# DESIGNING OF AN ARTIFICIAL LIGHT ENERGY CONVERTER BY COMBINING A NOVEL SHORT CHAIN DYAD WITH GRAPHENE NANOMATERIALS

*A thesis submitted towards partial fulfillment of the requirements for the degree of*

## Master of Technology in Laser Technology

Course affiliated to Faculty of Engineering and Technology and
offered by Faculty Council of Interdisciplinary Studies, Law and Management,
Jadavpur University

*submitted by*

**DEBMALYA HALDER**
**Examination Roll No. : M4LST19007**
**Registration No. : 141053 of 2017-2018**

*Under the guidance of*

**Prof. Dr. Tapan Ganguly**
School of Laser Science and Technology
Jadavpur University, Kolkata - 700032

**School of Laser Science and Engineering**

**Faculty Council of Interdisciplinary Studies, Law and Management**

**Jadavpur University**

**Kolkata -700032**

**India**

**2019**

**M. Tech in Laser Science & Technology**
**Course affiliated to**
**Faculty of Engineering and Technology**
**and offered by**
**Faculty Council of Interdisciplinary Studies, Law and Management**
**Jadavpur University**
**Kolkata, India**

---

## CERTIFICATE OF RECOMMENDATION

THIS IS CERTIFIED THAT THE THESIS ENTITLED "**DESIGNING OF AN ARTIFICIAL LIGHT ENERGY CONVERTER BY COMBINING A NOVEL SHORT CHAIN DYAD WITH GRAPHENE NANOMATERIALS**" IS A BONAFIDE WORK CARRIED OUT BY **DEBMALYA HALDER** UNDER MY SUPERVISION AND GUIDANCE FOR PARTIAL FULFILMENT OF THE REQUIREMENT FOR POST GRADUATE DEGREE OF MASTER OF TECHNOLOGY IN LASER TECHNOLOGY, DURING THE ACADEMIC SESSION 2018-2019.

---

**THESIS SUPERVISOR**
**Prof. Dr. Tapan Ganguly**
**School of Laser Science and Engineering**
**Jadavpur University, Kolkata-7000032**

Countersigned

---

**SRI. DIPTEN MISRA**
**Director**
**School of Laser Science and Engineering**
**Jadavpur University, Kolkata-700 032**

---

**DEAN**
**Faculty Council of Interdisciplinary Studies, Law and Management**
**Jadavpur University, Kolkata-700 032**

**M. Tech in Laser Science & Technology**
**Course affiliated to**
**Faculty of Engineering and Technology**
**and offered by**
**Faculty Council of Interdisciplinary Studies, Law and Management**
**Jadavpur University**
**Kolkata, India**

---

## CERTIFICATE OF APPROVAL **

This foregoing thesis is hereby approved as a creditable study of an engineering subject carried out and presented in a manner satisfactory to warrant its acceptance as a pre-requisite to the degree for which it has been submitted. It is understood that by this approval the undersigned do not necessarily endorse or approve any statement made, opinion expressed or conclusion drawn therein but approve the thesis only for the purpose for which it has been submitted.

---

**COMMITTEE OF FINAL EXAMINATION FOR EVALUATION OF THESIS**

---

---

---

** Only in case the recommendation is concurred

## DECLARATION OF ORIGINALITY AND COMPLIANCE OF ACADEMIC ETHICS

The author, hereby declares that this thesis contains original research work by the undersigned candidate, as part of his **Master of Technology in Laser Technology** studies during academic session 2018-2019.

All information in this document has been obtained and presented in accordance with academic rules and ethical conduct.

The author also declares that as required by this rules and conduct, the author has fully cited and referred all material and results that are not original to this work.

**NAME:** DEBMALYA HALDER

**EXAMINATION ROLL NUMBER: M4LST19007**

**THESIS TITLE:** DESIGNING OF AN ARTIFICIAL LIGHT ENERGY CONVERTER BY COMBINING A NOVEL SHORT CHAIN DYAD WITH GRAPHENE NANOMATERIALS

SIGNATURE: DATE:

# ACKNOWLEDGEMENT

I express my sincere gratitude to my supervisor ***Prof. Dr. Tapan Ganguly*** for his invaluable guidance, whole-hearted support and encouragement for accomplishing the present investigation. His dynamism, fantastic stamina and day-to-day monitoring every minute detail were a constant source of inspiration to me.

I express my great depth of gratitude to ***Dr. Somnath Paul & Ishani Mitra*** for their inspiration and encouragement and helping me through the research work.

I would also like to express my deep sense of thankfulness to ***Sri. Dipten Misra*** providing me necessary atmosphere to work on.

I record my acknowledgement to ***School of Laser Science and Engineering*** for giving me the opportunity to pursue my research work.

Lastly but obviously not the least I would like to pay my special admiration thanks to my parents and brother for their constant support, love and faith.

My eternal gratitude goes to god.

.

**DEBMALYA HALDER**

**Examination Roll No.: M4LST19007**

**Registration No. :141053 of 2017 – 2018**

# *Preface*

This dissertation entitled "Designing of an artificial light energy converter by combining a novel short chain dyad with graphene nanomaterials" is involved in designing such device by combining novel synthesized organic dyads with graphene oxide (GO) and reduced graphene oxide (RGO) for fulfillment of the strong need for the development of low cost light energy conversion devices having high efficiency, good stability and of biocompatible and biosafe in nature**.**

As the large amount of energy of the sun remains unused for future needs even after consumption of present requirements, this energy could be used to develop light energy conversion device in a biocompatible and biosafe manner which will not only be efficient and stable but also economically cheap.

**Chapter 1** is the introduction which mainly contains brief review of existing theoretical and experimental knowledge relevant to the present work and an outline of purpose studied in the present investigation.

**Chapter 2** contains description of the experimental techniques and materials used in the present investigation, works primarily be involved in designing such device by combining novel synthesized organic dyads with graphene oxide (GO) and reduced graphene oxide (RGO) composite systems for fulfillment of the strong need for the development of light energy conversion devices having low cost, high efficiency, good stability and of biocompatible and biosafe nature.

C**hapter 3** presents the results made from UV-vis absorption, steady state and time resolved spectroscopic investigations, both in pico and nanosecond time domain. Investigations are made on a novel synthesized dyad, (*E*)-4-(((9*H*-fluorene-2-yl)imino)methyl)-N,N-dimethylaniline (**NNDBF**) in its pristine form and when combined with GO & RGO i.e. in its nanocomposite form in the different concentration.

**Chapter 4** Comparisons of the photo-physics of the short chain dyad-GO & dyad RGO with the previously investigated different dyad nanocomposite.

**Chapter 5** consists of overall conclusion above the investigated work.

*Dedicated to my beloved Parents, brother, my supervisor &*

*God*

# Contents

# Chapter : 1

# *Introduction*

# Chapter 1: **Introduction**

Energy is an essential ingredient to our life. It is used to produce heat and work. If we live better than our primitive ancestors, it is because we use more energy to do work. Energy can exist in various forms. All of the energy sources that we use, except geothermal and nuclear energies, are derived initially from solar energy. Fossil fuel that we use today – coal oil and natural gas – are derived from organisms that grew over several hundreds of millions of years, storing the solar energy which reached the earth's surface. Renewable energies – hydro, biomass, wind are also directly or indirectly derived from our sun[1].

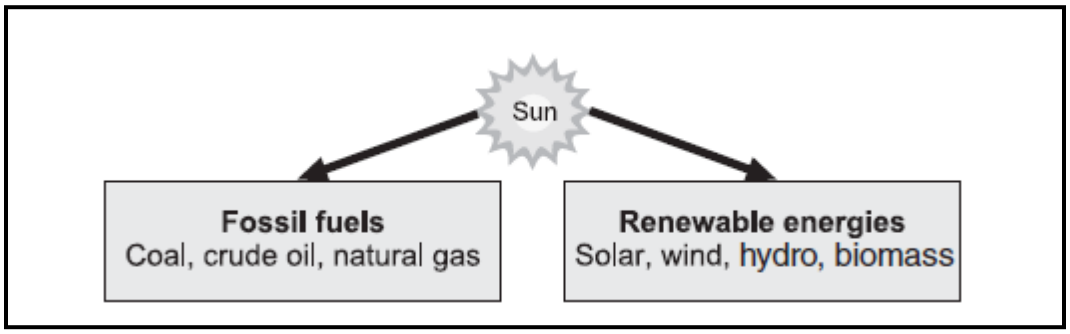


**Fig. 1.1**. Origin of different sources of energy used by humans[1].

Modern civilization is highly dependent on fossil fuel. The growing demand of energy, the non renewable fossil fuels are running out rapidly. This crisis of conventional energy resources is standing on the way of socio economic growth in the developing and developed countries. Petroleum products like kerosene, diesel, petrol are much more used in India to run pump sets, agricultural field and in transportation. So in 21$^{st}$ century, energy crisis is a severe problem[2].

In historical terms, the epoch of stored photosynthesis has been comparatively brief. Coal was seen as an inferior substitute when its use became widespread as a result of a shortage of wood in the late eighteenth century. The era of petroleum fuels began in the late nineteenth century. There are three reasons for believing that we are approaching the end of the present epoch: resource limitations, environmental problems, and social issues. A special series of reports on energy in New Scientist recently pointed out that pessimists now believe that the peak of world

oil production was actually in the year 2000 and that we are already on the downhill slope. There are still optimists who think that it might be 10 years away or more, but there is no substantial disagreement with the geological fact that the peak of world oil production, if it hasn't already happened, will happen in most of our lifetimes. In that near-future world, oil will become scarcer and more expensive. So we will have to change the basis of our energy use, while the current expectations are that we will have cheap petroleum for few decades. This beliefs is based on two heroic assumptions. The first is that there will be continuing stability in, and willingness to export oil from the Middle East region. The second assumption is that the majority of the world's population will continue to do without the transport options we take for granted while we dissipate the dwindling supplies of petroleum in such selfish indulgences as car races, jet skis, motor boats, and using heavy four-wheel-drive vehicles for suburban trips. So the first and most basic reason for moving away from the present pattern of fuel energy use is that we are dissipating a limited resource, making change inevitable.

The second reason for change is that the use of fossil fuels is causing serious environmental problems, at all levels from the local to the global. At the local level, fuel use in urban areas is the main cause of air pollution that is bad enough to pose serious health risks in many large cities (UNEP 2002). Here Delhi is the most air polluted city in India. At the regional level, the problem of acid precipitation has caused policy changes to reduce the production of sulfur dioxide as a byproduct of using fossil fuels (UNEP 2002). At the global level, the burning of increasing amounts of fossil fuels is the main cause of human-induced climate change; concern about this problem led to the development of the Framework Convention on Climate Change and its associated Kyoto Protocol, an agreement to curb emissions of carbon dioxide and other "greenhouse gases." The current scientific opinion is that emissions of carbon dioxide are about 2.5 times the capacity of natural systems to absorb the gas (IPCC 2001). In other words, global use of fossil fuels needs to be reduced to about 40% of the present level to bring emissions into balance with the natural carbon cycle. Recent scientific thinking suggests that climate change is accelerating and influencing other global cycles, posing a very serious threat to the future of human civilization.

The only feasible way of squaring this circle is to move away from stored photosynthetic products to new forms of artificial photosynthesis. The case for moving in this direction recognizes the scale of the available resources. The natural flows of solar energy are four orders of magnitude greater than the present global energy use and therefore are larger than any conceivable future energy demand. In fact, the amount of solar energy that hits in one summer day is of the same order of magnitude as the global annual energy use for all purposes[3]. Practical, cost effective technologies for conversion of sunlight directly into useful fuels do not currently exist, and will require new basic science.

Photosynthesis provides a blueprint for solar energy storage in fuels. All of the fossil-fuel based energy consumed today derives from sunlight harvested by photosynthetic organisms. The quality of human life is threatened unless renewable energy resources can be developed in the near future. The solar energy, the gift of nature, fills most of humanities energy needs. Utilization of solar energy is a very interesting aspect of science[1]. The photochemistry research involving chemical change, occurred by the absorption or emission of visible light or ultraviolet radiation, emphasizes fundamental processes aimed at the capture and conversion of solar energy[4]. Upon absorption of a photon (a quantum of light) a molecule goes to the excited state from its ground state. If upon electronic photo- excitation the molecule loses its chemical identity then the process is called photochemical but if the molecule preserves its chemical identity then the process is called photo physical. Photochemical processes form the basis of light. The most important and best-known photochemical reaction is photosynthesis, the mechanism by which plants derive their energy using solar energy. So the various types of artificial photosynthesis are effectively competing for the right to harness incoming photons and use them for the community's benefit. The development of artificial photosynthetic systems using a large portion of the solar spectrum would be a major advance in energy production, and a critical breakthrough with respect to the rising concern of environmental pollution caused by the use of fossil fuels [5]. To solve this problem one attractive strategy discussed in this thesis is the development of solar cells that are based on the organic dyad, graphene oxide (GO) and reduced graphene oxide (RGO).The present thesis addresses the current research issue in the field of a new solar cell based on charge electron injection separation a short chain dyad as a light energy converter.

The burgeoning new field of nanotechnology, opened up by rapid advances in science and technology, creates new opportunities for advancing medical science and disease treatment in human health care and has a promising solution of energy cricis. The conventional silicon based solid state solar cells are among the very few devices that are commercially available for converting solar energy to electricity. But there are many drawbacks i.e. they are brittle and harvest small amount of solar spectrum of light. For instance, silicon is transparent to infrared light. Which means a lot of solar potential energy is not harvested. An alternative approach is the use of quantum dots. These are nanoscale particles where the response to different wavelengths can be tuned by altering their sizes. While the efficiency of quantumdot solar cells reported in recent studies is increasing to as high as 9%, the real breakthrough is that the new devices can be produced at room temperature and in an atmosphere, rather than an expensive and hard-to-maintain vacuum. Perhaps the most exciting aspect of quantum-dot solar cells, though, is that the quantum dots can be dispersed in other materials, leading to "spray on" low-cost and large-area solar cells that can be applied to buildings or vehicles[6,7].

Scientists believe that hydrogen could be an effective solution to reducing the world's dependence on non-renewable carbon-producing fossil fuels because it is clean, portable and versatile. Hydrogen fossil fuel and artificial photosynthesis are the most important researches going on today. Apart from this type of research, a number of other promising approaches have appeared in recent years for working on artificial photosynthesis based on development of organic molecular systems which will provide nonradiative processes through photosensitized reactions like excitational energy transfer and photoinduced electron transfer (PET) [8,9]. Some novel chemical approaches are being attempted lately to design model compounds of artificial photosynthesis [55,57,60,64,67]. The short-chained dyads are capable of efficient light harvesting, excitation energy transfer, electron transfer and formation of long-lived chargeseparated states. The artificial or model light energy conversion devices will mimic the primarily charge-separation of natural photosynthetic system.

Artificial photosynthesis research applies the fundamental scientific principles of the natural process to the design of solar energy conversion systems. Solar energy has a great potential as a clean, cheap, renewable and sustainable energy source, but it must be captured and transformed

into useful forms of energy as plants do. An especially attractive approach is to store solar energy in the form of chemical bonds as performed in natural photosynthesis. So, dye-sensitized solar cells have emerged as promising alternatives to expensive solid state solar cells. The synthesis and characterization of a novel organic short chain dyad, NNDMBF ((E)-4-(((9H-fluorene-2-yl)imino)methyl)-N,N-dimethylaniline) have been made [2]. The primary aim is to fabricate new hybrid nanocomposites by combining the organic dyad with different noble metals, semiconductor nanoparticles and noble metal-semiconductor core/shell nanocomposite and finally with graphene to develop supercapacitor type storage system. The investigation would be carried out by using steady state and time resolved spectroscopic techniques on this novel synthesized short chain dyad and its hybrid nanocomposite systems. Some quantum chemical calculation should also been done using Gaussian 03 software to support the experimental findings by theoretical point of view. A better understanding of the various properties of these nanostructures is needed in order to realize their full potentials in the field of storage of energy. Our present and future investigations are directed in this way.

Recently we have synthesized a novel dyad [68] where the donor mathoxynpthalane is linked by a short chain with an acceptor p-methoxyacetophenone.

UV-vis absorption, steady state and time resolved spectroscopic investigation were made in different environment on this novel synthesized dyad in its pristine form and when combined with metal, metal-seconductor materials i.e. its nanocomposite form and the investigation using graphene oxide (GO) and redused graphene oxide (RGO) is underway. Primarily steady state measurement shows that the formation of charge separated species both in ground and excited states occur when the two redox components are attached with a short chain. In the present work the primary aim is to determine rates associated with charge separation and energy destructive charge recombination processes by using the steady state and time resolved spectroscopic techniques. The experimental date would help to reveal the suitability of the novel dyad to acting as an artificial light energy conversion device. Finally attempts will be made to design a nanocomposite system by combining dyad with GO and RGO. It is expected that with the help of short chain organic dyad system and combining them with the GO and RGO, a very efficient,

stable and low cost artificial light energy converter could be developed which should be of biocompatible and biosafe in nature. Development of much deeper understanding of how the complex interplays between the electronic and physical interactions of the active components ultimately affects the performance of this devices is the most promising challenge. Our primary attempts would be to combine the present organic short chain dyad NNDMBF with graphenes to compare our earlier results obtained on various nanoparticles or core shell of noble metal and semiconductor composite systems[refer some paper from t ganguly]. The rates associated with the charge separation ($k_{CS}$) and the energy destructive charge recombination ($k_{CR}$) processes would be measured with in the NNDMBF-graphene nanocomposite systems by using laser flash photolysis technique (pump probe method) and the observed charge separation and energy wasting charge recombination rate parameters would be compared with those of pure dyad system in order to evaluate the efficiency of the nanocomposite devices. Both charge separation and energy destructive charge recombination rates were measured from time correlated single photon counting (TCSPC) and transient absorption spectroscopic technique by laser flash photolysis (pump probe technique) methods.

It is expected that the present dyad NNDMBF when combined with graphene nanomaterials may form very stable energy storage systems and could behave as low cost supercapacitor. Our present investigations are directed in this way.

## 1 . Photophysics and Photochemistry in science and technology

Photochemical and photophysical processes have been intimately related to the development of man and his environment even before his appearance on the planet. A sophisticated series of photochemical and photophysical processes, now referred to as photosynthesis, made it possible for simple cells to become autotrophic, provided the necessities of life, stored solar energy in the form of fossil fuels, and still supply us with practically all our food. Photochemistry is heavily involved in processes that determine the composition of matter in the interstellar space, and in the formation of atmospheric pollutants. Here, photophysical processes also occur in nature. However, photochemistry and photophysics are also important from an artificial viewpoint.

Their impact in the chemical, physical, biological, and medical sciences and technologies, including nanotechnology, is being felt increasing in a spectacular manner. Photochemical and photophysical concepts are at the basis of important applications such as protection of dyes and plastics (and also human skin) from the damaging effect of sunlight, waste water cleaning, design of fluorescent compounds for a variety of sensing applications, creation of photochromic materials used in sunglasses, optical memories, solar-powered green synthesis, molecular photovoltaics, and solar energy conversion by water photodissociation etc.[10].

## 2 . A new dimension of chemistry and physics

Light excitation with a photon of suitable energy promotes a molecule from its ground state to an electronically excited state. Light excitation causes changes in the electronic structure of a molecule, so that each type of excited state has its own electronic structure, different from that of the ground state. Because the chemical and physical properties of a molecule depend on its electronic structure, each excited state has its own chemical and physical properties.

The ground state of a molecule uses the conventional chemical reactions, called thermal reactions, as they need heat to occur; the ground state is also responsible for the absorption spectrum, that is, for the color. The excited states are responsible for deactivation processes that can be chemical in nature or involve energy loss processes, either radiative or nonradiative. Therefore, light excitation opens new dimensions to chemistry and physics. In chemistry, the excited states can react in different ways, both qualitatively and quantitatively, compared with the ground state. In physics each excited state not only exhibits its own absorption spectrum (color) but can also be deactivated by its own photophysical processes, including light emission[10].

## 3 . Laws of photochemistry

All photochemical and photophysical processes are initiated by the absorption of a photon of visible or ultraviolet radiation leading to the formation of an electronically excited state.

$$R + h\nu = R^*$$

In the beginning of the 19th century, the qualitative approach to photochemistry was initiated by Grotthus and Draper. Then it was realized that all the incident light was not effective in bringing about a chemical changes and the first law of photochemistry is known as Grotthus-Draper law, which states that only that light which is absorbed by a system can cause chemical change.

The extent of absorption of light varies greatly from one substance to another, the rate of absorption is given by the Lambert- Beer law. The Lambert law states that the fraction of incident light absorbed by the transparent medium is independent of the incident radiation and each successive layer of the medium absorb equal fraction of incident radiation. The Beer law states that the amount of radiation absorbed is proportional to the number of molecules absorbing the radiation. The combined form of this law can be expressed as –

$$log_{10} \frac{I_{in}}{I_{out}} = \varepsilon cl$$

'$I_{in}$' is the intensity of light entering the substance, is greater than the intensity of emerging light '$I_{out}$'. Here 'c' is concentration and 'l' is path length of the absorbing substance[10], 'ε' is called molar absorption coefficient or extinction coefficient which is characteristic of a particular substance and a particular wavelength. Here the left hand side quantity is called absorbance (A).

$$A = \varepsilon cl$$

The Beer – Lambert law can generally be applied, except where very high - intensity light beams such as lasers are used. In such cases, a considerable proportion of the irradiated species will be in the excited state and not in the ground state. The Beer – Lambert law is frequently usedin the analytical determination of concentrations from absorbance measurements.

The second law of photochemistry is known as Stark-Einstein law, which states that one quantum of light is absorbed per molecule of absorbing and reacting substance that disappears. Molecules which absorb photons become physically 'excited', and this must be distinguished from becoming chemically 'active'. Excited molecules may lose their energy in nonchemical ways, or alternatively may trigger off thermal reactions of large chemical yield. This provides essential information about the primary photochemical process. The efficiency of a photochemical reaction can be expressed by quantum yield or quantum efficiency (φ).

$$\phi_{reaction} = \frac{number\ of\ molecules\ decomposed\ or\ formed}{number\ of\ quanta\ absorbed}$$

When high intensity light sources as from flash lamps or lasers are used 'biphotonic' photochemical effects may occur which modify the application of the Einstein law[11]. So the nature of the photo-products and the quantum yields are dependent on the light intensity.

## 4 . Light absorption by molecule

Molecules which contain antenna group, absorbs light energy. These groups are known as chromophores or chromophoric group. When oscillating electromagnetic radiation incident on an appropriate chromophore, an electron in the chromophore is promoted to the higher energy excited state. When this electronic transition occurs, the absorbing chromophore undergoes an electric dipole transition and the energy of the photon becomes part of the total energy of the excited - state molecule. The transition dipole moment lasts only for the duration of the transition and arises because of the process of electron displacement during the transition. The intensity of the resulting absorption is proportional to the square of the transition dipole moment. However, it is not possible to explain fully the effects of electronic excitation in molecules unless we also take into account the motions of the nuclei. Here, the total energy of molecules is made up of electronic energy and energy due to nuclear motion (vibrational and rotational):

$$E_t = E_e + E_v + E_r$$

where the subscripts refer to the total energy, electronic energy, vibrational energy and rotational energy, respectively. Because of the large differences between electronic, vibrational and rotational energies, it is assumed that these can be treated separately. This assumption is known as the Born – Oppenheimer approximation[12].

The energy gap between rotational states is much smaller than the gap between two vibrational states, similarly, energy gap between two vibrational states is much smaller than between two electronic states. So we can adequately describe the effect of electronic transition within the molecule by considering quantized electronic and vibrational states. The electronic transition results by the absorption of visible and UV light, in which changes in both electronic and vibrational states occur. These transitions are called vibronic transition.

At thermal equilibrium the population of energy levels is described by the Boltzmann distribution law . If $N_0$ molecules are in the ground state and $N_1$ be the number in any higher energy level then the equation becomes:

$$\frac{N_1}{N_0} = e^{-\frac{\Delta E}{RT}}$$

ΔE is the energy difference between the two energy levels, R is the gas constant and T is the absolute temperature. At room temperature, most molecules will be in the v = 0 vibrational state of the electronic ground state and so absorption almost always occurs from $S_0$ (v = 0) state.

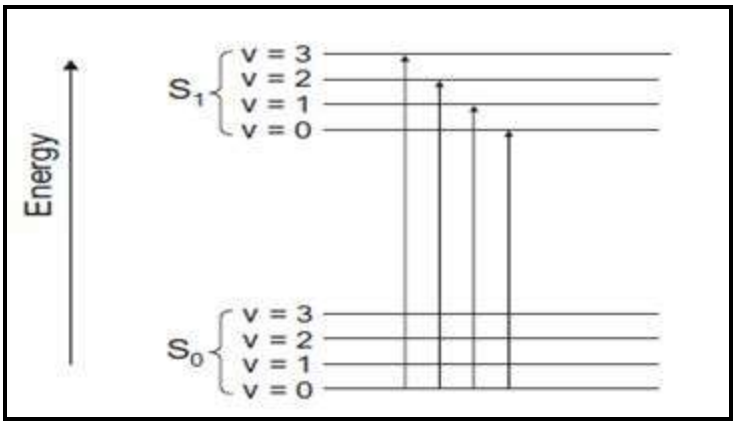


**Fig. 1.2**. Schematic diagram of the electronic ground state and the fi rst excited electronic state, with their associated quantised vibrational energy levels, for an organic molecule. The vertical arrows show vibronic transitions due to the absorption of photons[12].

The potential energy curve for a diatomic molecule often referred to as a Morse curve, which refers the way in which the potential energy of the molecule changes with its bond length. At the points where the horizontal lines meet the Morse curve, the energy is wholly potential. In between, the energy is partly kinetic and partly potential.

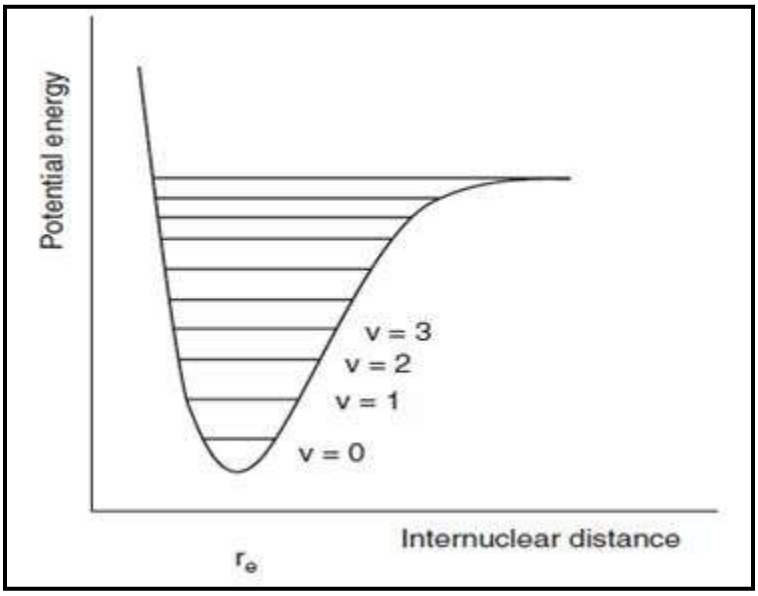


**Fig. 1.3.** Morse curve for a diatomic molecule, the minimum on the curve represents the equilibrium bond distance, $r_e$ [12].

Each vibrational energy level is associated with a wavefunction, the square of which relates to the most probable internuclear distance for a given vibrational quantum number, v. For the v = 0 level, the square of the wavefunction shows that the molecule spends most of its time in the region of the equilibrium configuration. However, for an excited vibrational energy level, the magnitude of the $\psi^2$ function is greatest close to the turning points of the vibrational motion, which shows that the bond spends most of its time in the fully compressed or fully - extended configuration. Nuclei are much heavier than electron, so nuclei move much slower than electron. When a transition occurs from one electronic state to another, it takes place so rapidly that the nuclei of the vibrating molecule can be assumed to be fixed during the transition. This is called the Franck – Condon principle.

Transitions between the vibrational levels in lower and upper electronic states will be most intense when the two states have similar internuclear separation, i.e. there will be a greater probability of an electronic transition when the $\psi^2$ functions for the upper and lower vibronic states have a greater overlap. This overlap, called the Franck – Condon factor.

## 4.1 Light absorption by organic molecule

In organic molecule we can see that small fingers are superimposed on a broader band. These fingers are called vibrational fine structures. Each finger corresponds to a transition from the v=0 of the ground electronic state to the v=0,1,2,3 etc. vibrational level of the excited electronic state.

The absorption spectra of rigid hydrocarbons in nonpolar solvents may show vibrational fine structure, but absorption spectra of other organic molecules in solution tend to be broad, featureless bands with little or no vibrational structure. This is due to the very large number of vibrational levels in organic molecules and to blurring of any fine structure due to interaction between organic molecules and solvent molecules.

## 5 . Electronic transition

In organic molecule the electronic transition between the molecular orbitals is possible by absorption of radiation. Usual ordering of such molecular orbitals is shown in fig – 1.4. Figure shows that in principle, there are sis type of electronic transition is possible: $\sigma \rightarrow \sigma^*$, $\sigma \rightarrow \pi^*$, n $\rightarrow \sigma^*$, $\pi \rightarrow \pi^*$, $\pi \rightarrow \sigma^*$,and n $\rightarrow \pi^*$. Of these possible transitions, only those of the last three normally account for the transitions in UV-Vis region. The others require too great an energy.

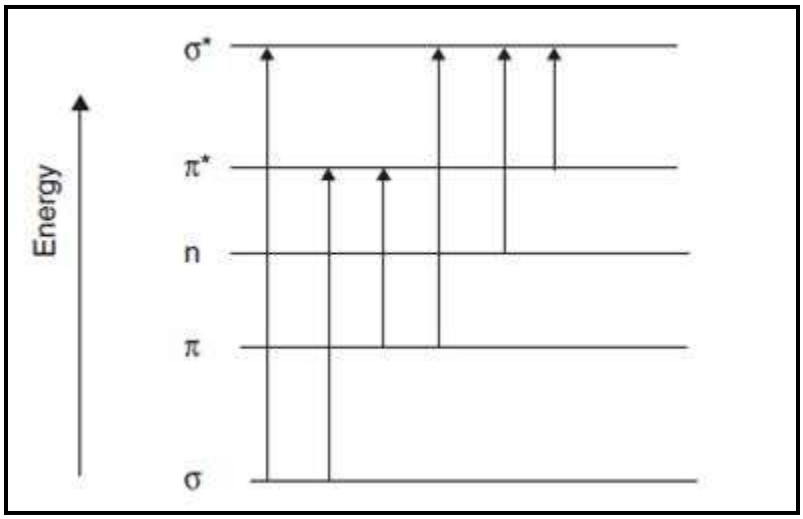


**Fig. 1.4.** Generalised ordering of molecular orbital energies for organic molecules and electronic transitions by excitation with light [12].

Four types of electronic excitation need to be considered for most organic molecules. They are listed below in order of decreasing energy:

(i) $\sigma \rightarrow \sigma^*$ transitions: These require too great an energy. These correspond to radiation absorption in the vacuum UV region. Alkanes, which have no *n* or *π* electrons, can be excited only in this way.

(ii) n $\rightarrow \sigma^*$ transitions: Alcohols, amines, ethers etc. can be excited in this manner. These are symmetry forbidden and low intensity transitions. The required radiation range for these transitions is 150-250 nm. Most peaks appear < 200 nm.

(iii) $\pi \rightarrow \pi^*$ transitions: The absorption peaks for these transitions fall in an experimentally convenient region of the spectrum (200 - 700 nm). These transitions need an unsaturated group in the molecule to provide the $\pi$ electrons.

(iv) (iv) $n \rightarrow \pi^*$ transitions: Aldehydes, ketones, carboxylic esters, etc. can undergo this promotion as well as the other three. The absorption peaks for these transitions fall almost in the same spectral region as that of $\pi \rightarrow \pi^*$ transitions.

Molar absorbtivities from $n \rightarrow \pi^*$ transitions are relatively low, and range from 10 to100 L $mol^{-1}$ $cm^{-1}$. $\pi \rightarrow \pi^*$ transitions normally give molar absorbtivities between 1000 and 10,000 L $mol^{-1}$ $cm^{-1}$.

The solvent in which the absorbing species is dissolved also has an effect on the spectrum. Peaks resulting from $n \rightarrow \pi^*$ transitions are shifted to shorter wavelengths (blue shift) with increasing solvent polarity. This arises from increased solvation of the lone pair, which lowers the energy of the *n* orbital. Often (not always) the reverse (red shift) is seen for $\pi \rightarrow \pi^*$ transitions. This is caused by attractive dipole forces between the solvent and the absorber, which lower the energy levels of both the excited and unexcited states. This effect is greater for the excited state, and so the energy difference between the excited and unexcited states is slightly reduced. This results in a small red shift. This effect also influences $n \rightarrow \pi^*$ transitions, but is overshadowed by the blue shift resulting from solvation of lone pairs.

In using the concept of molecular orbital theory to discuss the absorption of light by organic molecules, we concentrate on two molecular orbitals in particular. The highest occupied molecular orbital (HOMO) is the ground - state molecular orbital of highest energy with electrons in it and the lowest unoccupied molecular orbital (LUMO) is the ground - state molecular orbital of lowest energy with no electrons in it. Thus, the lowest energy transition in an organic molecule will be the HOMO - LUMO transition[12].

## 5.1 Excited states and the ground states

Electronic states of a molecule are obtained by considering the properties of all the electrons in the unfilled shells as they are the main contributors. Representation by overall symmetry of the molecule is the most useful way of designating energy states of a polyatomic molecule [11,13]. Classification by the quantized component of the orbital angular momentum along the line of centres, $\Sigma$, $\pi$, $\Delta$, is possible for linear molecules only. When details of the electronic structure of states are unknown or not necessary, the most common method is to denote them by their multiplicities, S (singlet) or T (triplet). In most organic molecules, all electrons in the ground state are paired, with each member of a pair possessing opposite spin as demanded by the Pauli principle. When one of a pair of electrons is promoted to an orbital of higher energy, the two electrons no longer share an orbital, and the promoted electron may, in principle, have the same spin as its former partner or the opposite spin. A molecule in which two unpaired electrons have the same spin is called a triplet (T), while one in which all spins are paired is a singlet (S). The lowest-energy excited state is called $S_1$, the next $S_2$, etc., and triplet states are similarly labeled $T_1$, $T_2$, $T_3$ etc. Therefore, $S_0$ indicates the ground state. In most cases promotions from the $S_0$ state to any T states are improbable (these are called "forbidden" transitions). Thus it can be stated that in most molecules only singlet-singlet promotions take place.

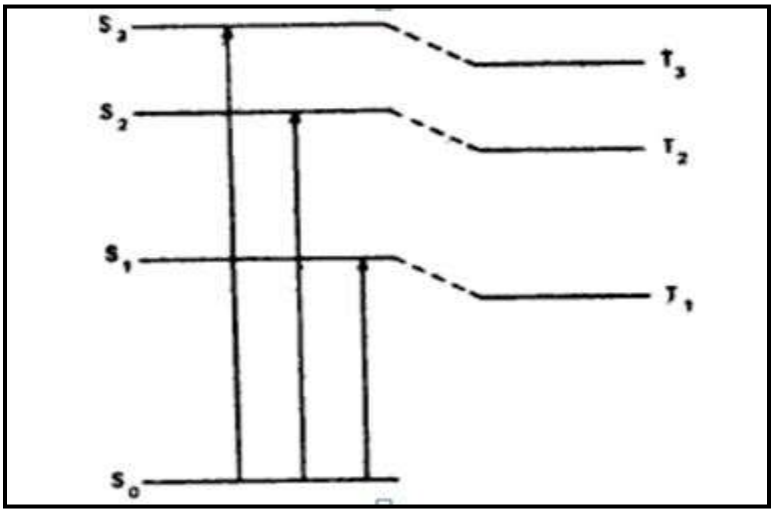


**Fig. 1.5.** - Relative energies of singlets $S_0$, $S_1$, $S_2$ and triplets $T_1$, $T_2$ state of a typical organic molecule [11]

## 6. Physical deactivation of excited state

A molecule, photo-chemically promoted to an excited state by photon absorption. These excited states are short - lived, loses their energy within a very short period of time through a verity of deactivation process. When the excited molecule returns to its ground state then the deactivation process is called physical process and if a new molecular species is formed then the deactivation process is accompanied with the chemical change.

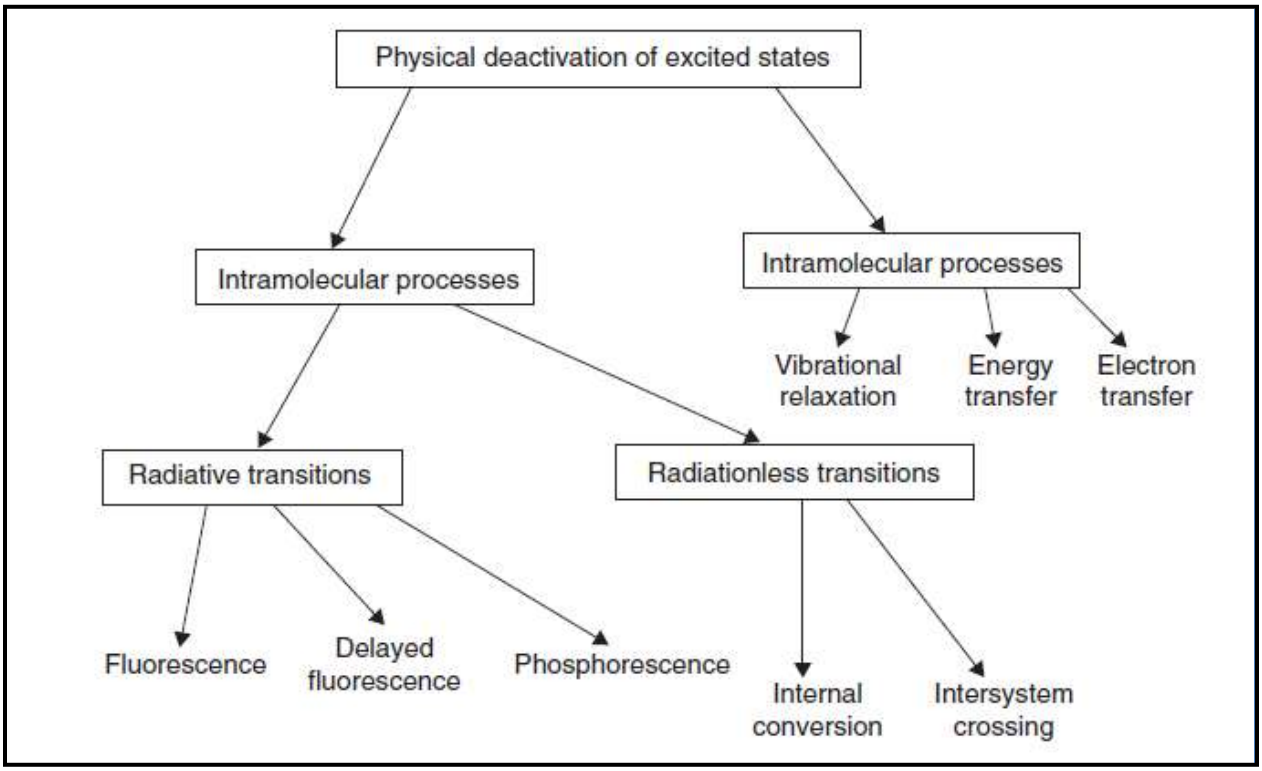


**Fig. 1.6.** Physical deactivation of excited states of organic molecules [12]

Physical relaxation processes may be categorized as:

i. Intramolecular processes

a. Radiative transitions: it emits electromagnetic radiation when excited molecule goes to the ground state. Fluorescence and phosphorescence are known collectively as luminescence.

b. Radiationless transitions: There is no emission of electromagnetic radiation during the relaxation process.

ii. Intermolecular processes

a. Vibrational relaxation: Here the molecules of excited vibrational level which have excess energy, undergoes rapid collision with one another or with the solvent molecule in the lowest vibrational level of a particular electronic level.

b. Energy transfer: The electronically – excited state of one molecule (the donor) is deactivated to a lower electronic state by transferring energy to another molecule (the acceptor), which is itself promoted to a higher electronic state.

c. Electron transfer: It involves a photoexcited donor molecule interacting with a ground - state acceptor molecule. An ion pair is formed, which may undergo back electron transfer, resulting in quenching of the excited donor.

## 6.1 Jabloski diagram

The photophysical processes, including light absorption, are conveniently discussed making use of the Jablonski diagram (Fig. 1.7). In that diagram, the electronic states are represented by thick horizontal lines that are arranged in vertical order to indicate the relative energies. According to Kasha, [14] for most photo-physical processes we need to consider only the lowest excited singlet state ($S_1$) or the lowest triplet state ($T_1$) as likely candidates for the initiation of a process. It is assumed that the ground state is a singlet for organic molecules. For clarity, only

the first few excited states are considered and the states of different multiplicity are separated horizontally. Vibrational levels are represented by thin lines, with the lowest one indicating the $\nu$ =0 level. Rotational levels are not indicated. Radiative transitions, associated with the absorption or emission of a photon, are indicated by straight arrows, while radiationless transitions are shown by wavy arrows. It is assumed, as it usually happens for organic molecules, that $S_0 \rightarrow T_n$ absorptions cannot take place because of the spin selection rule, while symmetry selection rules cannot be taken into account for two reasons: they are less severe than the spin one, and molecules have a variety of different symmetries.

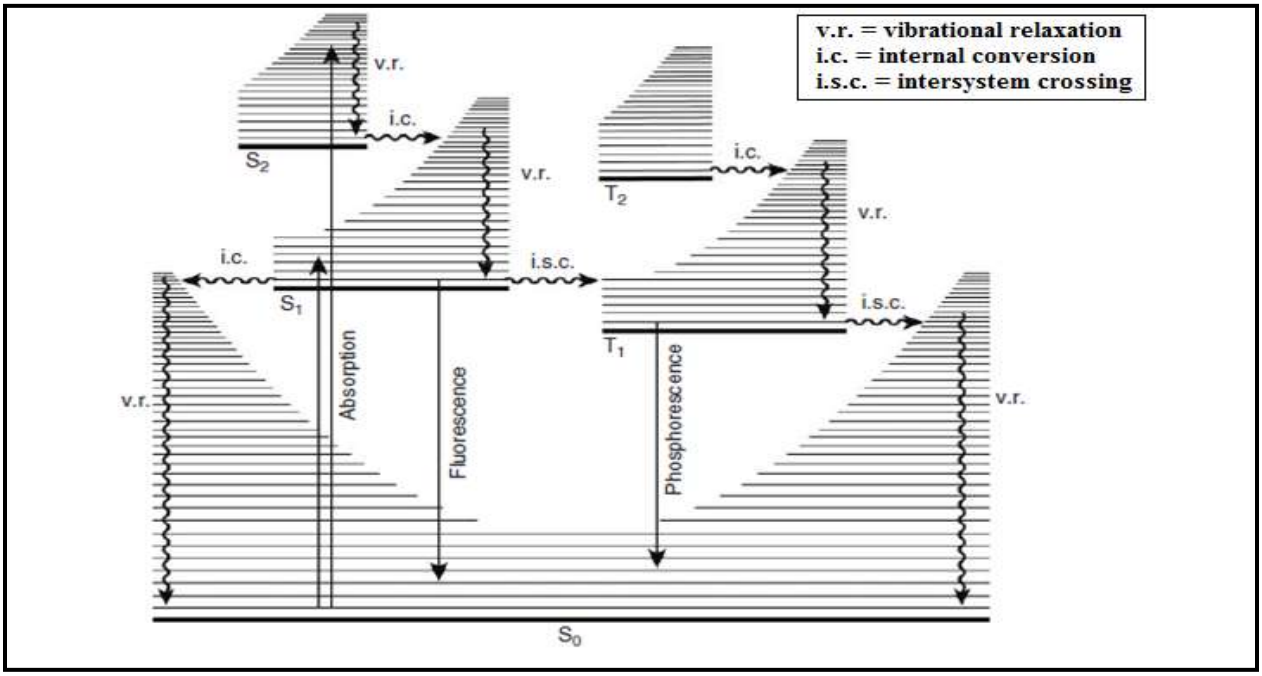


**Fig. 1.7.** Energy diagram (Jablonski diagram) used to depict the photophysical processes between ground state and excited states [10].

## 6.1.1 Radiative transition

Luminescence is the emission of light by a substance. It occurs when an electron returns to the electronic ground state from an excited state and loses its excess energy as a photon.

Luminescence is divided into two types, depending upon the nature of the ground state and excited states. The emission of radiation is also governed by Franck-Condon principle.

### 6.1.1.1 Fluorescence

Absorption of UV radiation by a molecule excites it from a vibrational level in the electronic ground state to one of the many vibrational levels in the electronic excited state. This excited state is usually the first excited singlet state. A molecule in a high vibrational level of the excited state will quickly fall to the lowest vibrational level of this state by losing energy to other molecules through collision. The molecule will also partition the excess energy to other possible modes of vibration and rotation. Fluorescence occurs between states of same multiplicity (spin allowed), usually from the lowest vibrational level of the lowest excited singlet state, $S_1$ (v=0).

$$S_1 \rightarrow S_0 + h\nu$$

The emission rate is typically near 108 Hz. These high emissive rate result in fluorescence lifetime are of the order of $10^{-12}$ – $10^{-6}$ s.

### 6.1.1.2 Phosphorescence

The phenomenon of phosphorescence involves an intersystem crossing, or transition, from the singlet to the triplet state. A triplet state results when the spin of one electron changes so that the spins are same, or unpaired. The transition from the ground state to the triplet excited state is a forbidden transition of different multiplicity. Usually the transition occurs from the lowest vibrational level of the lowest excited triplet state, $T_1$ (v=0).

$$T_1 \rightarrow S_0 + h\nu$$

Typical timescales for photon emission by phosphorescence are of the order of $10^{-3}$ – $10^{-2}$ s. Hence a characteristic feature of phosphorescence is an afterglow, that is, emission that continues after the exciting source is removed.

### 6.1.2 Vibrational relaxation

Electronically - excited states is usually associated with an excess of vibrational energy in addition to its electronic energy, unless it is formed by a transition between the zero - point vibrational levels (v = 0) of the ground state and the excited state ($0 \rightarrow 0$ transition). Vibrational relaxation involves transitions between a vibrationally - excited state (v > 0) and the v = 0 state within a given electronic state when excited molecules collide with other molecules, such as solvent molecules. Typical lifetime for the process is of the order of $10^{-13}$ – $10^{-9}$ s in condensed phases, and the excess vibrational energy is dissipated as heat.

## 6.1.3 Non-radiative transitions

Non-radiative transitions occur between iso-energetic (or degenerate) vibrational-rotational levels of different electronic states. Since there is no change in the total energy of the system, no photon is emitted, and the process is represented by a horizontal wavy arrow on a Jablonski diagram (Fig. 1.7.). The non-radiative deactivation pathways are of two general types, namely internal conversion (IC) and intersystem crossing (ISC).

### 6.1.3.1 Internal conversion

Relaxation from an upper excited electronic state ($S_2$ , $S_3$ , etc.) to a lower electronic excited state with the same multiplicity takes place rapidly by the radiationless process of internal conversion. Because the difference in energy of these upper excited states is relatively small, there is a high probability of the v = 0 level of, say, $S_2$ being very close in energy to a high

vibrational level of $S_1$, allowing rapid energy transfer between the two electronic levels to occur. Internal conversion involves intramolecular radiationless transitions between vibronic states of the same total energy and the same multiplicity. Typical timescales are of the order of $10^{-14}$–$10^{-11}$ s (internal conversion between excited states) and $10^{-9}$ – $10^{-7}$ s (internal conversion between $S_1$ and $S_0$ ).

Generally internal conversion between $S_1$ and $S_0$ occurs more slowly than that between excited states. Therefore, irrespective of which upper excited state is initially produced by photon absorption, rapid internal conversion and vibrational relaxation processes mean that the excited - state molecule quickly relaxes to the $S_1$ ($v_0$) state from which fluorescence and intersystem crossing compete effectively with internal conversion from $S_1$ . This is the basis of Kasha ' s rule , which states that because of the very rapid rate of deactivation to the lowest vibrational level of $S_1$ (or $T_1$ ), luminescence emission and chemical reaction by excited molecules will always originate from the lowest vibrational level of $S_1$ or $T_1$.

### 6.1.3.2 Intersystem crossing

Intersystem crossing involves intramolecular spin - forbidden radiationless transitions between isoenergetic states of different multiplicity. The transition can takes place either by direct spin orbit coupling $S_1$ to the higher vibrational level of $T_1$ or by the spin orbit coupling to one of the higher states $T_n$ followed by rapid internal conversion $T_n \rightarrow T_1$. The rate determining the steps in the spin inversion is in the range $10^7$ – $10^{11}$ Hz [6]. This depends on the extent of spin orbit coupling as well as on the energy gap between the states involved. Intersystem crossing has a timescale of the order of $10^{-11}$ – $10^{-8}$ s.

## 6.1.4 Excited states lifetime

The rapid nature of vibrational relaxation and internal conversion between excited states of an electronically - excited molecule will usually relax to the lowest vibrational level of the lowest

excited singlet state. It is from the $S_1$ (v = 0) state that any subsequent photophysical or photochemical changes will generally occur. This is called Kasha's rule.

### 6.1.4.1 Excited singlet state lifetime

The competing intramolecular photophysical processes that can occur from $S_1$ ($v_0$) are fluorescence, intersystem crossing and internal conversion, with first - order rate constants of $k_f$, $k_{ics}$ and $k_{ic}$ , respectively (Fig. 1.8 ). Applying a standard treatment of first - order chemical kinetics, the rate of disappearance of the excited $S_1$ molecules, ${}^1J_{total}$ , is given by:

$$ {}^1J_{total} = -\frac{d[S_1]}{dt} = \left(K_f + K_{isc} + K_{ic}\right)[S_1] = K_{total}\,[S_1] $$

'-' sign indicates that the $S_1$ state decays with time, i.e. it's concentration decreases with time. The solution of the above equation is

$$ [S_1]_t = [S_1]_0 \exp\left(-t/\tau\right) $$

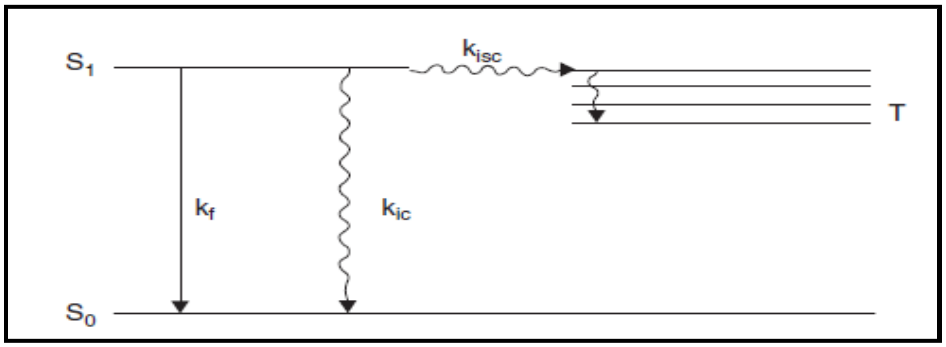


**Fig. 1.8.** Competing photophysical processes occurring from $S_1$[12]

where $[S_1]_0$ is the concentration of excited $S_1$ molecules at time t = 0 resulting from the initial exciting pulse, $[S_1]_t$ is the concentration of excited $S_1$ molecules at time t and τ is the excited

singlet - state lifetime of the $S_1$ excited state. The excited singlet state life time,$\tau$ is the time taken for the concentration of $S_1$ to decrease to 1/e times of its initial value.

Here time correlated single photon counting technique is used to measure the excited singlet state life time, $\tau$. The sample is irradiated with a very short duration laser light pulse (<< 1 ns) to ensure any given molecule will only be excited once during the pulse. As soon as the population of the molecules are excited, the molecules randomly begin to relax to the ground state by fluoresce.

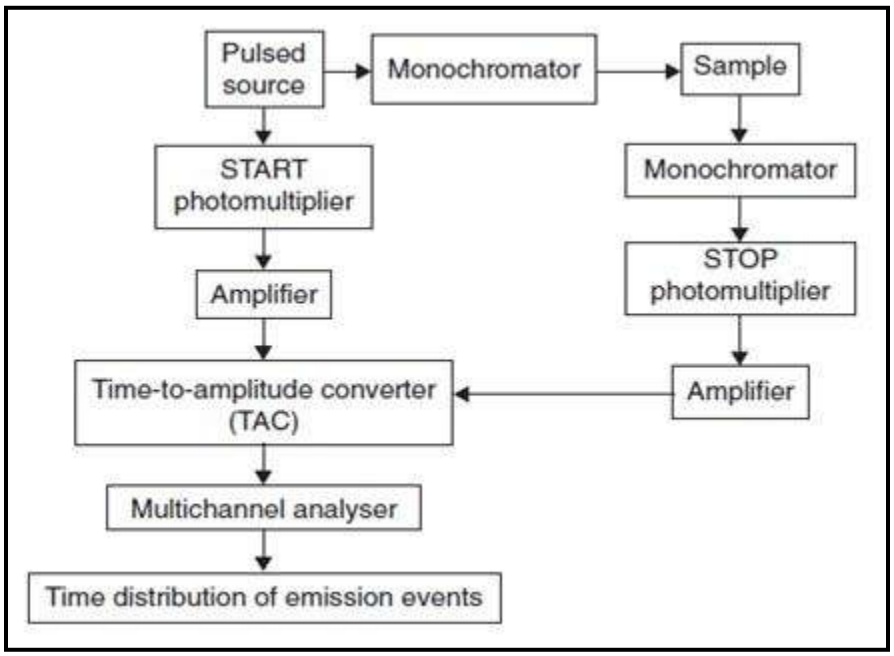


**Fig. 1.9.** Schematic diagram of a time correlated single photon counting apparatus[12]

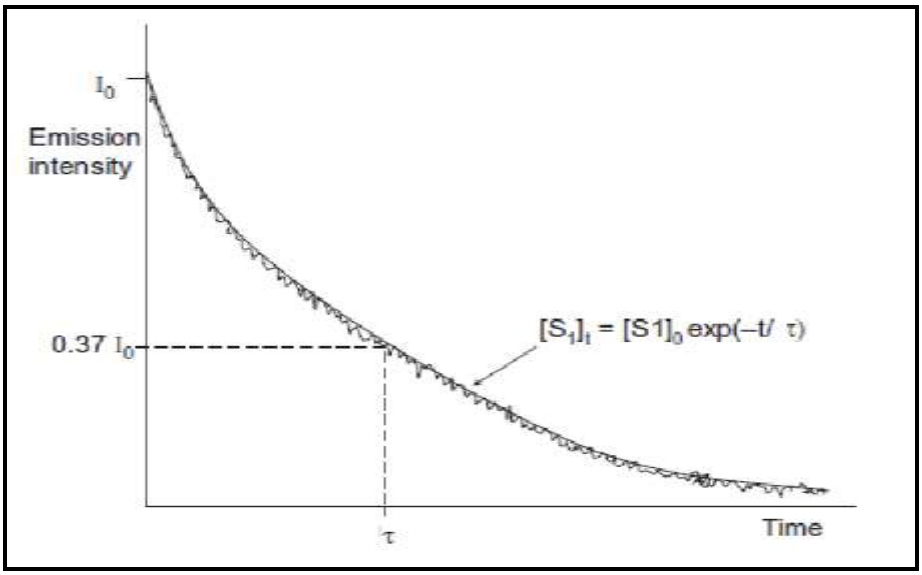


**Fig. 1.10.** Time resolved fluorescence decay measured by time correlated single photon counting[12]

The pulsed source produces its pulse of light to irradiate the sample, and then the START photomultiplier sends a signal to the TAC, which then linearly builds up a voltage until a signal is received from the STOP photomultiplier. When the STOP signal is received, the magnitude of the voltage is measured and stored in a multichannel analyser. The multichannel analyser divides the voltage range into a sequence of several hundred channels, each channel building up the count of the number of times a certain voltage level is detected. The electronics of the system allows the process to be repeated millions of times a second, building up a histogram representing the time distribution of the emission events (Fig. 1.10).

## 6.1.4.2 Excited singlet state radiative lifetime

It is the life time, $\tau_0$ of $S_1$ state in absence of any radiationless transitions. $\tau_0$ is the reciprocal of the rate constant for fluorescence, $k_f$ :

$$\tau_0 = \frac{1}{k_f}$$

Similarly for excited singlet state lifetime:

$$\tau = \frac{1}{k_f + k_{ics} + k_{ic}} = \frac{1}{k_{total}}$$

Since $k_{total}$ is greater than $k_f$, the observed excited singlet state lifetime is less than the excited singlet state radiative lifetime. $\tau$ only approaches $\tau_0$ as intersystem crossing and internal conversion from $S_1$ and become much slower processes than fluorescence.

### 6.1.4.3 Fluorescence quantum yield ($\phi_f$)

This is the fraction of excited molecules that fluoresce. It can be represented as

$$\phi_f = \frac{rate\ of\ fluorescence\ (J_f)}{rate\ of\ absorption\ (J_{abs})}$$

Under the steady illumination condition, a steady state will be reached, where the rate of formation of excited molecules is equal to the rate of deactivation by the intramolecular processes.

$$J_{abs} = J_{total}$$

Therefore,

$$\phi_f = \frac{J_f}{J_{total}}$$

$$\phi_f = \frac{k_f [S_1]}{k_{total} [S_1]}$$

$$\phi_f = \frac{k_f}{k_{total}}$$

Now,

$$\tau_0 = \frac{1}{k_f} \quad \text{and} \quad \tau = \frac{1}{k_{total}}$$

Thus,

$$\phi_f = \frac{\tau}{\tau_0}$$

An order of magnitude estimate of the radiative lifetime of $S_1$ is given by:

$$\tau_0 \approx \frac{10^{-4}}{\varepsilon_{max}}$$

Where $\tau_0$ has units of s and $\varepsilon_{max}$ has units of $mol^{-1}\ cm^{-1}$. Here $\pi \rightarrow \pi^*$ transition with $\varepsilon_{max}$ is the order of $10^3$-$10^5$ $mol^{-1}\ cm^{-1}$ gives $\tau_0$ of the order of ns-μs. For $n \rightarrow \pi^*$ transition $\varepsilon_{max}$ has the value of the order 10-100 $mol^{-1}\ cm^{-1}$ giving $\tau_0$ of the order of μs-ms.

### 6.1.4.4 Lifetimes of the $T_1$ excited state

By analogy with the expressions for the lifetimes of $S_1$, the values for $T_1$ are given by

$$\tau_0 = \frac{1}{k_p}$$

$$\tau = \frac{1}{k_{total}} = \frac{1}{k_p + k_{ics}^{TS}}$$

The order of magnitude estimate of the radiative lifetime of $T_1$ is given by:

$$\tau_0 \approx \frac{10^{-4}}{\varepsilon_{max}}$$

Where $\tau_0$ has units of s and $\varepsilon_{max}$ has units of $mol^{-1}$ $cm^{-1}$. The process $S_0 + h\nu \rightarrow T_1$ is spin forbidden. So the molar absorption coefficient of such transition will be very small and so $T_1$ state will have a longer life time than $S_1$ state. In general, $\pi \rightarrow \pi^*$ transition have longer radiative lifetime (1-$10^2$ s) than $n \rightarrow \pi^*$ states ($10^{-4}$-$10^{-2}$ s). As excited triplet state decay more slowly than excited singlet states then it is much easier to determine the excited triplet state lifetime than excited singlet state lifetime.

### 6.1.5 Electron transfer

Electron transfer (ET) represents one of the most fundamental pathways in many physical and biological processes. In general, reactions which involve the transfer of an electron are called redox reactions. The particle that is actually transferred in redox reactions need not be just a single electron. Redox reactions play an important role in everyday life. Understanding and control of ET reactions comprise one of the broadest and most active research areas of physical chemistry today [16,17]. There are many such different systems as organic and inorganic, colloids, photoconducting polymers, metal-liquid electrode interfaces, mimicking of photosynthesis, semiconductor-liquid electrodes, liquid-liquid interfaces and proteins, where ET reactions come into play. The oldest and most important photoinduced electron transfer system in nature is photosynthesis. The photosynthetic machinery is located in the thylakoid membrane inside the chloroplasts [18]. The reaction centers Photosystem II (PS II) and Photosystem I (PS I), are large protein complexes positioned in the membrane. To increase the light harvesting efficiency the reaction centers are surrounded by many chlorophyll molecules, capable of absorbing the sunlight, that are arranged in large light harvesting complexes. In PS II the excitation energy harvested by the antenna complexes eventually leads to excitation of P680, which is the primary electron donor chlorophyll(s) in the reaction center. Electron transfer then occurs in a series of subsequent reactions, from the excited P680* to the electron acceptor pheophytin and further to two quinones, eventually leading to the formation of ATP, and further to the buildup of carbohydrates, proteins and fat. The chlorophyll that initially lost an electron in the excited state reaction, receives an electron from another donor, and can go through another excitation and electron transfer cycle. The electron from the donor comes from water molecules,

attached to a manganese cluster. After four completed cycles with removal of electrons from the water, oxygen is released as a bi-product. On the other end of the complicated electron transfer system, $CO_2$ is converted to build carbohydrates, proteins and fat.

Many other reactions exist in which electron transfer is followed by the formation or breaking of bonds or the trapping of a charge transfer state, followed by further chemical reactions. In organic chemistry, mechanisms involving bond breaking or bond making very often proceed by an ET mechanism.

In inorganic chemistry mixed valence systems are characterized by ET between linked metal sites. In the modern world, probably photography is the most powerful medium. Electron transfer forms the basis of conventional colour photography; the absorption of light by an organic dye placed on a small silver halide semiconductor crystal induces the transfer of an electron from the dye to the crystal. There, the electron reduces a $Ag^+$ ion to $Ag^0$ and a few of these silver atoms can catalyze the reduction of the whole crystal in the development process [19,20]. Again, based on the same principle, organic solar cells are developed employing $TiO_2$ as the semiconductor. $TiO_2$ is reversibly reduced in this process and acts as an electrode as it passes the electron to an electronic circuit. These so-called Grätzel cells are very promising because they can be produced much more cheaply than conventional Si based solar cells [21]. Electrode reactions such as those encountered in a battery or in aluminium production always involve a pure ET step. An advanced device as the scanning tunneling microscope (STM) is fully based on the possibility to transfer an electron between the scanning tip and the substrate under study. The STM is capable of visualizing details in the electron density of atoms and molecules [22,23]. Molecular electronics [24,25] is a newly developed field in which ET plays a crucial role. Electrically conducting wires, memories, electronic switches, rectifiers, light sensitive detectors, electroluminescent devices, photoconductors, Grätzel cell may be thought of as molecular electronic devices. Molecular electronic devices may potentially replace the current semiconductor based technology, whose progress is expected to reach saturation due to size limitation in a device.

The future ability to design nanostructures actually affects all aspects of our technological modern life. It has implications on the storage and processing of information, on communication technology and material science, but also on developing new nano machines for biological and medical benefit. For example, molecular devices can interact directly with the molecular components of the cell, and thus serve as probes in studying fundamental processes within the cell. A biological probe that has been already demonstrated is a nanosensor that can detect in real time biological and chemical species. Using this sensor, detection of ligand-receptor binding was demonstrated and picomolar protein concentration could be monitored [26].

### 6.1.5.1 History of electron transfer

The first electron transfer reactions that were studied were self-exchange electron transfer reactions of inorganic ions in aqueous solution. The modern experimental basis for ET reactions in solutions began 1920 with studies of ionic oxidation reduction reactions. In the late 1940's, early 1950's with the reports of new absorption band in solutions of aromatic hydrocarbons and iodine of Benesi and Hildebrand (1949) and the idea of partial charge transfer in the ground state of Brackman, the understandings of organic charge transfer complexes were started. In 1949 Franck and Libby [27] showed that ET transfer rates in solution are determined by horizontal Franck-Condon factors, in analogy to radiative processes where the transition probabilities are determined by vertical Franck-Condon factors. The Mulliken model (1952) for electron donor acceptor complexes, and the discovery of excimer formation by Forster and Kaspar in 1954 were essential steps that have led to the extensive developments in the field of electron donor-acceptor systems in the last decades.

During 1956-1960 R. A. Marcus made use of potential energy surfaces and statistical mechanics to provide a detailed classical description of the ET process [28-32]. He reduced the many-dimensional potential energy surfaces for reactants and products to harmonic free energy curves which were functions of a single reaction coordinate. The so-called Marcus Inverterted Regime was thus predicted and later experimentally proved. In 1969, Verhoeven and coworkers were reported donor and acceptor that are covalently linked. Studies on photoinduced

intramolecular electron transfer in covalently linked donor-bridge-acceptor compounds that incorporate a hydrocarbon bridge of e.g. the steroid, cyclohexyl, or norbornlogous type, to link two chromophoroes, have been numerous during the past decades. The so-called Marcus inverted regime predicted by R. A. Marcus in 1960 were first confirmed by this type of donor bridge acceptor system.

In 1970s photochemists were appointed with flash spectroscopic studies. Along with that conductometric, magnetic techniques and other sophisticate techniques added a new dimension to the electron transfer research. The application of time-resolved laser flash spectroscopy permitted the direct observation of radical ion intermediates in reactions where theory predicted an ET pathway [33]. Chemically induced dynamic nuclear polarization (CIDNP) was found to be invaluable in probing kinetics of ET [34]. Photosensitized reactions proceeding by ET were also investigated and quickly found to have important synthetic applications.

In particular, organic chemists discovered that photosensitized ET could generate radical cations of electron-rich olefins and strained cyclic molecules, which could undergo a wide variety of interesting transformation.

Considerable progress was also made in the photochemistry of transition-metal complexes during 1970's. Much of this effort was concerned with the bimolecular quenching of the excited states of transition-metal complexes by energy and electron transfer. These examples stimulated the development of theoretical descriptions of ET quenching which were rooted in the ideas of Taube [35], Libby [36], Marcus [31] and Hush [37].These concepts were extended to the ET quenching of photoexcited metal complexes by Sutin [38] and Balzani [39], who demonstrated the enormous scope and applicability of these reactions to solar energy conversion and the photoinduced decomposition of water.

Electron transfer research activity nowadays continues a wide variety of fronts, including the employment of new experimental schemes to test the predictions of classical and nonclassical theories of ET [38], the scope of photosensitized catalysis [40], the solution dynamics of

exciplexes of radical ions [41,42] , photoinduced ET in biological system [43-45] , the search for novel reactions of organic molecules photosensitized by electron transfer [46] and the role of ET in solar energy conversion. Till photoinduced electron transfer remains a subject of intellectual challenge.

## 6.1.5.2 Forward electron transfer and related reactions

Photoinduced electron transfer plays a central role in a broad array of process in the physical, chemical and biological sciences [47-49]. Photoinduced electron transfer can be described as the movement of an electron caused by the result of the absorption of light, from an electron rich species (an electron donor D) to an electron deficient species (an acceptor A). Either the donor or the acceptor or a ground state complex between the donor and the acceptor (often termed as a charge transfer complex) may be the light absorbing species.

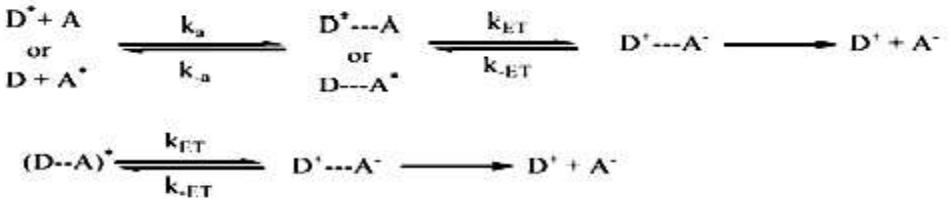


When D and A are freely diffusing in a solvent the electron transfer process, after photoexcitation, is bimolecular, i.e., the two reactants have to diffuse together to form an outer sphere precursor complex ($D^*$---A or D---$A^*$), where ka usually is diffusion controlled. The precursor complex undergoes reorganization towards a transition state in which the electron transfer takes place at a certain distance and arrangement, resulting in the successor complex $D^+$-----$A^-$ .The precursor complex can either be in close contact, or in a solvent-separated configuration, and electron transfer may occur at a distribution of different donor-acceptor configurations. The successor complex finally dissociates to form the product ions,the $D^+$ and $A^-$, as shown below [28, 50].

However, when D and A are linked to each other, no diffusion processes are needed prior to electron transfer and an intra-molecular electron transfer, obeying uni-molecular reaction kinetics, occurs that is more rapid.

$$(D - A)^* \underset{K_{-ET}}{\overset{K_{ET}}{\rightleftharpoons}} D^+ - A^-$$

Enhancement of redox activity is the main cause for transfer of an electron from an electron donor to an electron acceptor molecule [51]. The probability of electron transfer increases with increasing electronic interaction between the redox centers and with the nuclear reorganization of the reactants so that the transfer occurs with minimal change in nuclear configuration and momentum.

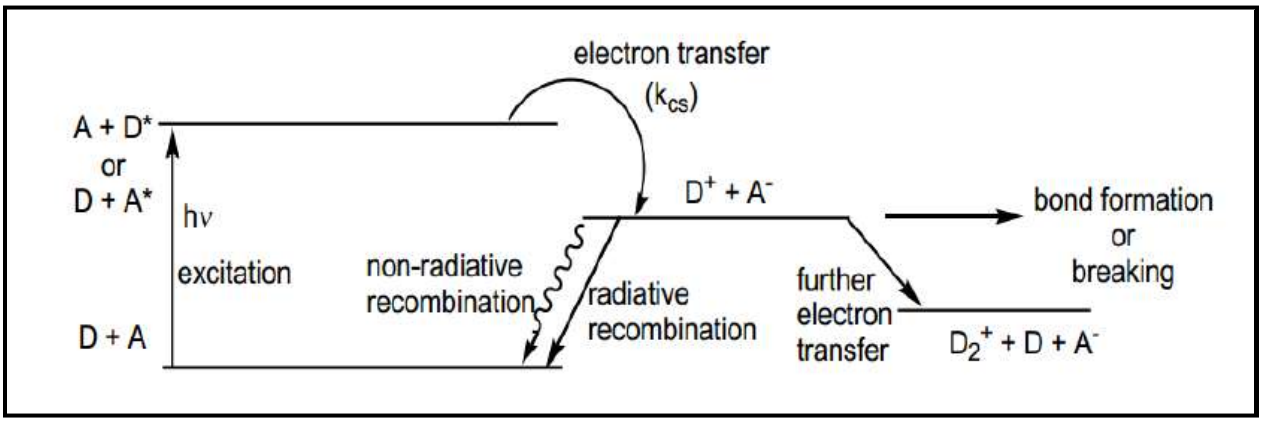


**Fig. 1.11.**Fate of a charge separated state.

In many other reactions, electron transfer is followed by the formation or breaking of bonds or the trapping of a charge transfer state, followed by further chemical reactions.(Fig.1.11.) shows the representation of the several possibilities that a charge separated state can undergo. Another process that can follow charge separation (or forward electron transfer) is simple charge recombination (or back electron transfer) leading to the initial state. This is in fact a very common process, which is often the fate of a charge transfer state.

Generally this charge recombination can occur by a dark (non-radiative) process, but there exist many systems in which the charge transfer state undergoes a radiative charge recombination. The energy of the emission of this process (often called charge transfer fluorescence or, more accurately, charge recombination fluorescence) is very dependent on the environment of the dipolar charge transfer state. A polar environment stabilizes this state and thus lowers its energy and thereby shifts the emission to the red. These types of systems can be used as a polarity (and mobility) probe.

## 7. Graphene oxide (GO) and Reduced Graphene oxide (RGO)

Graphene is allotropes of carbon. This name was introduced by Boehm, Setton, and Stumpp in 1994 [52]. Graphene oxide (GO) and reduced graphene oxide (RGO) is an oxidized and redox compound of graphene respectively. Graphene is a single layer (monolayer) of carbon atoms which is tightly bound in a hexagonal honeycomb lattice. It is in the form of a $sp^2$ bonded carbon atoms in a plane with molecular bond length 0.142 nm. Layers of graphene stacked on top of each other form graphite, with an interplanar spacing of 0.335 nm. The separate layers of graphene in graphite are held together by van der Waals forces, which can be overcome during exfoliation of graphene from graphite. Graphite exhibits a remarkable anisotropic behavior with respect to thermal and electrical conductivity. It is highly conductive in the direction parallel to the graphene layers because of the in-plane metallic character, whereas it exhibits poor conductivity in the direction perpendicular to the layers because of the weak van der Waals interactions between them [53]. The carbon atoms in the graphene layer form three $\sigma$ bonds with neighboring carbon atoms by overlapping of $sp^2$ orbitals while the remaining $p_z$ orbitals overlap to form a band of filled $\pi$ orbitals. The valence band and a band of empty $\pi^*$ orbitals forms the conduction band, which are responsible for the in-plane conductivity.

Here incertion of guest molecules in the graphene layer modifies the spacing, this results the structural modification of the graphene planes because the hybridization of the reacting carbon

atoms changes from $sp^2$ to $sp^3$. A simple example is the introduction of strong acid and oxidizing reagents that creates oxygen functional groups on the surfaces and at the edges of the graphene layers giving rise to graphite oxide. In 1958 Hummers and Offeman [54] reported the oxidation of graphite and the production of graphite oxide on immersing natural graphite in a mixture of $H_2SO_4$, $NaNO_3$, and $KMnO_4$ as a result of the reaction of the anions intercalated between the graphitic layers with carbon atoms, which breaks the aromatic character. The strong oxidative action of these species leads to the formation of anionic groups on graphitic layers, mostly hydroxylates, carboxylates, and epoxy groups. The out of planar C–O covalent bonds increase the distance between the graphene layers from 0.35nm in graphite to about 0.68nm in graphite oxide [55]. This increased spacing and the anionic or polar character of the oxygen groups formed impart to graphene oxide (GO) a strongly hydrophilic behavior, which allows water molecules to penetrate between the graphene layers and thereby increase the interlayer distance even further. Thus graphite oxide becomes highly dispersible in water. The formation of $sp^3$ carbon atoms during oxidation disrupts the delocalized $\pi$ system and consequently electrical conductivity in graphite oxide deteriorates reaching between $10^3$ and $10^7$ Ω-cm depending on the amount of oxygen [53].

## 7.1 Graphene Oxide

Graphene oxide (GO) can be considered as a monolayer of graphite oxide. The main difference between graphite oxide and GO is the interplanar spacing between the individual atomic layers of the compounds, which is caused by water intercalation. This increased spacing, caused by the oxidization process, $sp^2$ also disrupts the bonding network, meaning that both graphite oxide and GO are often described as electrical insulators. GO is a poor conductor but its treatment with light, heat, or chemical reduction can restore most properties of the famed pristine graphene. After fabrication of graphite oxide, GO can be obtained by exfoliating graphite oxide into monolayer sheets through a variety of thermal and mechanical methods [52]. Among these methods thermal exfoliation becomes a popular method of GO exfoliation. During heating, the oxygen-containing functional groups attached on carbon plane decompose into gases such as $H_2O$, $CO_2$ and CO, which will diffuse along the lateral direction. This exfoliation occurs only if

the decomposition rate of functional groups surpasses the diffusion rate of evolved gases. Here the interlayer pressure existing among adjacent layers is large enough to overcome their van der Waals interactions and pushes the layers separated from each other. Generally, a minimum temperature of 550 °C is necessary for the successful exfoliation at atmospheric pressure [56]. Similarly, the mechanical method of exfoliation can be done by sonicating graphite oxide in water or polar organic media. Especially, sonicating and mechanical stirring can be combined together to exfoliate graphite oxide with a better efficiency than using any individual method. But the sonication has a great disadvantage that it causes substantial damage of GO platelets. It can reduce them in surface size from microns to nanometers.

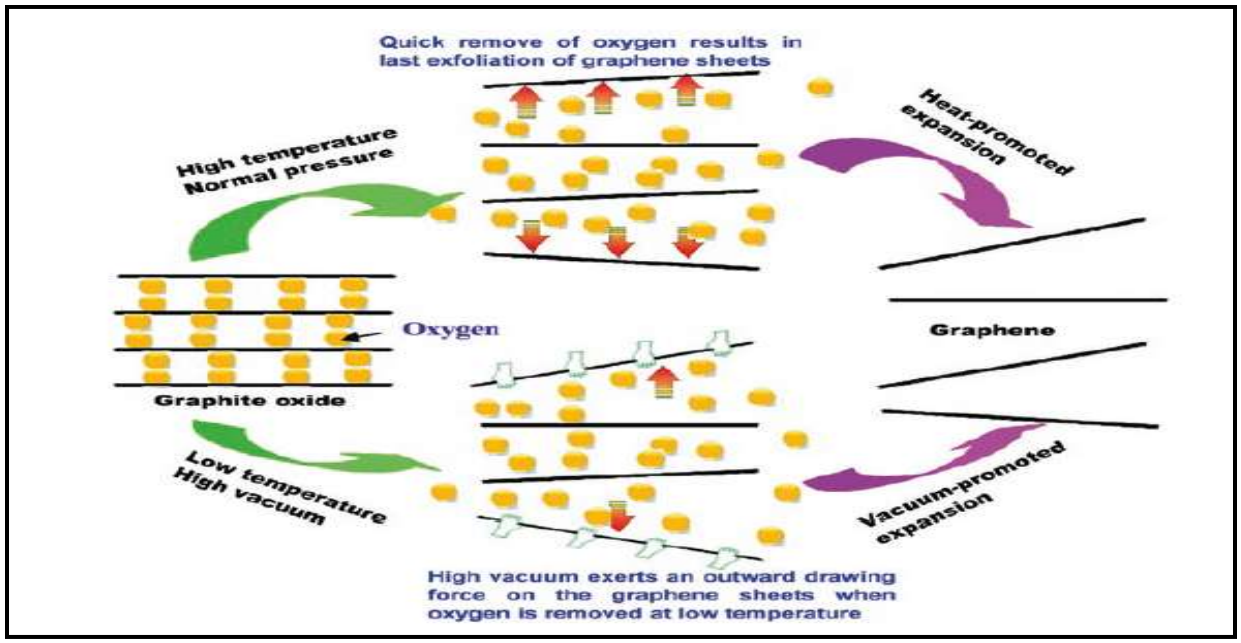


**Fig. 1.12.** Thermal exfoliation of graphite oxide [58]

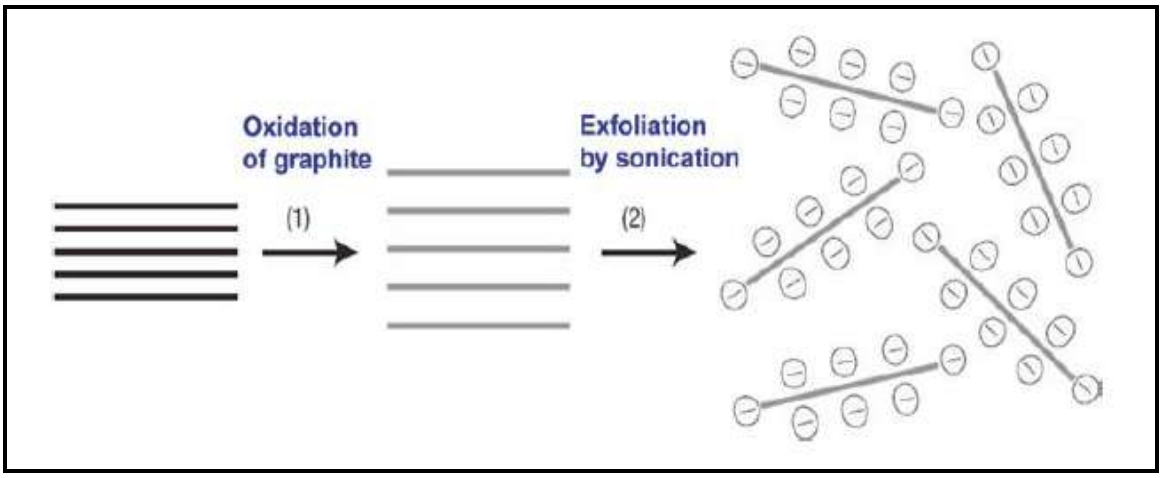


**Fig. 1.13.** Exfoliation of graphite oxide in water by sonication [59]

## 7.2 Reduced Graphene Oxide (RGO)

Reducing GO to produce RGO is an extremely vital process because it has a large impact on the quality of the RGO produced; therefore, it will determine how close RGO will come in terms of structure to pristine graphene [57]. There are a number of ways reduction can be achieved, although they are all methods based on chemical, thermal, or electrochemical means. Some of these techniques are able to produce very high-quality RGO, similar to pristine graphene, but they can be complex or time-consuming to perform. RGO produced by chemical reduction has relatively poor yields in terms of surface area and conductivity. Thermally reducing GO at temperatures of 1000 $^0$C or more creates RGO that has been shown to have a very high surface area, close to that of pristine graphene. This thermal process damages the graphene platelet as pressure builds up, produces $CO_2$ and reduces mechanical strength by creating imperfections, vacancies etc. in it's structure. Electrochemical reduction of GO produce high quality RGO, similar to the pristine graphene. Primary benefit of this process is that there are no hazardous chemical is used, so no toxic waste comes out.

## 7.3 Advantages and disadvantages of GO and RGO

The advantages of GO is its easy dispersability in water and other organic solvents because of the presence of oxygen functionalities. This solubility of GO remains a very important property when it is mixed with other material to improve their conductivity. Though GO is often described as an electrical insulator because of the disruption of its $sp^2$ bonding networks. To recover the honeycomb hexagonal lattice, and the electrical conductivity, the reduction of GO has to be achieved. Functionalization of GO can fundamentally change the properties of GO. The resulting chemically modified graphenes could then potentially become much more adaptable for many applications. For optoelectronics, biodevices, or as a drug-delivery material, it is possible to substitute amines for the organic covalent functionalization of graphene to increase the dispersability of chemically modified graphenes in organic solvents. It has also been proven that porphyrin-functionalized primary amines and fullerene-functionalized secondary amines could be attached to GO platelets, ultimately increasing nonlinear optical performance. Although the chemical reduction of GO is currently seen as the most suitable method of mass production of graphene, it has been difficult for scientists to complete the task of producing graphene sheets of the same quality as mechanical exfoliation but on a much larger scale.

## 8. Aim of thesis

The synthesis and characterization of the novel organic dyad NNDMBF would be made. The primary aim would be to fabricate some new hybrid nanocomposites by combining the organic dyad with graphenes. The investigations are being carried out by using steady state and time-resolved spectroscopic techniques on the novel synthesized short chain dyad and its hybrid nanocomposite systems. Some quantum chemical calculations are being carried out by using Gaussian 03 software to support the experimental findings by theoretical point of view. Both from the theoretical predictions and NMR studies it reveals that in the ground state only

extended (E-type) conformation of the pristine dyad exist, whereas on photoexcitation these elongated conformers are converted into folded forms (Z-type). Time resolved fluorescence spectroscopic (fluorescence lifetime by TCSPC method) measurement demonstrates that in acetonitrile medium and in presence of GO and RGO nanoparticles the organic- inorganic hybrid nanocomposite possesses larger amount of extended conformers relative to folded one, even in the excited singlet state. This indicates the possibility of slower energy destructive charge recombination rates relative to the rate possesses associated with charge-separation within the dyad. In the present investigation the steady state and time resolved spectroscopic investigations would be made on the same dyad when combined with graphenes to examine the suitability of the nanocomposite to construct efficient charge-storage device so that it can act as cost-effective supercapacitor system.

## 9. Literature Review

The suitability of a novel synthesized short-chain dyad as a light energy converter has a wide application in optical data storage, light emitting diode (LEDs), optical solar cell, photovoltaic cell etc. The primary aim of this thesis is to develop several nanocomposite devices where the novel synthesized dyad being combined with noble nanomaterial graphene oxide (GO) and reduced graphene oxide (RGO), which behalves as a artificial light energy converters which should highly efficient, biocompatible and bio-safe and of low cost. Here the novel organic dyad is NNDMBF where the donor part is 4 (N, Ndimethylamine) benzaldehyde with acceptor fluorine (F).

Ganguly et al.[60] observed different photo physical properties of gold (Au)-dyad MNTMA (where the electron donor methoxy naphthalene (MNT) is connected with the acceptor p-methoxyacetophenone (MA) by a short spacer) system by using UV-vis and time resolved spectroscopic tecnique and the observed results are compared with pristine dyad. Significant differences have been observed between the photophysics of the pristine dyad and Au-dyad composite.

Ganguly et al.[61] measured different photo physical properties of Silver (Ag)-dyad MNTMA (where the electron donor methoxy naphthalene (MNT) is connected with the acceptor p-methoxyacetophenone (MA) by a short spacer) system by using UV-vis, steady state and time resolved spectroscopic techniques and the observed results are compared with the Gold (Au)-dyad MNTMA hybrid nanomaterials. Significant differences have been observed between the photophysical properties of two nanocomposite. Here considerable enhancement of the plasmonic absorption band observed in case of Ag-dyad system, which is absent in case of other Au-dyad nanocomposite system. From the fluorescence lifetime measurement we get folded conformation which facilitates charge recombination, was observed even in excited state in case of Ag-dyad nanocomposite system unlike the situation observed for Au-dyad hybrid nanocomposite system where elongated conformation were found to prevail significantly on photoexcitation. From transient absorption measurement by laser flash photolysis method, observed faster energy destructive charge recombination rate in case of Ag-dyad nanocomposite system relative to the Au-dyad hybrid nanocomposite system.

Ganguly et al.[62] observed by using UV–vis absorption, steady state and time resolved fluorescence and absorption spectroscopic investigations demonstrated that the short chain dyad MNTMA when combined with gold-silver core-shell (Au@Ag) nanocomposite , forms elongated conformers in the excited state whereas for the dyad – Ag (spherical) system the majority of dyads remains in a folded conformation. In the dyad-core-shell nanocomposite system, energy wasting charge recombination rate slows down primarily due to elongated conformation and thus it may be anticipated that this hybrid nanocomposite system may serve as a better light energy conversion device.

Ganguly et al. [63] demonstrated that the investigation were made by the electrochemical, steady state and time resolved spectroscopic (time correlated single photon counting and laser flash photolysis) technique on a novel synthesized dyad, 1-(4-cloro-phenyle)-3-(4-methoxy-napthalen-1-yl)-propenone (MNCA) where the donor 1-methoxy-napthalene (MNT) is connected with the acceptor p-cloroacetophenone (PCA) by an unsaturated olefinic bond. This dyad

possesses mainly extended (E-type) conformation both in the ground and excited state. Here E-type isomeric structure dominates in the ground state, considerable amount of Z-type (folded) species are produced in the excited state. It is hinted that the proximity effect of mithoxi functionality in donor moiety, may be the reason for the formation of mostly E-isomeric species in the MNCA dyad system. From the observed unchanged values of charge recombination and ion-pair lifetime estimated from the analysis of transient absorption spectra of the dyad in presence of βCD (β-cyclodextrin) and without it, confirms the proposition about the maintenance of the extended conformation even upon photoexcitation. From the transient absorption measurement it appears that due to increase of delay time between the exciting and probe pulses, higher triplet $T_n$ of the donor being generated gets involved in PET reaction with the surrounding medium CAN. So from the present findings, MNCA in aqueous medium seems to be good candidate to build a light energy conversion device.

Ganguly et al.[64] explained from the UV-vis, steady state and time resolved spectroscopic investigations on the pristine dyad, dyad-spherical gold nanoparticles (GNP) and dyad-star shaped gold nanoparticles (GNS), it was observed that though in the ground state the dyad in its pristine form possesses trans-type (elongated and planar) isomer but on photoexcitation trans-form converts into cis-structure (folded). Interestingly, the dyad exhibits different behavior when it combines with GNP or GNS. In nanocomposite form, even on photoexcitation some ground state trans-structure still retains its identity in the excited state. The 60% of the trans-species remains unchanged in the excited state due to excitation of dyad-GNS system and possibly this configuration facilitates the hindrance of energy destructive charge recombination processes as in this conformer the donor and acceptor moieties tend to move far away from each other causing lack of overlapping of charge clouds within the two redox components. The dyad-GNS nanocomposite appears to be the best possible light energy conversion or storage device within the three system studied in the present investigation.

Ganguly et al.[65] studied with the help of electrochemical, steady state and time resolved fluorescence (fluorescence lifetimes by using time correlated single photon counting technique) and nanosecond laser flash photolysis methods, the nature of charge separation along with the

energy wasting charge recombination processes within a short-chained organic dyad 1-(4-bromo-phenyl)-3-(2-methoxynapthalen-1-yl)-propenone (MNBA) has been revealed. In MNBA, the donor 2-methoxynapthalen (2MNT) is connected with the acceptor p-bromoacetophenone (PBA) by an unsaturated olefinic bond. Though in the ground state elongated type structure (E-form) is observable from NMR spectra but on photoexcitation, another conformers possibly of the nature of folded type isomeric species (Z-form) were also apparent from time resolved fluorescence measurements. However preponderance of elongated form in the excited singlet state has been established from this time resolved measurement. The energy wasting charge recombination rate is determined from the transient absorption measurement by nano second laser flash photolysis technique, was found to be significantly lower than the charge separation rate, which is measured from time resolved fluorescence. This observation demonstrates that MNBA may serve as an efficient candidate to construct artificial light energy conversion device or components of molecular photovoltaic cells.

J.H. Kim et al.[66] demonstrated that the photosensitive conjugated polymer with electron donor-acceptor dyad which contains a terthiophene unit, can modulate charge accumulation by photoirradiation resulting in a threshold voltage shift in the polymer field-effect transistors (PFETs) while this effect of the photoinactive polymer containing a thienothiophene unit is negligible. These results suggest that the feasible molecular design strategies can provide an effective platform to achieve controllable threshold voltage modulation in PFETs.

E. Rivera eet al.[67] were synthesized and characterized a series of pyrene-fullerene $C_{60}$ dyad bearing pyrene units ($PyFC_{12}$, PyFPy, $Py_2FC_{12}$ and PyFN) and studied their optical properties by absorption and fluorescence spectroscopy. Dyads were designed in this way because the pyrene moieties act as light-harvesting molecules and are able to produce "monomer" ($PyFC_{12}$) or excimer emission (PyFPy, $Py_2FC_{12}$ and PyFN). The fluorescence spectra of the dyads exhibited a significant decrease in the amount of pyrene monomer and excimer emission, without the appearance of a new emission band due to fullerene $C_{60}$. The pyrene fluorescence quenching was found to be almost quantitative, ranging between 96%–99% depending on the construct, which is

an indication that energy transfer occurred from one of the excited pyrene species to the fullerene $C_{60}$.

Ganguly et al.[68] studied the photophysical properties and the nature of the photoinduced electron transfer (PET) reactions within a synthesized anisole (A)-thioindoxyl (T) dyad system (24MBTO) by using electrochemical, steady state, and time-resolved spectroscopic techniques. Computations on the dyad were performed both in gas phase as well as solvent environment by TD-DFT method with B3LYP density function. The electrochemical measurements indicate the possibility of occurrence of PET reactions within 24MBTO between the linked redox centers A and T. Both steady-state and time-resolved spectroscopic measurements on the novel synthesized 24MBTO dyad demonstrate the formations of the two types of isomeric species: Z- and E-forms, resulted from the charge separation reactions. From the detailed studies it reveals that the present thioaurone may behave as a versatile photoswitchable system.

Ganguly et al.[69] investigated the Photoswitchable characteristics of a novel dyad, 1-(4-chloro-phenyl)-3-(1-methoxy-3,4-dihydro-naphthalen-2-yl) propenone (MNCADH) in both experimentally and theoretically. In the ground state MNCADH is found exclusively as 'trans' isomer. From experimental findings, obtained by steady state and time resolved spectroscopic techniques, it is apparent that both 'cis' and 'trans' isomers are present in the excited state. 'Trans' isomer prefers to populate in polar medium, whereas 'cis' isomer mainly populates in nonpolar medium. Potential energy surface calculations at density functional theory unveil that the interconversion energy barrier is quite high in ground state as compared to that of excited state, so that switching form one conformer to another only becomes possible in excited state.

Ganguly et al.[70] described the method of synthesis and characterization of a novel organic dyad, 3-(1-Methoxy-3,4-dihydro-naphthalyn-2-yl-)-1-p-chlorophenyl propenone. Here they fabricate new hybrid nanocomposites by combining the organic dyad with different noble metals, semiconductor nanoparticle and noble metal semiconductor core/shell nanocomposites. In this organic dyad, donor part is 1-Methoxy-3, 4-dihydro-naphthalen- 2-carboxaldehyde with the acceptor p-chloroacetophenone. They have carried out steady state and time-resolved

spectroscopic measurements on the dyad and its hybrid nanocomposite systems. Both from the theoretical predictions and NMR studies it reveals that in the ground state only extended (E-type or trans-type) conformation of the dyad exists whereas on photoexcitation these elongated conformers are converted into folded forms (Z- or cis-type) of the dyad, showing its photoswitchable character. Time resolved fluorescence spectroscopic (fluorescence lifetime by TCSPC method) measurements demonstrate that in chloroform medium all the organic–inorganic hybrid nanocomposites possess larger amount of extended conformers relative to folded ones, even in the excited singlet state. This indicates the possibility of slower energy destructive charge recombination rates relative to the rate processes associate with charge-separation within the dyad. This indicates the suitability to construct efficient light energy conversion devices especially with the Ag-dyad nanocomposites.

Ganguly et al.[71] were made steady state and time resolved spectroscopic measurements at the ambient temperature on an organic dyad, 1-(4-Chloro-phenyl)-3-(4-methoxy-naphthalen-1-yl)-propenone (MNCA), where the donor 1-methoxynaphthalene (1 MNT) is connected with the acceptor p-chloroacetophenone (PCA) by an unsaturated olefinic bond, in presence of Ag@TiO2 nanoparticles. Time resolved fluorescence and absorption measurements reveal that the rate parameters associated with charge separation within the dyad increases whereas charge recombination rate reduces significantly when the surrounding medium is changed from only chloroform to mixture of chloroform and Ag@TiO2 (noble metal-semiconductor) nanocomposites. The observed results indicate that the dyad being combined with core–shell nanocomposites may form organic– inorganic nanocomposite system useful for developing light energy conversion devices.

Ganguly et al.[72] reveals from steady state and fluorescence lifetime measurements that due to photoexcitation of benzotriazole (BZ) part of the bichromophore, 9(1-H-benzotriazole-lylmethyl)-9H-carbazole (BHC), singlet–singlet energy transfer takes place to populate the lowest excited singlet of carbazole (CZ). CZ, thus being excited indirectly via energy transfer process, undergoes strong charge transfer (CT) reaction with the surrounding polar medium acetonitrile (ACN). On the other hand, very weak CT band was apparent when CZ part, within

BHC, was directly excited. In less polar tetrahydrofuran (THF) and polar benzonitrile (BN) environment, lack of formation of CT band strongly suggests in favor of the electron-accepting behavior of ACN. Moreover, by measuring the emission spectra of BHC in micro crystals and of 30 bilayers mixed LB film at high mole fraction of BHC molecules, the possibility of excimer formation or aggregation has been ruled out. Thus, BHC, when dissolved in ACN, acts as a triad system of BZ–CZ–ACN where BZ acts as an antenna molecule and CZ as a reaction center. The possible role of the bichromophoric system BHC as an artificial photosynthetic or solar energy conversion device has been hinted.

O. Ito et al.[73] investigated intramolecular photoinduced charge-separation and charge-recombination processes in two $C_{60}$-spacer-TTF dyads, in which $C_{60}$ and TTF (tetrathiafulvalene) are connected through a flexible spacer of different lengths, have been investigated in polar solvents by time-resolved absorption and fluorescence techniques. Weak interaction between the $C_{60}$-moiety and TTF-moiety in the ground state was suggested by the steady-state absorption spectra; the dyad with the shorter spacer shows slightly stronger interaction than that with the longer spacer. The observed short fluorescence lifetimes of these dyads, compared with that of their precursor fullerene derivative in THF and benzonitrile indicate that the charge separation takes place via the singlet excited state of the $C_{60}$-moiety, producing the ion pairs ($C_{60}^{-}$-spacer-$TTF^{+}$) as shown from the transient absorption spectra in the 800–1100 nm region. In polar benzonitrile solvent, the ion-pair state with the long flexible chain shows longer lifetime than that with the short chain, suggesting that weaker interaction between $C_{60}$ and TTF moieties is preferred to the long ion-pair lifetime.

Ganguly et al.[74] observed the photophysical properties of the synthesized short-chain organic dyad, 1-(4-chlorophenyl)-3-(4-methoxy-naphthalen-1-yl)-propenone (MNCA) in isotropic media and gel (P123) environment by using steady state, time-resolved spectroscopic techniques and fluorescence anisotropy decay. From the NMR and time-resolved spectroscopic studies E-isomeric form (elongated nature) of the charge-transfer species of the dyad MNCA appears to be the only isomeric form in the ground state and this conformation retains even after

photoexcitation whatever be the nature of the environment, the isotropic solution or micro-heterogeneous medium (gel phase of P123).

Ganguly et. al.[75] described the methods of synthesis and characterization of the bichromophores (4MBA and 4MBAS) comprising 4-methoxybenzo[b]thiophene (4MBT) as donor and p-chloroacetophenone (PCA) as acceptor linked together by an olefinic (unsaturated in the former bichromophore and saturated in the case of the latter one) bridge. Here they compared the monomolecular photophysical properties of the bichromophores with the photophysics of the bimolecular systems. Both from the steady-state electronic absorption and fluorescence emission spectra it shows that the bichromophores exhibit charge transfer (CT) complex both in the ground and excited states. In intermolecular interactions it appears that a weak excited singlet ($S_1$) CT complex of contact nature is formed, whereas in intramolecular systems (bichromophores 4MBA and 4MBAS) relatively stronger excited CT complexes of two types: cis (folded) and trans (extended) isomers for 4MBA and two conformers for 4MBAS are formed and transient absorption measurements clearly demonstrate the occurrences of photoinduced intermolecular ET reactions. Transient absorption spectral measurements by laser flash photolysis technique reveal that energy wasting charge recombination process within the bichromophore is largely precluded on changing the nature of the spacer from unsaturated to more flexible saturated one. So, it is necessary to incorporate two spacers (cyclophane type) instead of one to enhance the charge separation rate and to minimize the energy wasting recombination process.

Ganguly et al.[76] measured different photophysical properties of silver (Ag)-dyad MNTMA system by using UV-vis, steady state and time resolved spectroscopic technique and the observed result is compared with the gold (Au)-MNTMA hybrid nanomaterials. Considerable enhancement of the plasmonic absorption band observed in the case of Ag-dyad system, which is absent in case of the other Au-dyad nanocomposite system. From the measured fluorescence lifetime values, preponderance of folded conformation which facilitates charge recombination was observed even in the excited state in the case of Ag-dyad hybrid nanocomposite system unlike the situation observed for Au-dyad hybrid nanocomposite where elongated conformations

were found to prevail significantly on photoexcitation. Transient absorption measurements by laser flash photolysis method state that energy destruction rate is much faster in case of Ag-dyad system relative to the Au-dyad nanocomposite device.

S.Fukuzumi et al.[77] examined photoinduced charge separation (CS) and charge recombination (CR) processes in various porphyrin-fullerene linked systems (i.e., dyads and triads) by means of time-resolved transient absorption spectroscopy and fluorescence lifetime measurements. Here lowest lying chargeseparated state of all the investigated systems, namely, that of ferrocenium ion ($Fc^{+}$) and the $C_{60}$ radical anion ($C_{60}^{*-}$) pair in the Fc-ZnP-$C_{60}$ triad, has been generated with the highest quantum yields. Determination of CS and CR rate constants, together with the one-electron redox potentials of the donor and acceptor moieties in different solvents, has allowed us to examine the driving force dependence of the electron-transfer rate constants. Interestingly, the Marcus plot has provided clear evidence for intramolecular CR located in both the normal and inverted regions of the Marcus parabola.

T. Torres et al.[78] investigated the photophysical properties of new dyad molecule, which is composed of a covalently linked Zn-phthalocyanine (donor) and a $C_{60}$ derivative (acceptor). They presented an experimental evidence of long lived charge separation in solid state with a life time several order higher than in solution. It is the basis of possible photovoltaic application.

S. Fukuzumi et al. [79] observed that the photoindused process in zinc porphyrin-$C_{60}$ dyad (ZnP-$C_{60}$) in different organic solvents by fluorescence lifetime measurements and picosecond and nanosecond time-resolved transient absorption spectroscopies. The charge-separated state ($ZnP^{*+}$-$C_{60}^{*-}$) is formed via photoinduced electron transfer from the excited singlet state of the porphyrin to the $C_{60}$ moiety. In nonpolar solvents such as benzene ($\varepsilon$= 2.28), the charge-separated state undergoes charge recombination to yield the $C_{60}$ singlet excited state, followed by intersystem crossing to the $C_{60}$ triplet excited state. More polar solvents such as anisole ($\varepsilon$= 4.33) render the energy level of the charge-separated state lower than the $C_{60}$ singlet excited state, resulting in the direct formation of the $C_{60}$ triplet excited state (1.50 eV) from the charge-separated state. In polar solvents such as benzonitrile ($\varepsilon$=25.2), where the energy level of the

charge-separated state (1.38 eV) is low compared with the $C_{60}$ triplet excited state, the charge-separated state, produced upon excitation of the both chromophores, decays directly to the ground state. Such solvent dependence of charge recombination processes in ZnP-$C_{60}$ can be rationalized by small reorganization energies of porphyrins and fullerenes in electron-transfer processes.

K. Maruyama et al. [80] investigated photoindused intramolecular charge separation (CS) and charge recombination (CR) of the product ion pair (IP) state of a series of fixed-distance dyads consisting of free-base porphyrin or zinc porphyrin and quinines by using femtosecond laser sopectroscopy, to determine energy gap and temperature dependences of CS and CR reactions in nonpolar media. Obtained CS rates were in the normal region and CR rates were in the inverted region. They have confirmed that the activation barrier for the CS reaction increases with a decrease of the energy gap, while the CR process is activationless, indicating the dominant effect of the high-frequency quantum mode in the inverted region. They also examined solvent polarity effect upon the energy gap dependence upon CS rate constant and CR rate constant. Here solvent reorganization energy increases with the solvent polarity, with the CS rate constant but CR rate constant shows little solvent polarity dependence.

# References


1. C. Ngo and J. B. Natowitz, "Our energy future – resources, alternative and the environment", Wiley, 1, 2009.
2. S. Paul, I. Mitra, R. Dutta, M. Bardhan, M. Bose, S. Das, M. Saha and T. Ganguly, "Comparative analysis to explore the suitability of a short chain dyad in its pristine and nanocomposite forms for designing artificial light energy conversion device", J Nanosci Nanotechnol, 18, 1, 2018.
3. A.F. Collings and C. Critchley, "Artificial Photosynthesis", chapter 1, Artificial Photosynthesis: Social and Political Issues by I. Lowe, Wiley-VCH, 2005.
4. E.A. Rohlfing, W.J. Stevens, M.E. Gress, "Project of Chemical Sciences, Geosciences and Bio-sciences", 2003.
5. N.S. Lewis and D.G. Nocera, "Powering the planet: Chemical challenges in solar energy utilization", Proc.Natl.Acad Sci. U.S.A, 103, 15729, 2006.
6. G.M. Whitesides, "The right size in nanobiotechnology", Nat. Biotechnol, 21, 1161, 2003
7. The national nanotechnology initiative strategic plan, nanoscale science, engineering, and technology subcommittee, national science and technology council, The White House December, 2007.
8. M. Hilgendorff and V. Sundström, "Dynamics of electron injection and recombination of dye-sensitized $TiO_2$ Particles", J. Phys. Chem. B, 102, 10505, 1998.
9. J. Pan, G. Benkö, Y. Xu, T. Pascher, L. Sun, V. Sundström, T. Polivka, "Photoinduced electron transfer between a carotenoid and $TiO_2$ Nanoparticle", J. Am. Chem. Soc, 124, 13949, 2002.
10. V. Balzani, P. Seroni, A. Juris, "Photochemistry and Photophysics: Concepts, Research, Applications", Wiley-VCH, 2014.
11. K.K.R. Mukherjee, "Fundamentals of photochemistry" New Age Publication, Third Edition
12. B. Wardle, "Principals and application of photochemistry", Wiley, 2009.
13. G.G. Guilbault, "Principle of luuminescence spectroscopy. Luminescence determination of clinically and agriculturally important samples", Pure & Appl. Chem., 57, 495, 1985.

14. M. Kasha, “Characterization of electronic transition in complex molecules”, Disc. Faraday Soc., 9, 14, 1950.
15. M. Klessinger and J. Michl, “Excited states and photochemistry of organic molecules”, VCH Publishers, 1995.
16. H.D. Routh, “Twentieth century developments in photochemistry. Brief historical sketches”, Pure Appl. Chem., 73, 395, 2001.
17. M.A. Hilu and U. Peskin, “Promotion of deep tunneling through molecular barriers by electronic-nuclear coupling”, J Chem. Phys., 122, 021103, 2005.
18. D.R. Ort, C.F. Yocum and I.F. Heichel, “Oxygenic photosynthesis: The light reactions”, Kluwer Academic Publishers, 4, 2004.
19. J. Belloni, M. Treguer, H. Remita and R.D. Keyzer, “Enhanced yield of photoinduced electrons in doped silver halide crystals”, Nature, 402, 865, 1999.
20. I.R. Gould, J.R. Lenhard, A.A. Muenter, S.A. Godleski and S. Farid, “Two electron sensitization: A new concept for silver halide photography”, J. Am. Chem. Soc., 122, 11934, 2000.
21. M.K. Nazeeruddin, A. Key, I. Rodicio, R.H. Baker, E. Muller, P. Liska, N. Vlachopoulos and M. Gratzel, “Conversion of light to electricity by cis $X_2$Bis (2,2-bipyridyl-4,4-dicarboxylate) ruthenium(II) charge transfer sensitizers (X=$Cl^-$, $Br^-$, $I^-$, $CN^-$ and $SCN^-$) on nanocrystallyne $TiO_2$ electrodes”, J Am. Chem. Soc., 115, 6382, 1993.
22. C. Rogero, J.I. Pascual, J. Go´mez-Herrero and A. M. Baro, “Resolution of site-specific bonding properties of $C_{60}$ adsorbed on Au(111)”, J. Chemical Physics, 116, 832, 2002
23. J. M. Zuo, M. Kim, M. O'Keeffe, J. C. H. Spence, “Direct observation of d-orbital holes and cu-cu bonding in $Cu_2O$”, Nature, 401, 49, 1999.
24. M. C. Petty, “Molecular Electronics: prospects for instrumentation and measurement science”, Meas. Sci. Technol., 7, 725, 1996.
25. I. B. Martini, E. R. Barthel, B. Schwartz, “Optical control of electrons during electron transfer”, Science, 293, 462, 2001.
26. Y. Cui, Q. Wei, H. Park, C. M. Lieber, “Nanowire nanosensors for highly sensitive and selective detection of biological and chemical species”, Science, 293, 1289, 2001.
27. W.F. Libby, “Theory of electron exchange reactions in aqueous solution”, J. Phy. Chem., 56, 863, 1952.

28. R. A. Marcus, “On the theory of oxidation reduction reactions involving electron transfer”, J. Chem. Phys., 24, 966, 1956.
29. R. A. Marcus, “Electrostatic free energy and other properties of states having non-equilibrium polarization”, J. Chem. Phys., 24, 979, 1956.
30. R. A. Marcus, “On the theory of oxidation reduction reactions involving electron transfer. II. applications to data on the rates of isotopic exchange reactions”, J. Chem. Phys., 26, 867, 1957.
31. R. A. Marcus, “On the theory of electron transfer reactions. VI. unified treatment for homogeneous and electrode reactions”, J. Chem. Phys., 43, 679, 1965.
32. R. A. Marcus, “Exchange reactions and electron transfer reactions including isotopic exchange: Theory of oxidation-reduction reactions involving electron transfer”, Discuss. Faraday Soc., 29, 21, 1960.
33. N. Mataga, M. Mitiga, T. Nishimura, “Picoseconds chemistry of some exciplex systems”, J. Mol. Struct., 47, 199, 1978.
34. L. T. Muus, P.W. Atkins, K. McLauchlan, J.B. Pedersen, “Chemically Induced Magnetic Polarization”, D. Reidel Publishing Company, 39, 1977.
35. H. Taube, “Electron transfer between metal complex – A retrospective view (Nobel Lecture)”, Angew. Chem. Int. Ed., 23, 329, 1984.
36. W.F. Libby, “Electron tunneling in chemistry and biology”, Ann. Rev, Phys. Chem., 28, 105, 1977.
37. N. S. Hush, “Homogenous and heterogeneous optical and thermal electron transfer”, Electrochimica. Acta., 13, 1005, 1968.
38. N. Sutin, “Electron exchange reaction”, Annu. Rev. Nucl. Sci., 12, 285, 1962.
39. V. Balzani, F.Bolletta, M.T.Gandolfi, M. Maestri, “Bimolecular electron transfer reaction of the excited states of the transition metal complexes”, Top. Curr. Chem., 75, 1, 1978.
40. M. Julliard, M. Chanon, “Photoelectron transfer catalysis: its connection with the thermal and electrochemical analogues”, Chem. Rev., 83, 425, 1983.
41. K. Chibisov, “Electron transfer in photochemical reactions”, Russ. Chem. Rev. ( Eng. Transl.), 50, 1169, 1981.

42. M. Jurczok, T. Gustavsson, J. Mialocq, W. Rettig, “Electron transfer and solvation in 9,9-bianthryl and derivatives: a sub-ps fluorescence upconversion study”, Chem. Phys. Lett., 344, 357, 2001.
43. R.F. Anderson, G.A. Wright, “Energetics and rate of electron transfer in DNA from base radical anions to electron-affinic intercalators in aqueous solution”, Phys. Chem.Chem.Phys., 1, 4827, 1999.
44. I. Diazadeh, E.S. Medvedev, A. A. Stuchebrukhov, “Effect of protein dynamics on biological electron transfer”, Proc. Natl. Acad. Sci. USA, 94, 3703, 1997.
45. C. Aubert, P. Mathis, A. P. M. Eker, K. Brettel, “Intraprotein electron transfer between tyrosine and tryptophan in DNA photolyase from Anacystis nidulans”, Proc. Natl. Acad. Sci. USA, 96, 5423, 1999.
46. S. Nad, H. Pal, “Photoinduced electron transfer from aliphatic amines to coumarin dyes”, J. Chem. Phys., 116, 1658, 2002.
47. V. Balzani, “Electron transfer in chemistry”, Wiley-VCH, 2001.
48. F. C. De Schryver, S. De Feyter, G. Schweitzer, “Femtochemistry”, Wiley-VCH, 2001.
49. J. Jortner, M. Bixon, “Electron Transfer: From Isolated Molecules to Biomolecules”, Wiley, 107, 1999.
50. R. A. Marcus, N. Sutin, “Electron transfers in chemistry and biology”, Biochim. Biophys. Acta, 811, 265, 1985.
51. M. A. Fox, “Photoinduced electron transfer”, J Photochem. Photobiol. A. Chem., 52, 617, 1990.
52. H.P. Boehm, R. Setton and E. Stumpp, “Nomenclature and terminology of graphite intercalation compounds”, Pure & Appl. Chem., 66, 1893, 1994.
53. D.D.L. Chung, “Review Graphite”, J. Mater. Sci., 37, 1475, 2002.
54. W.S. Hummers and R.E. Offeman, “Preparation of Graphitic Oxide”, J Am. Chem. Soc., 80, 1339, 1958.
55. A.B. Bourlinos, D. Gournis, D. Petridis, T. Szabo, A. Szeri and I. Dekany, “Graphite Oxide: chemical reduction to graphite and surface modification with primary aliphatic amines and amino acids”, Langmuir, 19, 6050, 2003.
56. M.J. McAllister, J.L. Li, D.H. Adamson, H.C. Schiniepp, A.A. Abdala, J.Liu, M.H. Alonso, D.L. Milius, R. Car, R.K. Prud’homme and I.A. Aksay, “Single sheet

functionalized graphene by oxidation and thermal expansion of graphite", J. Am. Chem. Soc., 19, 4396, 2007.

57. C.H. Chuang, Y.F. Wang, Y.C. Shao, Y.C.Yeh, D.Y. Wang, C.W. Chen, J.W. Chiou, S.C. Ray, W.F. Pong, L.Zhang, J.F.Jhu and J.H. Guo, "The effect of thermal reduction on the photoluminescence and electronic structures of graphene oxides", Sci. Rep., 4, 4525, 2014.
58. W. Lv, D.M. Tang, Y.B. He, C.H. You, Z.Q. Shi, X.C. Chen, C.M. Chen, P.X. Hou, C. Liu and Q.H. Yang, "Low-temperature exfoliated graphenes: vacuum-promoted exfoliation and electrochemical energy storage", ACS Nano., 3, 3730, 2009.
59. D. Li, M.B. Muller, S. Gilje, R.B. Kaner and G.G. Wallace, "Processable aqueous dispersions of graphene nanosheets", Nat. Nanotechnol., 3, 101, 2008.
60. G. Dutta, A. Paul, S. Yadav, M. Bardhan, A. De, J. Chowdhury, A. Jana and T. Ganguly, "Time resolved spectroscopic studies on a novel synthesized photoswitchable organic Dyad and its nanocomposite form in order to develop Light Energy Conversion Devices", J Nanosci Nanotechnol., 15, 1, 2015.
61. G. Dutta, P. Chakraborty, S. Yadav, A. De, M. Bardhan, P. Kumbhakar, S. Biswas, H.S. DeSarker and T. Ganguly, "Time resolved spectroscopic investigations to compare the photophysical properties of a short-chain dyad when combined with silver and gold nanoparticles to form nanocomposite systems", J Nanosci Nanotechnol., 15, 1, 2015.
62. G. Dutta, S.Paul, M. Bardhan, A. De and T. Ganguly, "Designing of an artificial light energy converter in the form of short-chain dyad when combined with core-shell gold/silver nanocomposites", Spectrochim Acta Part A: Mol and Biomol Spectrosc., 180, 168. 2017.
63. S. Bhattacharya, M. Bardhan, A.K. De, A. De and T. Ganguly, "Photo induced electron transfer within a novel synthesized short-chain dyad", J. Lumin., 130, 1238, 2010.
64. S. Paul, I. Mitra, R. Dutta, M. Bardhan, M. Bose, S. Das, M. Saha and T. Ganguly, "Comparative analysis to explore the suitability of a short chain dyad in its pristine and nanocomposite forms for designing artificial light energy conversion device", J Nanosci Nanotechnol., 18, 1, 2018.

65. S. Bhattacharya, J. Chowdhury and T. Ganguly, "Nature of charge separation and recombination processes within an organic dyad having short spacer", J. Lumin., 130, 1924, 2010.
66. J. Kim, J.E. Kwom, A.A. Boampong, J.H. Lee, M.H. Kim, S.Y. Park, T.D. Kim and J.H. Kim, "Threshold voltage modulation of polymer transistors by photoinduced charge–transfer between donor–acceptor dyads", Dyes Pigm., 142, 387, 2017.
67. G.Z. Galan, J.O. Palacios, B.X. Valderrama, A.A.C. Davila, D.C. Flores, V.H.R. Sanchez and E. Rivera, "Pyrene-fullerene $C_{60}$ dyads as light-harvesting antennas", Molecules, 19, 352, 2014.
68. S. Bhattacharya, T.K. Pradhan, A. De, S.R. Choudhury, A.K. De and T. Ganguly, "Photophysical processes involved within the anisole-thioindoxyl dyad system", J. Phys. Chem. A, 110, 5665, 2006.
69. A. Chakraborty, S. Chakraborty and T. Ganguly, "Photoisomerization within a novel synthesized photoswitchable dyad: experimental and theoretical approaches", Indian J Phys, 87, 1113, 2013.
70. G. Mondal, A. Chakraborty, U.K. Sur, B. Ankamwar, A. De and T. Ganguly, "Synthesis, characterization, photophysical properties of a novel organic photoswitchable dyad in its pristine and hybrid nanocomposite forms", J. Nanosci Nanotechnol., 12, 4591, 2012.
71. G. Mondal, S. Bhattacharya, S. Das and T. Ganguly, "The rates of charge separation and energy destructive charge recombination processes within an organic dyad in presence of metal-semiconductor core shell nanocomposites", J. Nanosci Nanotechnol., 12, 187, 2012.
72. P. Mondal, T. Misra, A.De, S. Ghosh, S.R. Choudhury, J. Chowdhury and T. Ganguly, "Phtophysical processes involved within the bichromophoric system 9-benzotriazole-1-ylmethyl-9H-carbazole and its role as an artificial photosynthetic device", Spectrochim Acta Part A, 66, 534, 2007.
73. E. Allard, J. Cousseau, J. Orduna, J. Garin, H. Luo, Y. Araki and O. Ito, "Photoinduced electron-transfer processes in C60 tetrathiafulvalene dyads containing a short or long flexible spacer", Phys. Chem. Chem. Phys., 4, 5944, 2002.

74. M. Bardhan, T. Misra, J. Chowdhury and T. Ganguly, “Comparative studies by using spectroscopic tools on the charge transfer (CT) band of a novel synthesized short-chain dyad in isotropic media and in a gel (P123)”, Chem. Phys. Lett., 481, 142, 2009.
75. M Maiti, T Misra, T Bhattacharya, C Basu (nee Deb), A De, S K Sarkar,T Ganguly, “Comparative studies on inter- and intramolecular electron transfer processes within 4-methoxybenzo[b]thiophene (4MBT) and p-chloroacetophenone (PCA) reacting systems by using steady-state and laser flash photolysis techniques “, J. Photochem. Photobiol. A: Chem., 152, 41, 2002.
76. G. Dutta, P. Chakraborty, S. Yadav, A De, M. Bardhan, P. Kumbhakar, S. Biswas, H.S. DeSarkar and T. Ganguly, “Time resolved spectroscopic investigations to compare the photophysical properties of a short-chain dyad when combined with silver and gold nanoparticles to form nanocomposite systems”, J. Nanosci Nanotechnol., 16, 7411, 2016.
77. H. Imahori, K. Tamaki, D.M. Guldi, C. Luo, M. Fujitsuka, O. Ito, Y. Sakata and S. Fukuzumi, “Modulating charge separation and charge recombination dynamics in porphyrin-fullerene linked dyads and triads: marcus-normal versus inverted region”, J. Am. Chem. Soc., 123, 2607, 2001.
78. M.A. Loi, P. Denk, H. Hoppe, H. Neugebauer, C. Winder, D. Meissner, C. Brabee, N.S. Sariciftci, A. Gouloumis, P. Vazquez and T. Torres,“Long lived photoindused charge separation for solar cell applications in phthalocyanine-fulleropyrrolidine dyad thin films”, J. Mater. Chem., 13, 700, 2003.
79. H. Imahori, H.E. El-Khouly, M. Fujitsuka, O. Ito, Y. Sakata and S. Fukuzumi, “Solvent dependence of charge separation and charge recombination rates in porphyrin-fullerene dyad”, J. Phys. Chem. A, 105, 325, 2001.
80. T.Asahi, M. Ohkohchi, R. Matsusaka, N. Mataga, R.P. Zhang, A. Osuka and K. Maruyama, “Intramolecular photoinduced charge separation and charge recombination of the product ion pair states of a series of fixed-distance dyads of porphyrins and quinones: energy gap and temperature dependences of the rate constants”, J. Am. Chem. Soc., 115, 5665, 1993.

# Chapter : 2

# *Materials and Experimental Techniques*

# Chapter 2: **Materials and Experimental Techniques**

## 1 . Materials

The solvents acetonitrile (ACN) (SRL) and cyclohexane (CH) of spectroscopic grade (purchased from Sigma-Aldrich) are purified following the standard procedures and tested before use for the absence of any impurity emission in the concerned wavelength region.Water is deionized using a Millipore Milli-Q system.

## 1.1 Synthesis and characterization of the dyad NNDMBF

The synthesis procedure of the investigated dyad is given in Fig- 2.1. In brief, 2-amino fluorene has been synthesized according to the literature. A mixture of 1.5 mmol 2-amino fluorene and 1.5 mmol 4-(dimethylamino)benzaldehyde was taken in a round bottle flask, 7 mL of anhydrous ethanol was added to it. The reaction mixture was stirred at room temperature for 2 h. After completion of the reaction (monitored by thin layer chromatography, TLC), the solvent was removed under high vacuum and crude reaction mass was washed several times with hexane to get the pure product which is the dyad[1].

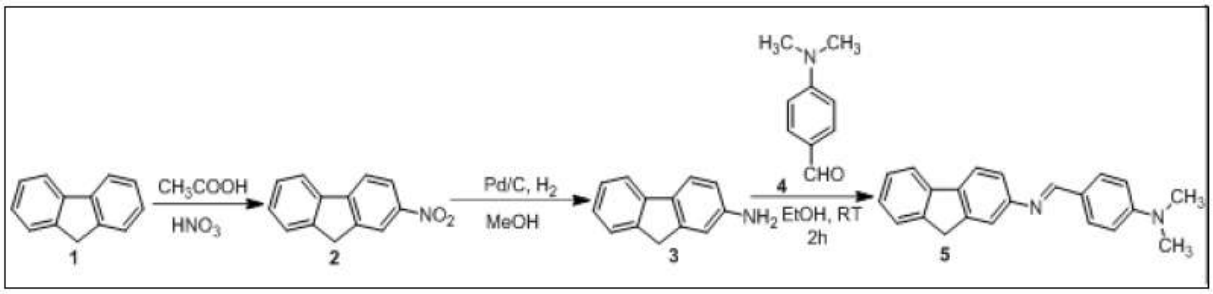


**Fig. 2.1.** synthesis procedure of NNDMBF dyad

$^{1}H$ and $^{13}C$ NMR spectra (Fig. 2.2., 2.3.) were recorded on Bruker AVIII- 500. Chemical shifts were reported in ppm. Coupling constants (J values) were reported in Hertz. $^{1}H$ NMR

chemical shifts were referenced to $CDCl_3$. $^{13}C$ NMR chemical shifts were referenced to $CDCl_3$. (E)-4-(((9H-fluorene-2-yl)imino)methyl)-N,N-dimethylaniline (Compound 5). $^1H$ NMR (500 MHz, $CDCl_3$): δ =2.90 (s, 6H), 3.81 (s, 2H), 6.62 (d, 2H, *J* = 8.5Hz), 7.13-7.18 (m, 2H), 7.24-7.28 (m, 2H), 7.41 (d, 1H, *J* = 7.5 Hz), 7.64-7.69 (m, 4H), 8.31 (s, 1H). $^{13}C$ NMR (125 MHz, $CDCl_3$):δ = 36.9, 40.2, 111.6, 117.5, 119.5, 120.2, 120.3, 124.5, 125.0, 126.2, 126.8, 130.4, 138.9, 141.6, 144.4, 151.9, 152.4, 159.6.

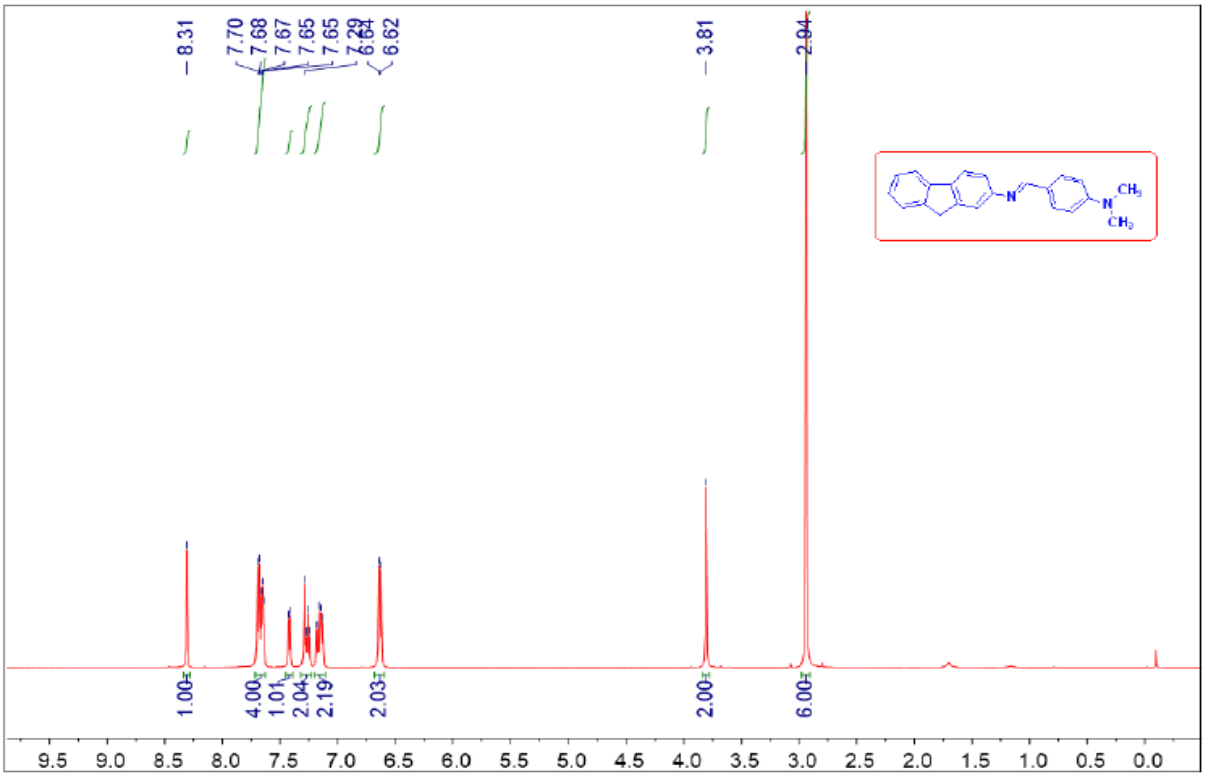


**Fig. 2.2.** $^1H$ NMR of (E)-4-(((9H-fluorene-2-yl)imino)methyl)-N,N-dimethylaniline

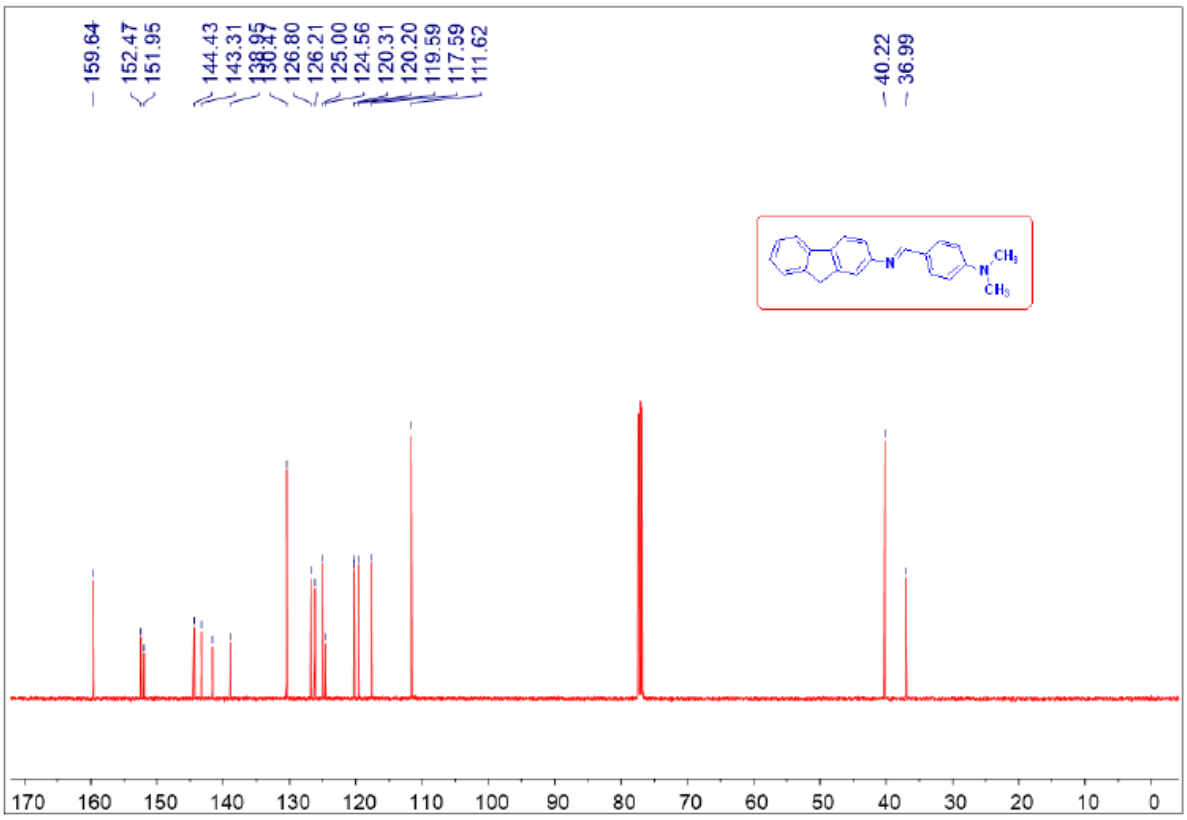


**Fig. 2.3.** $^{13}$C NMR of (E)-4-(((9H-fluorene-2-yl)imino)methyl)-N,N-dimethylaniline

From the molecular structure of the dyad, one can presume the possibilities of the two conformers: Trans- and Cis- (Fig. 2.4.) of the dyad.

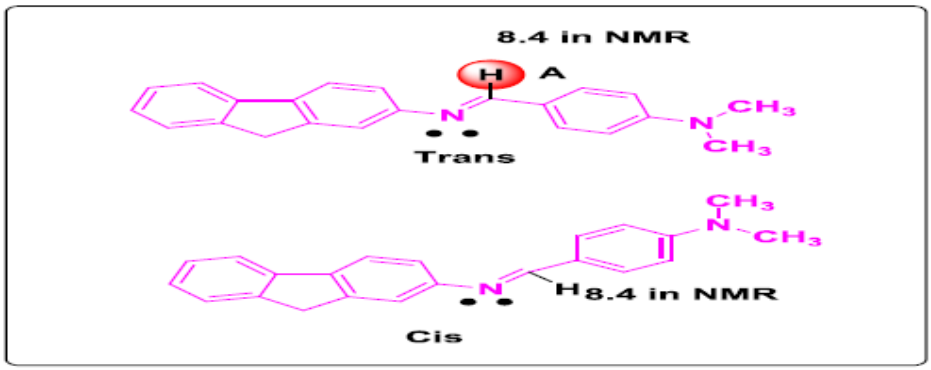


**Fig.2.4.** Two conformers of dyad

Since there is no proton on the N atom, we cannot predict the possible ground state conformation of the dyad by coupling constant value from NMR. From the theoretical computations on ground state optimized geometry of the dyad NNDMBF by using BL-LYP/6-311 g (d,p) level of theory on HOMO –LUMO surfaces it shows that there may be the two types of conformers Cis- and Trans- , in which the latter form is found to be more stable in the ground state. Thus the above theoretical predictions suggest that both cis- and trans- forms of the dyad exist in the ground state with the preponderance of the latter.

## 1.2 Novel short-chain dyad (NNDMBF)

A novel short-chain dyad (NNDMBF) (Fig. 2.5.) has been synthesized (the synthesis and characterization were given below) in which electron donor 4(N,Ndimethylamine)benzaldehyde (NNDMB) is linked by a short chain with the acceptor fluorene (F).

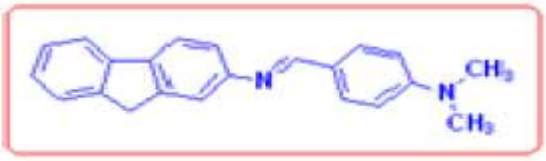


**Fig. 2.5.** novel short-chain dyad (NNDMBF)

## 1.3 Graphene oxide (GO) and Reduced Graphene oxide (RGO)

### 1.3.1 Graphene oxide (GO)

The exact structure of GO is difficult to determine but it is clear that for GO the previously contiguous aromatic lattice of graphene is interrupted by epoxides, alcohols, ketone carbonyls, and carboxylic groups. In 1958 Hummers method is most commonly is used today, though it produces some toxic gases like $NO_2$, $N_2O_4$ or $CIO_2$. D.C. Marcano et al. [2] reported that the scalable preparation of graphene oxide nanoribbon (GONRs) from multiwalled carbon nanotube with the treatment of $KMnO_4$ and concentrated $H_2So_4$. This method reduces the defects in the basal plane of GO than that produced by Hummers method. Otherwise this method provides us a

greater amount of hydrophilicity relative to the old Hammer's procedure. The advantages of the modified Hammer's method, with its simpler protocol, higher yield and equivalent conductivity upon reduction, make it attractive for preparing material on a large scale. It may also show improved performance in materials applications, such as in membranes, TEM grids, or temperature-sensitive device fabrication.

A. Mallick et al [3] reported that GO can be produced by using modified Hammer's method. Here, 2 g of graphite powder was mixed with 1 g of NaNO3 by keeping it in an ice bath. Now, concentrated $H_2SO_4$ (130 ml) was added to the mixture under a stirring condition. Under the vigorous stirring condition, 6 g of $KMnO_4$ was added slowly maintaining the reaction temperature of the mixture around $20^0$ C. Gradually, the reaction temperature was elevated up to $40^0$ C and stirred for 6 h. At this stage, the colour of the mixture changes from dark grey to grayish green. An additional 6 g of $KMnO_4$ were added to the mixture and stirred for another 6 h so that the color of the mixture becomes grayish brown. Now, 250 ml of triple distilled water was slowly added to the solution which raises the temperature of the solution to around $96^0$ C at which the mixture was stirred for 30 min. The solution was then cooled down to room temperature. Now, an additional 500 ml triple distilled water and 15 ml 30% $H_2O_2$ were added to the solution to stop the oxidation. At this stage, the color of the solution becomes yellow ochre signifying the high oxidation level of graphite. The yellow solution was washed two times with 1M HCl solution and repeated washing was done with triple distilled water until a pH of 5 was obtained. This was done by centrifugation of the solution and decantation of the supernatant. A rigorous washing and decantation step is necessary to exfoliate the graphene oxide layers and to remove the unexfoliated graphene oxide layers. The thick yellow brown gel was filtered and dried overnight to get a fine yellow graphene oxide (GO) powder. A stoichiometric amount of GO was then taken in triple distilled water and ultrasonicated for 30 min to get a homogeneous solution.

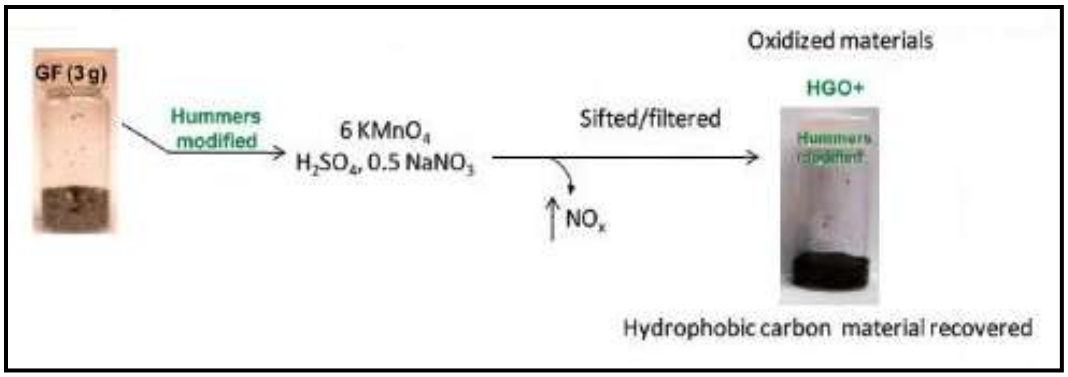


**Fig. 2.6.** Synthesis process of GO [2]

In our experiment we used GO where the level spacing is around 9.0 Å (from XRD spectra). The X-ray photoelectron spectroscopy (XPS) confirms that GO produced by modified Hammer's method is more oxidized than GO produced by Hammer's methods. XPS confirms that improved GO has 63% oxidized carbon and 37% graphitic carbon. From $^{13}C$ NMR we get the apperant peak of oxidized carbon of GO at around 287 eV. TEM images confirms the structure regularity of GO. UV-Vis spectra supports the regular structure of GO is due to greater retention of carbon ring in basal plane. Large extinction coefficient of GO indicate that it has large number of aromatic ring or isolated aromatic domain. The $\lambda_{max}$ data from electronic transition indicate that these aromatic rings are not extended conjugation but overall absorption indicates that GO produced by modified Hammer's method has more aromatic rings retained than Hammer's methods GO [2].

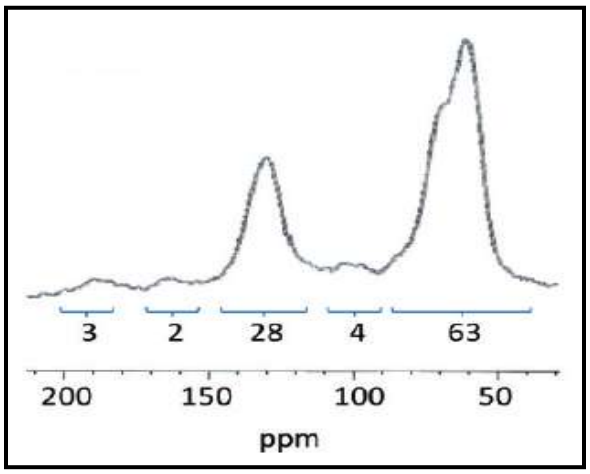


**Fig. 2.7.** $^{13}C$ NMR spectra of GO [2]

### 1.3.2 Reduced Graphene Oxide (RGO)

Bulk samples of the oxidized materials were reduced using hydrazine hydrate and then annealed at 300 and 900 °C in $Ar/H_2$. In general, for the hydrazine reduction, 100 mg of the improved GO materials is dispersed in 100ml DI water, stirred for 30 min and then 1 ml of hydrazine hydrate is added. The mixture is heated at 95 $^0$C using water bath for 45 min, a black solid precipitated from reaction mixture. Products are isolated by filtration and washed with DI water, producing 54 mg of chemically reduced improved GO (RGO). After reduction no signal from oxidized carbon is detected by NMR spectra. This indicates the quality of RGO is very good. From AFM data we can say that individual flacks of RGO have a thickness ranging from 1 to 3 nm [2].

## 2 . NMR Spectroscopy Technique

Nuclear magnetic resonance (NMR) is a physical phenomenon in which nuclei in a magnetic field absorb and re-emit electromagnetic radiation. This energy is at a specific resonance frequency which depends on the strength of the magnetic field and the magnetic properties of the isotope of the atoms; in practical applications, the frequency is similar to VHF and UHF television broadcasts (60–1000 MHz). NMR allows the observation of specific quantum mechanical magnetic properties of the atomic nucleus. Many scientific techniques exploit NMR phenomena to study molecular physics, crystals, and non-crystalline materials through nuclear magnetic resonance spectroscopy. NMR is also routinely used in advanced medical imaging techniques, such as in magnetic resonance imaging (MRI).

## 2.1 Theory and Principle of NMR

All isotopes that contain an odd number of protons or neutrons have an intrinsic magnetic moment and angular momentum i.e. a nonzero spin, while all nuclides with even numbers of both have a total spin of zero. The most commonly studied nuclei are $^1$H and $^{13}$C, although nuclei from isotopes of many other elements (e.g.$^2$H, $^6$Li etc.) have been studied by high-field NMR

spectroscopy as well. The property of nuclear spin is fundamental in NMR spectroscopy. The nuclei which has a non zero nuclear spin angular momentum, L, then the associated magnetic moment, μ is

$$\mu = \gamma L$$

Where γ is gyromagnetic ratio. Here magnatic moment and angular momentum are both vector quantity. So, when this placed in an external static magnetic field, the microscopic magnetic moment aligns themselves along the magnetic field in a discrete number of states, as energy levels are quantized. This applied field imposes a torque on the magnetic moment, so it traces a circular path around the applied field. This motion is called larmor precession.

The nuclear magnetic resonance occurs when the nucleus changes it's spin state, driven by the absorption of quantum of energy. The applied radiation frequency must match with the larmor precessional frequency to satisfy the resonance condition. So the energy involved is given by

$$\Delta E = h\nu = \frac{h\gamma B_0}{2\pi}$$

Where h is planks constant and $B_0$ is the applied magnetic field. The population of the differently oriented nuclear particle in different energy state can be described by the Boltzmann distribution law.

$$\frac{N_\alpha}{N_\beta} = e^{\Delta E/K_B T}$$

Where $N_\alpha$ , $N_\beta$ are the number of nuclei of different orientation. The difference between the spin energy level is very small, so the corresponding population difference will be very small. This is why NMR is very sensitive relative to the other technique, such as IR and UV, where energy difference between the ground and excited state is quite large [4].

## 2.2 Basic NMR apparatus

The heart of an NMR instrument is a magnet of adequate field strength and adequate homogeneity. Nowadays superconducting solenoid magnets manufactured from niobium alloy wire is exclusively used to provide static magnetic field. This can produce up to 18.8 tesla magnetic field with the proton frequency of 800 MHz.

To excite NMR spectra we need radio frequency (RF) power, which is generated in the transmitter. The source of RF is normally an electronic device called a frequency synthesizer, which produces a very narrow band at one or more selected frequencies. Most of NMR spectrometer requires two or more separate frequency. Then it is amplified and RF power is applied to the sample by electrical coils in a probe. The probe holds the sample in the magnetic field. Usually probe contains one or more coils to accommodate several radio frequencies simultaneously. Usually probe is long cylindrical coil, where axis of the coil coincides with the magnetic field. But the axis of the rf coil must be perpendicular to the magnetic field [5].

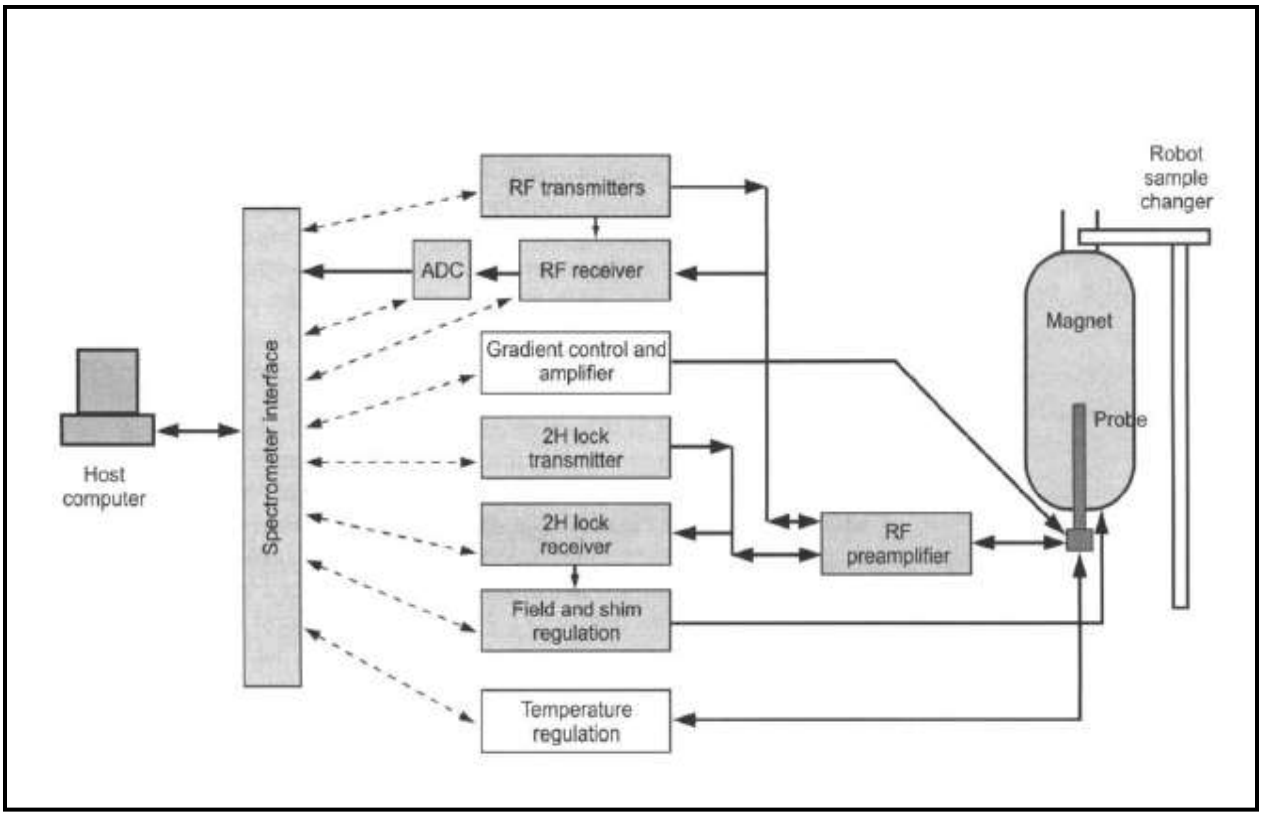


**Fig. 2.8.** A schematic illustration of modern NMR spectrometer[4]

In NMR spectroscopy the processing magnetization induces an electrical signal in a coil placed in the probe. In NMR spectrometer the coil is used to transmit the exciting RF to the

sample is used to measure extremely weak nuclear induction signal. Then it is amplified but the detected signal is in much lower (audio) frequency range, so it is further processed electronically.

The spectrometer cabinet consists of the radio-frequency transmitters and the detection system for the observation channel, additional transmitter channels, the lock channel and the pulsed field gradient transmitter. Most spectrometers come in either a two-channel or three-channel configuration, plus the lock channel. The spectrometer is controlled by a UNIX based host computer. This computer converts electrical analog NMR signal to the digital signal by analog to digital converter (ADC). The computer also processes the acquired data, although this may also be performed 'off-line' with one of the many available NMR software packages.

Various optional peripherals may also be added to the instrument, such as variable temperature units which allow sample temperature regulation within the probe, robotic sample changers and so on. Recently, the coupling of NMR with other analytical techniques such as HPLC, has gained popularity especially within the pharmaceutical industry. The need for these will obviously depend on the type of samples handled and the nature of the experiments employed [4].

## 3 . UV-Visible absorption spectrometer

Ultraviolet-visible spectroscopy is considered an important tool in analytical chemistry. In fact, this is one of the most commonly used techniques in clinical as well as chemical laboratories [6]. Ultraviolet-visible spectroscopy or ultraviolet-visible spectrophotometry refers to absorption spectroscopy in the ultraviolet-visible spectral region. This means it uses light in the visible and adjacent (near-UV and near-infrared (NIR)) ranges. UV-Vis spectrophotometer is used in the quantitative determination of concentrations of the absorber in the solutions of transition metal ions and highly conjugated organic compounds. Particles in suspension will scatter light. So, spectrophotometers may also be used to estimate the number of cells in suspension.

Basically, spectroscopy is related to the interaction of light with matter. As light is absorbed by matter, the result is an increase in the energy content of the atoms or molecules. The absorption of visible light or ultraviolet light by a chemical compound will produce a distinct spectrum. When ultraviolet radiations are absorbed, this results in the excitation of the electrons from the ground state towards a higher energy state. The theory revolving around this concept states that the energy from the absorbed ultraviolet radiation is actually equal to the energy difference between the higher energy state and the ground state.

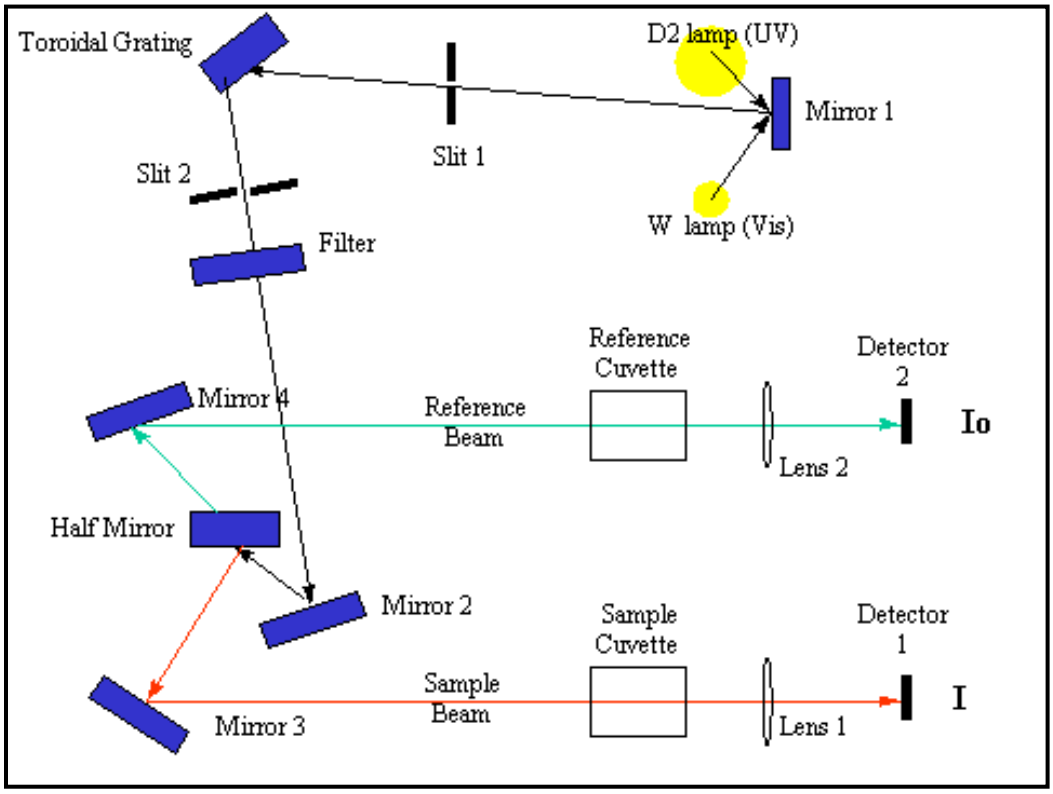


**Fig. 2.9.** UV-Vis Absorption Spectrophotometer[7]

The basic parts of this spectrophotometer are a light source, a holder for the sample, a diffraction grating in a monochromator or a prism to separate the different wavelengths of light, and a detector. The radiation source is often a Tungsten filament (300-2500 nm), a deuterium arc lamp, which is continuous over the ultraviolet region (190-400 nm), Xenon arc lamp, which is continuous from 160-2000 nm; or more recently, light emitting diodes (LED) for the visible wavelengths. The detector is typically a photomultiplier tube, a photodiode, a photodiode array

or a charge-coupled device (CCD). Single photodiode detectors and photomultiplier tubes are used with scanning monochromators, which filter the light so that only light of a single wavelength reaches the detector at one time. The scanning monochromator moves the diffraction grating to "step-through" each wavelength so that its intensity may be measured as a function of wavelength. Fixed monochromators are used with CCDs and photodiode arrays. As both of these devices consist of many detectors grouped into one or two dimensional arrays, they are able to collect light of different wavelengths on different pixels or groups of pixels simultaneously.

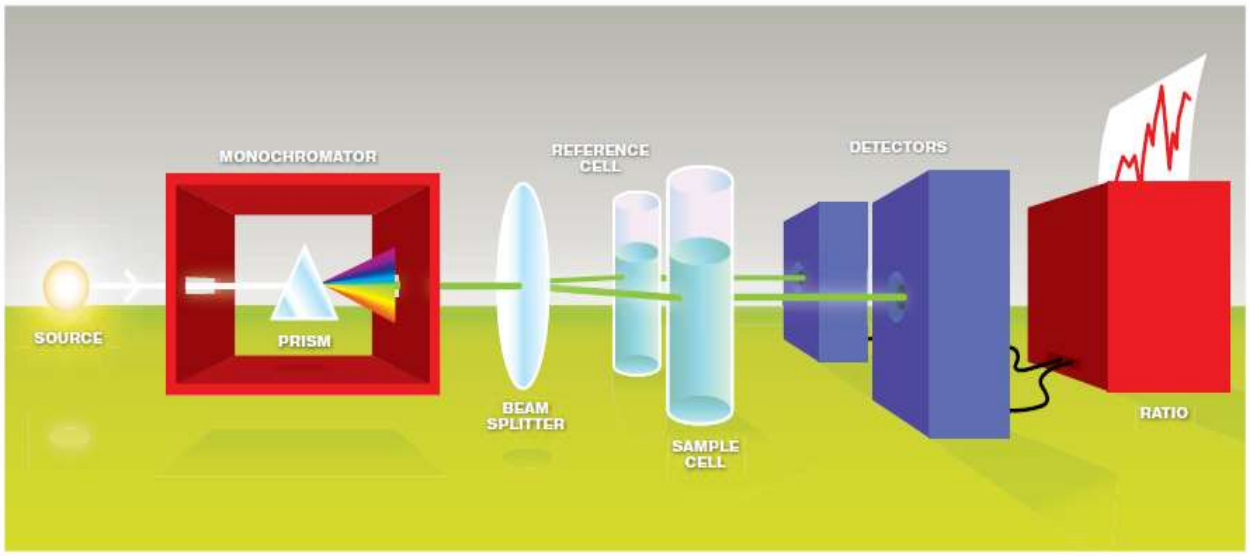


**Fig. 2.10.** UV-Visible absorption spectrometer basic block diagram [8]

When studying a compound in solution by spectrophotometry, we have to put it in a sample holder called a cuvette and place it in the spectrophotometer. Light of a particular wavelength passes through the solution inside the cuvette and the amount of light transmitted or absorbed by the solution is measured by a lightmeter. Then we compare the absorbance of our test solution to a reference blank. Ideally, the reference blank should contain everything found in the sample solution except the substance we are trying to analyze. In our experiment we will measure the absorbance of a organic dyad, that is dissolved in water. The reference blank in this case would be water alone.

## 3.1 Basic principle

For analytical purpose, there are two main propositions about the light absorption. The first, Lambert's Law states that the amount of incident light absorbed is independent of the intensity of incident light. So, successive layers of equal thickness will transmit an equal proportion of the incident energy.

$$\frac{I}{I_0} = T$$

Where $I$ is the intensity of the transmitted light, $I_0$ is the intensity of the incident light, and $T$ is the transmittance. Now, the transmittance as a percentage of incident light:

$$\%T = \frac{I}{I_0} \times 100$$

Since the compound being tested is not present in the reference blank, the transmittance of the reference blank is defined as 100%T. A certain portion of the light will be absorbed by the compound in the test cuvette; therefore its %T will be lower than that of the blank.

The second, Beer's Law states the absorption of light is directly proportional to both the concentration of the absorbing medium and the thickness of that medium (Beer, 1852). A combination of the two laws, the Beer-Lambert Law, defines the relationship between absorbance and transmittance.

$$A = log\frac{I}{I_0} = log\frac{100}{T} = \varepsilon cl$$

Where $A$ is the absorbance, $\varepsilon$ is the molar attenuation coefficient of the medium ($M^{-1}$ $cm^{-1}$), $c$ is the molar concentration (M), and l is the path length (cm). It is important to remember that the molar attenuation coefficient is a function of wavelength; therefore Beer-Lambert law is only true at a single wavelength i.e. at monochromatic light [9].

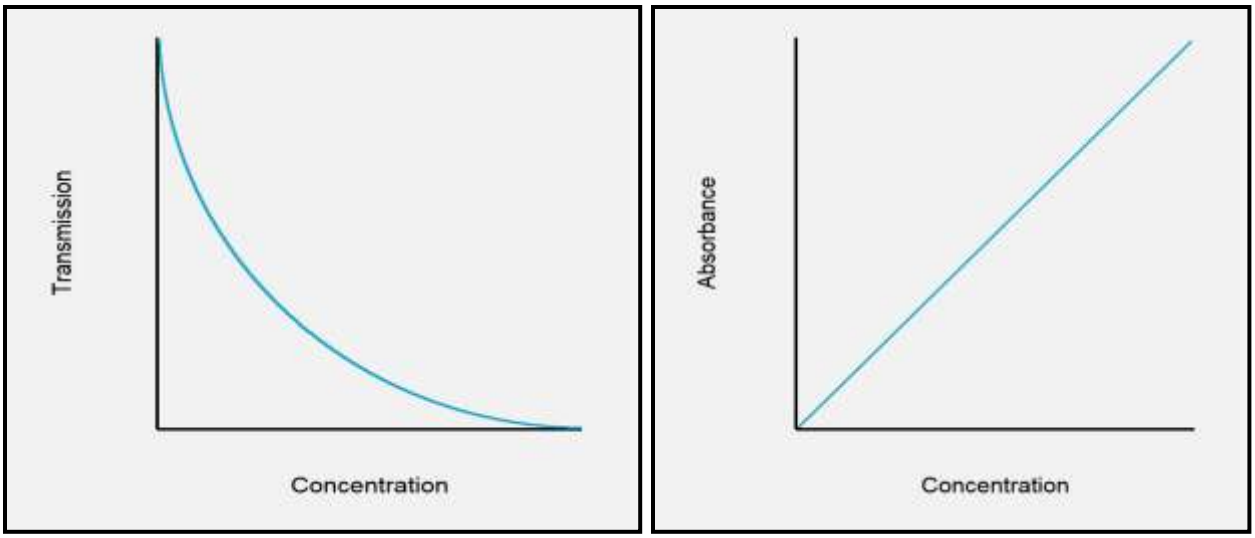


**Fig. 2.11.** 1st figure shows exponential curve associated with transmission plotted against concentration and 2nd figure shows the linear relationship associated with absorbance plotted against concentration [9]

An alternative use of the linear relationship between absorbance and concentration is to calculate a factor for a specific molecule of interest that can then be applied to subsequent sample of unknown concentrations of that same molecule. This avoids the relatively time consuming process of a plotting calibration curve. To calculate the factor (k), the absorbance of a known concentration of the molecule of interest needs to be determined.

$$k = \frac{concentration\ (c)}{absorption\ (A)}$$

## 3.2 Fluorescence Excitation Spectra

In order to supplement the absorption spectral data, particularly to locate lowest excited singlet and triplet states, the technique of excitation spectroscopy was employed. The excitation spectra has been recorded with FP-8300 fluorescence spectrophotometer (JASCO) with the emission monochromator set at the maximum of fluorescence or phosphorescence intensity and the exciting monochromator is scanned from shorter wavelength values in the vicinity of the emission band of the molecule.

## 3.3 Application of UV-Visible spectroscopy

It can be used to detect a functional group, to detect the absence or the presence of chromophore in a complex compound. This can also be used to detect the extent of conjugation in polyenes. When there is an increase in double bonds, the absorption shots to the longer wavelength. In addition, UV spectroscopy may be used to identify unknown compounds. UV spectroscopy can also help determine the configurations of a geometrical isomer. It has been established that cis-alkenes are absorbed at a different wavelength compared to trans-alkenes. If one of the isomers comes with non-coplanar structure, it can still be determined by UV spectroscopy. Also this tool can determine the purity of a substance.

## 4 . Spectrofluorometer

Fluorescence is an analytical tool for the determination of the presence of specific molecules in solutions, is now routinely used in biochemistry and biophysics for studying molecular interactions and dynamics, both in solutions and in cells; in drug discovery; in life sciences for DNA sequencing; in nanotechnology and material sciences for identification and characterization of new materials. Fluorescence is part of a general class of phenomena named luminescence. It is distinguished by the phosphorescence as the latter takes, typically, a time of the order of one microsecond ($10^{-6}$ s) or longer while the former takes a time of the order of one nanosecond ($10^{-9}$ s).

Generally spectrofluorometer is an instrument which takes advantage of fluorescent properties of some compounds in order to provide information regarding their concentration and chemical environment in a sample. A certain excitation wavelength is selected, and the emission is observed either at a single wavelength, or a scan is performed to record the intensity versus wavelength, also called an emission spectra.

Usually, spectrofluorometers use high intensity light sources to bombard a sample with as many photons as possible. This allows for the maximum number of molecules to be in an excited state at any one point in time. Normally, in all of the instruments, the fluorescence is collected at an angle of 90 degrees with respect to the optical axis set by the excitation light beam. This

geometry maximizes the efficiency of the emission collection and reduces the background due to the excitation light. A spectrofluorometer measures a signal over a zero background instead of, the difference in the intensity of two signals, which is measured in spectrometer. The key elements of a spectrofluorometer are the light source, the monochromator and the light detector.

The light source utilized in a spectrofluorometer is a high-pressure xenon arc lamp. The bulb of this lamp includes xenon at high pressure that is excited to higher level by the electrical arc established by the current running through the electrodes. The emitted light is a continuous spectrum from about 250 nm up to 1100 nm.

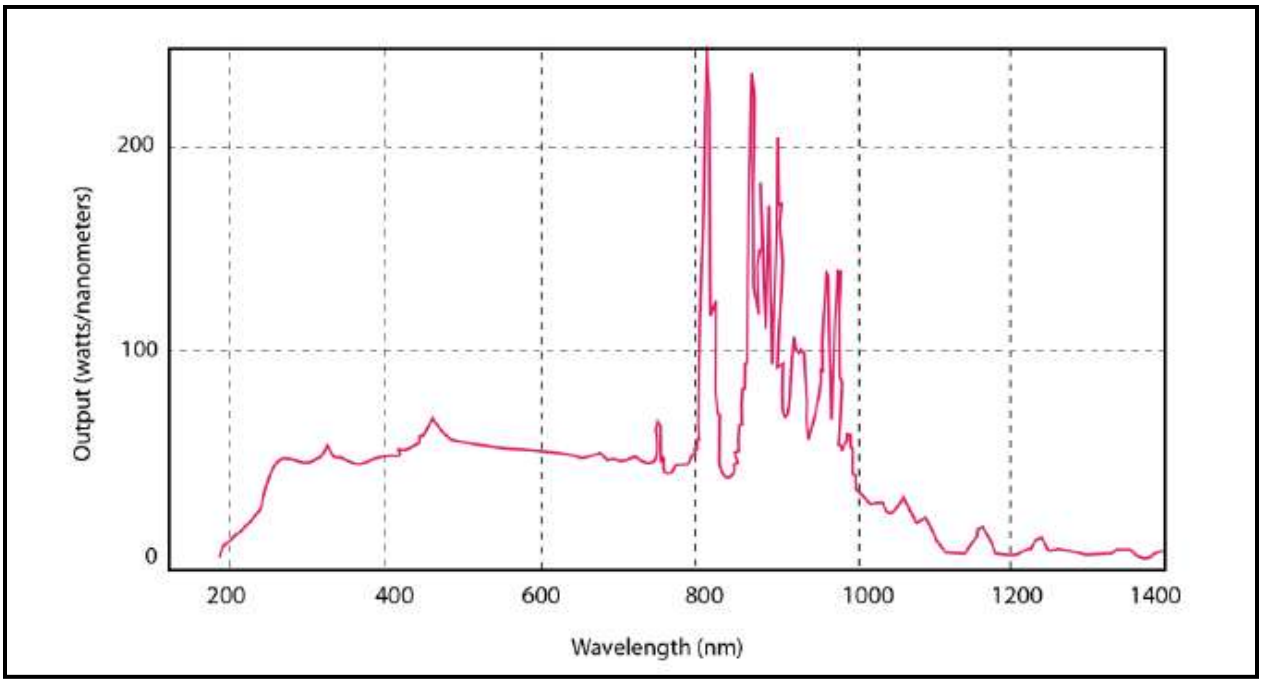


**Fig. 2.12.** Spectral distribution for the 300W xenon arc lamp[10]

Monochromators are utilized to select the wavelength used for irradiating the sample when using a xenon arc lamp; in the collection channel of a spectrofluorometer they are utilized to record the range of wavelengths emitted by a fluorophore. The simplest monochromator includes a diffraction grating and slits at the entrance and at the output. Light impinging at an angle on the grating is diffracted at a series of angles; usually, the first angle is selected for the measurement. It is important to remember that when a monochromator is set to deliver radiation at wavelength

λ, it also delivers radiation at 2λ. Typically the intensity of the second order is about 1/10 the intensity of the first order; still this amount is sufficient to contaminate the emission spectrum. The second order can be eliminated with a judicial selection of filters. A characterization of every monochromator is the amount of stray light i.e. radiation present at any wavelength other than the specific wavelength. Different strategies are available for the minimization of the stray light, the first being a judicial selection of the grating. There are two type of grating, ruled grating and holographic grating. Gratings can be arranged in different designs to build a monochromator, the two most popular being the Czerny-Turner and the Seya-Namioka.

Photomultiplier tube (PMT), or photodiode is used as a detector of light and convert it to the corresponding electrical signal. Photomultiplier tubes are sensitive within a set wavelength range that is determined by the material used in the photocathode. The PMT can be utilized in the region from about 230 nm to about 830 nm. It is apparent that even within the operational wavelength region, the sensitivity is not the same; the non-linearity of the sensitivity introduces an artifact in the data such that a correction to the data has to be introduced.

A spectrofluorometer includes other optical elements such as lenses and mirrors; moreover polarizers are utilized for anisotropy measurements. The operational region of the instrument is given by the superposition of the wavelength transmission of the various elements of the instruments. Even within this region, the variation in transmission has to be taken into account when measuring the fluorescence parameters [10]. The fluorescence is detected with photomultiplier tubes and quantified with the appropriate electronic devices. The output is usually presented in graphical form and stored digitally.

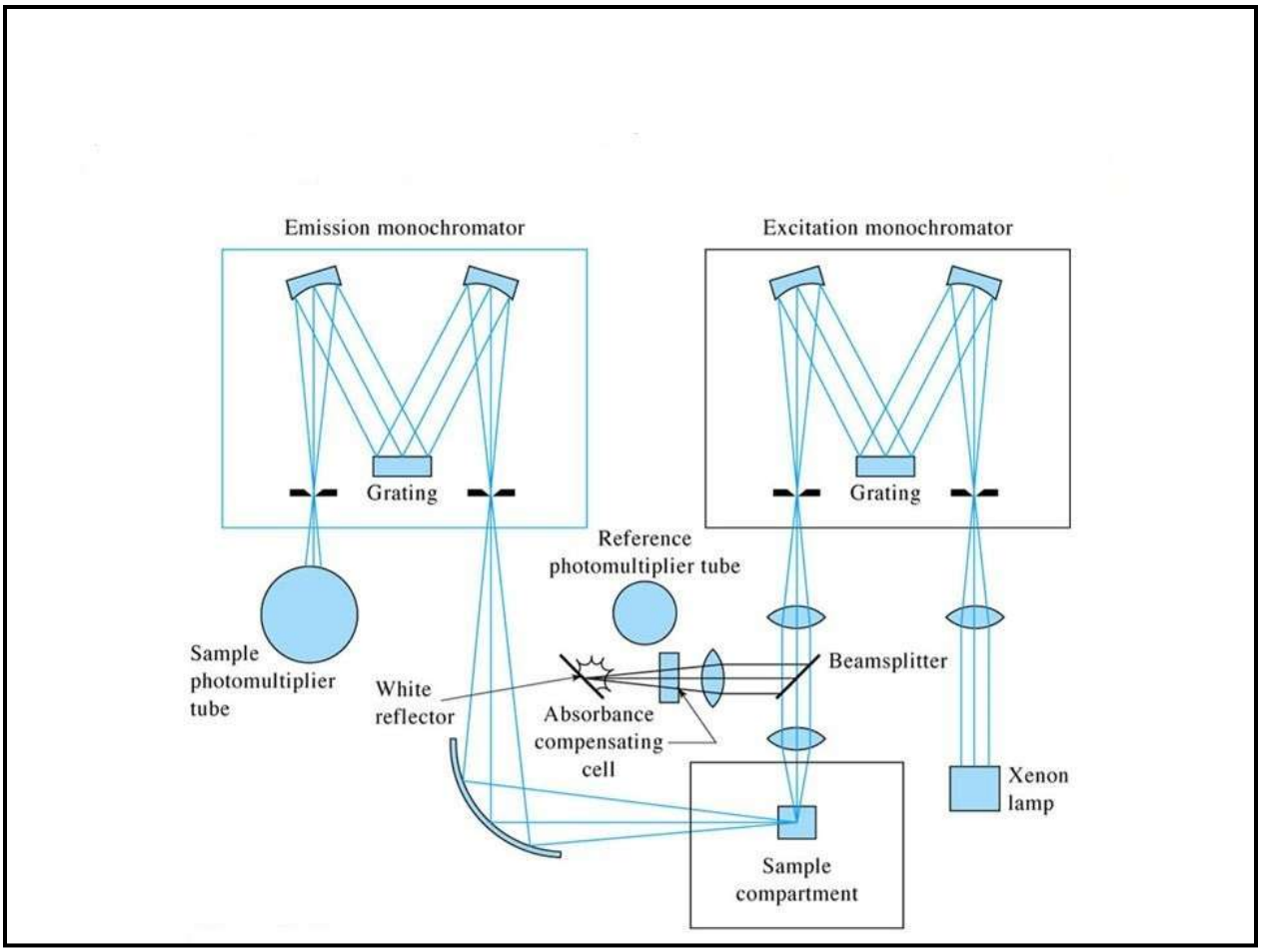


**Fig. 2.13.** Spectroflurometer basic ray diagram[11,12]

The instrument schematic also shows the components of the optical module that surrounds the sample holder. Shutters are provided to eliminate the exciting light or to close off the emission channel. A beam splitter is provided in the excitation light path. This splitter reflects part of the excitation light to a reference cell, which generally contains a stable reference fluorophore. The beam splitter consists of a thin piece of clear quartz, which reflects about 4% of the incident light. This amount is generally adequate for a reference channel that frequently contains a highly fluorescent quantum counter. The intensity from the standard solution is typically isolated with a bandpass filter, and is proportional to the intensity of the exciting light. Changes in the intensity of the arc lamp may be corrected for by division of the intensity from the sample by that of the reference fluorophore.Polarizers are present in both excitation and emission of light path.Generally the polarizers are removable so that they can inserted only for measurements of

fluroscenes anisotropy, or when it is necessary to select for particular polarized components for emission and excitation. Accurate measurement of fluorescence anisotropies requires accurate angular positioning of the polarizers. The polarizer mounts must be accurately indexed to determine the angular orientation.

## 5. Time resolved spectroscopy

In physics, chemistry and biology, a lot of effort and research is directed to understand the dynamics of various processes. Depending on the size of the object being watched, the time scales on which the changes take place may vary from very slow to extremely fast. Electronic devices provide access to the realm of microseconds, nanoseconds, down to hundreds of picoseconds. Even faster processes, the durations of which are tens of picoseconds and less, require the fastest tool available in nature – light itself. As light travels with a constant speed 3 x $10^8$ m/s in vacuum. All the processes that occurs faster than or within 1µs is called ultrafast processes. The area of science that explores ultrafast processes in atoms, molecules, crystals and glasses using light-based spectral techniques is called time-resolved spectroscopy.

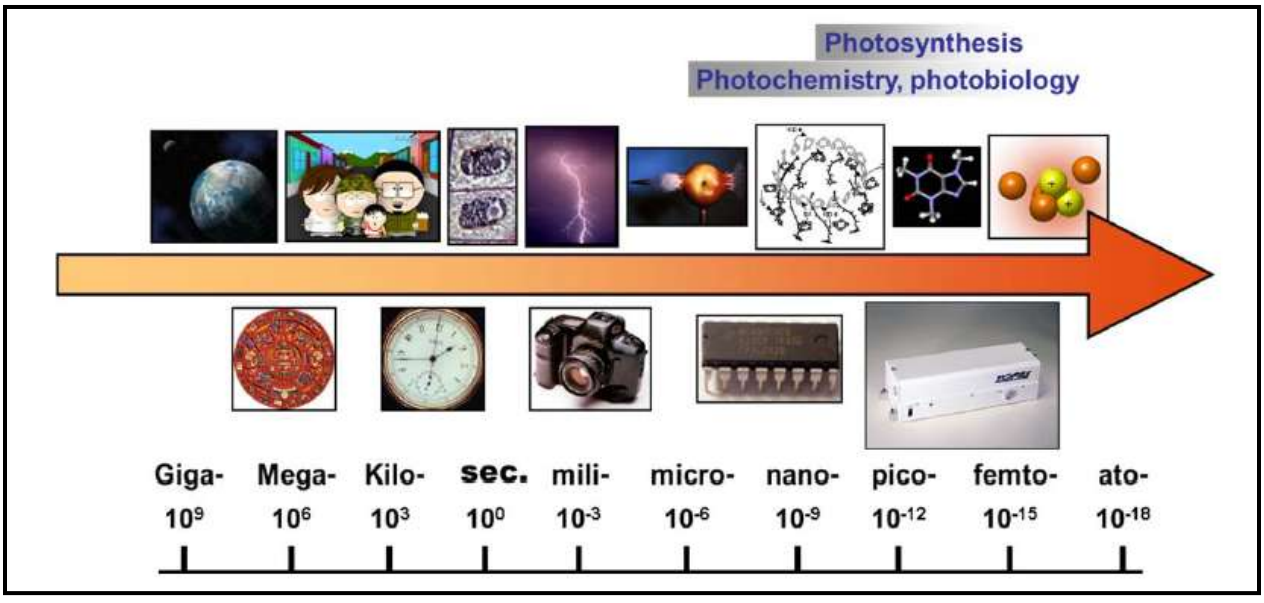


**Fig. 2.14.** Different natural processes, their time scale and instruments for following them

In order to follow ultrafast events, an experiment needs time resolution and time resolution in ultrafast spectroscopy comes from short laser flashes called pulses. There are two methods, which can produce laser pulses from the continuous wave laser source.

a) Q-switch or a variable attenuator inside the laser cavity
b) Mode-locking of the light modes inside the laser cavity

Most often the process is studied after the illumination of the materials but in principle the technique can be employed to any process that leads to a change in properties of the materials. With the help of pulsed lasers, it is possible to study processes that occur on time scales as short as $10^{-16}$ s. Time resolved fluorescence spectroscopy is an extension of fluorescence spectroscopy. Here, the fluorescence of a sample is monitored as a function of time after excitation by a flash of light. There are different spectroscopic methods for studying the time resolved spectroscopy:

I. Pump probe methods
    a) Time resolved absorption in UV-visible range
    b) Time resolved absorption in IR range
II. Time resolved emission spectroscopy: electronic methods
    a) Broad bandwidth photodetectors
    b) The streak camera
    c) Single photon counting
III. Time resolved emission spectroscopy: optical methods
    a) The kerr shutter
    b) Up-conversion method

In our experiment we have used time correlated single photon counting method, as we get the conformer species of order pecosecond. The two main types of pulsed-light sources used in time-resolved fluorescence spectroscopy are the flash lamp and the laser.

## 5.1 Time resolved optical detection at low light intensity

When light propagates through matter it can interact with the molecules in various ways. In the simplest case, the photons of the incident light may be reflected, absorbed, or scatted [13]. When the molecules of the sample absorbs photon then they are excited to the higher energy

level and return to the ground state after emitting a photon of longer wavelength. At high intensity several photons are interacts with the molecule, results a multiphoton excitation or second harmonic generation. Light transmitted or scattered or emitted from the sample carieses important information about the sample molecules. So, optical technique can be used to probe molecular parameter inside the sample.

Often the effects involved in the conversion of the light are extremely weak, or the concentration of the molecules involved in the conversion processes is low. So, the detected optical signal is very low. Optical signals have to be considered a stream of photons. At a given photon rate, the signal-to-noise ratio decreases with the square root of the detection bandwidth. Now consider the detection of a fast optical waveform, such as a fluorescence decay excited by short laser pulses. The fluorescence decay time is on the order of a few nanoseconds. So, it is quite hard to detect appreciable amount of signal from a single pulse, so we repeat the experiment several times and average the signal detected within a given period of time after the excitation pulses. Here a weak optical signal is a sequence of individual photon detection events. The signal waveform can therefore more efficiently be reconstructed by determining the arrival times of the photons, and counting them in several time bins according to their times after the excitation pulses.

## 5.2 Time correlated single photon counting (TCSPC)

Time resolved fluorescence spectroscopy is a powerful analysis tool in fundamental physics as well as in the life science. Implementing it in the time domain requires recording the time dependent intensity profile of the emitted light upon excitation by a short flash of light, typically a laser pulse. With periodic excitation it is possible to extend the data collection over multiple cycles and one can reconstruct the single cycle decay profile from single photon events collected over many cycles.

### 5.2.1 Principle of TCSPC technique

Time-Correlated Single Photon Counting (TCSPC) [13] is based on the detection of single photons of a periodical light signal, the measurement of the detection times of the individual photons and the reconstruction of the waveform from the individual time measurements. TCSPC makes use of the fact that for low-level, high-repetition rate signals the light intensity is usually low enough that the probability to detect more than one photon in one signal period is negligible.

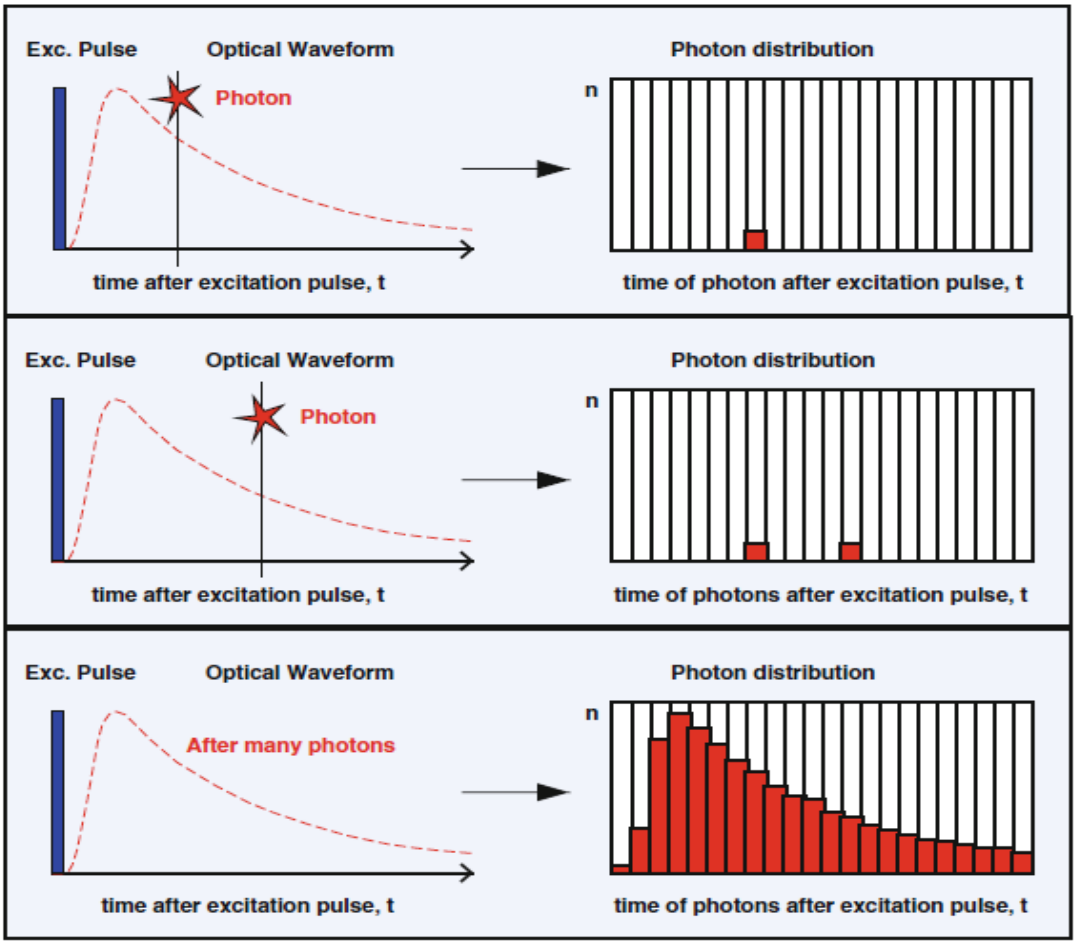


**Fig. 2.15.** Principle of TCSPC : The recording process builds up the distribution of photons over the time after the excitation pulses [13].

This electronic method is useful, when excitation is performed using high repetition rate lasers. After excitation of the molecule by a laser pulse, it will sit in the excited state for some time, and eventually, after time Δt, it will emit a photon. If we find a way of measuring Δt multiple times, the obtained waiting time values will be distributed according the probability of the radiation at particular time. This insight is employed in time-correlated single photon counting (TCSPC) experiment, the principle of which is illustrated in Fig. 2.15. High repetition rate laser is firing ultrashort pulses into the sample. Part of the laser light is split off by a beamsplitter and directed to a fast photodiode, creating an electrical pulse. This pulse further goes into a discriminator that converts this pulse of unknown temporal shape into a digital 'start' signal. Start signal is used to start a time-to-voltage, or time-to-amplitude converter (TAC). TAC is a device that produces an analogue voltage signal proportional to the delay between two digital electronic pulses ('start' and 'stop'). It is, in essence, just a capacitor charged by a constant current, or ramp generator. Fluorescence photon emitted by the sample is captured by a sensitive photomultiplier (PMT), the signal of which is also processed by the discriminator and directed to the TAC as a 'stop' signal. As a result, TAC ends up holding a voltage, proportional to the duration between 'start' and 'stop' photon, or, in other words, the period of time between excitation and emission. This voltage is stored in a multi-channel analyzer – a device consisting of a series of counters, one of each is incremented every time a voltage signal is received. The number of counter incremented corresponds to the observed voltage: e.g. if the voltage is between 0 and 0.1 V, counter No.1 is incremented and if it is between 0.1 and 0.2V then counter No.2 is incremented, and so forth. This way, a fluorescence decay histogram is recorded: the counters corresponding to often observed delay times between the excitation and emission accumulate highest numbers, whereas the counters corresponding to seldom occurring delays see just a few photons.

$$Charge\ seperation\ rate \sim \frac{1}{\tau_1} - \frac{1}{\tau_2}$$

Where $\tau_1$ is the fluorescence lifetime of the quenched donor in presence of the acceptor (quencher) and $\tau_2$ is the unperturbed lifetime of the donor in absence of the quencher.

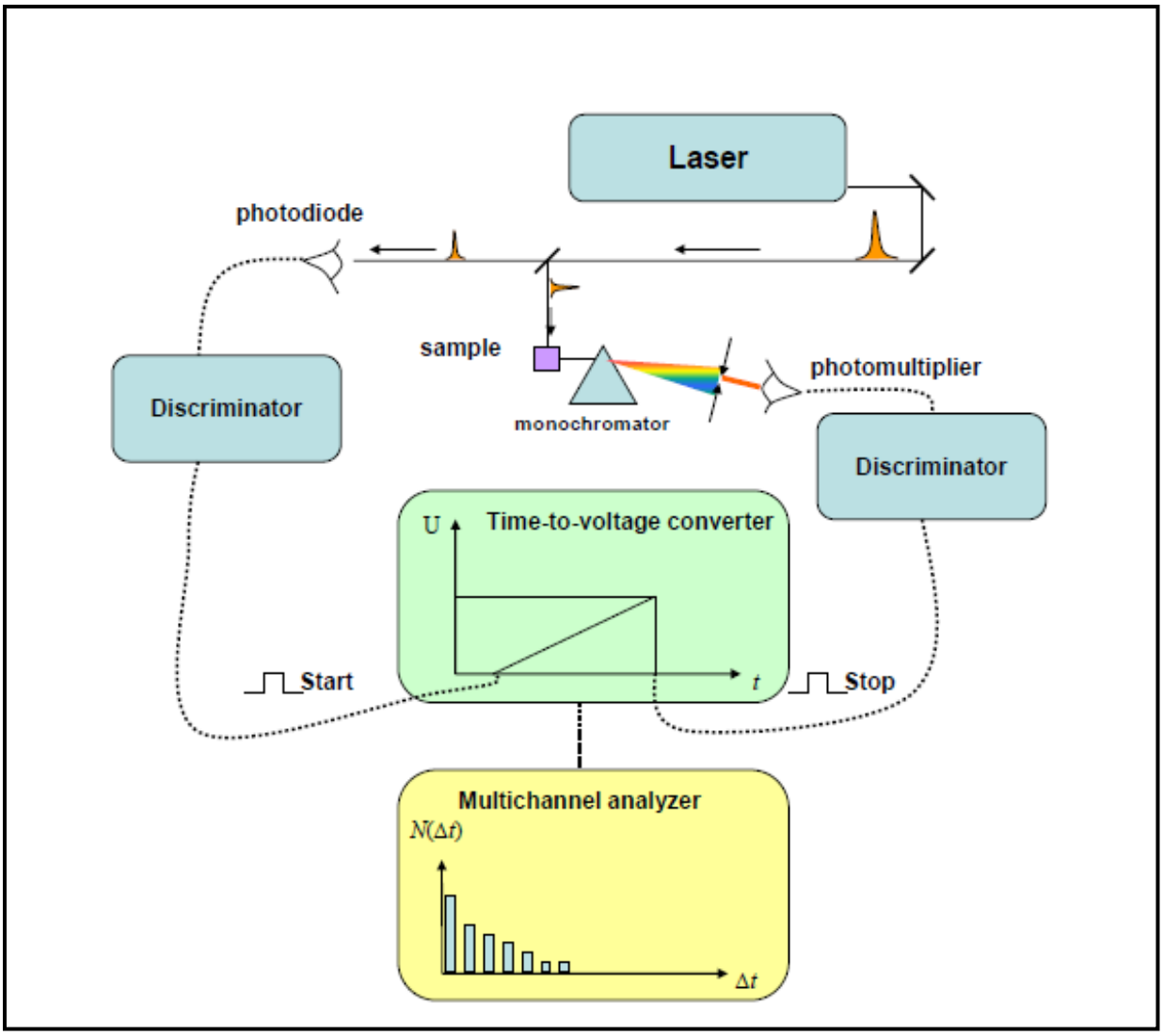


**Fig. 2.16.** The principle of time-correlated single-photon counting

In our experiment Fluorescence lifetime measurements are carried out by using the time correlated single photon counting method using HORIBA JOBIN YVON FLUOROCUBE. The quality of fit is assessed over the entire decay, including the rising edge, and tested with a plot of weighted residuals and other statistical parameters e.g., the reduced 2 and the Darbin–Watson (DW) parameters. The time resolution is ~ 20 ps and the excitation wavelength used is 375 nm and 455 nm with a diode laser.

## 5.2.3 Advantages of TCSPC

The main advantage of TCSPC is that it does not require intense excitation light. In each excitation pulse causes only one fluorescence photon to be detected. TCSPC is also completely insensitive to the stability of the laser pulse energy. The measurement is cumulative, i.e. one can count photons until the desired signal-to-noise ratio is reached, and the quality of the data allows answering the question posed by the experimenter.

Compared to the other time resolved spectroscopic methods, TCSPC is economical. It became popular after the advent of diode lasers providing laser pulses in the 100 ps range. Such lasers cost only a few percent the price asked for a 'real' ultrafast system. It also applied to the fluorescence life time measurement and it recorded by confocal microscope with time resolution. So, each pixel of fluorescence image contain decay information of the sample [15].

## 5.2.2 Disadvantages of TCSPC

Its main disadvantage is a limited time resolution. In fact it is not limited by the response time of the detector; the discriminators do not register the response itself, but rather fire their electronic pulses when the signal of the detector reaches a predefined percentage of the maximum. This way picosecond and nanosecond time resolution is accessible, even if the response of the detector to a light pulse is several microseconds. The measurement uncertainty comes from so called 'jitter', i.e. differences of signal shape from one pulse to another. Time resolution of TCSPC is usually measured by measuring the duration of light pulse elastically scattered by the sample. Scattering is an instantaneous process and its temporal shape is determined only by the time-response of the instrument. Another disadvantage of the TCSPC is the availability of single wavelength. At each time fluorescence kinetics is only registered at one detection wavelength.

## 5.3 Diode laser

A laser diode is electrically a P-I-N diode. The active region of the laser diode is in the intrinsic (I) region, and the carriers, electrons and holes, are pumped into it from the N and P regions respectively. While initial diode laser research was conducted on simple P-N diodes, all modern lasers use the double-heterostructure implementation, where the carriers and the photons are confined in order to maximize their chances for recombination and light generation. Unlike a regular diode used in electronics, the goal for a laser diode is that all carriers recombine in the I region, and produce light. Thus, laser diodes are fabricated using direct band gap semiconductors. The laser diode epitaxial structure is grown using one of the crystal growth techniques, usually starting from an N doped substrate, and growing the I doped active layer, followed by the P doped cladding, and a contact layer. The active layer most often consists of quantum wells, which provide lower threshold current and higher efficiency [16].

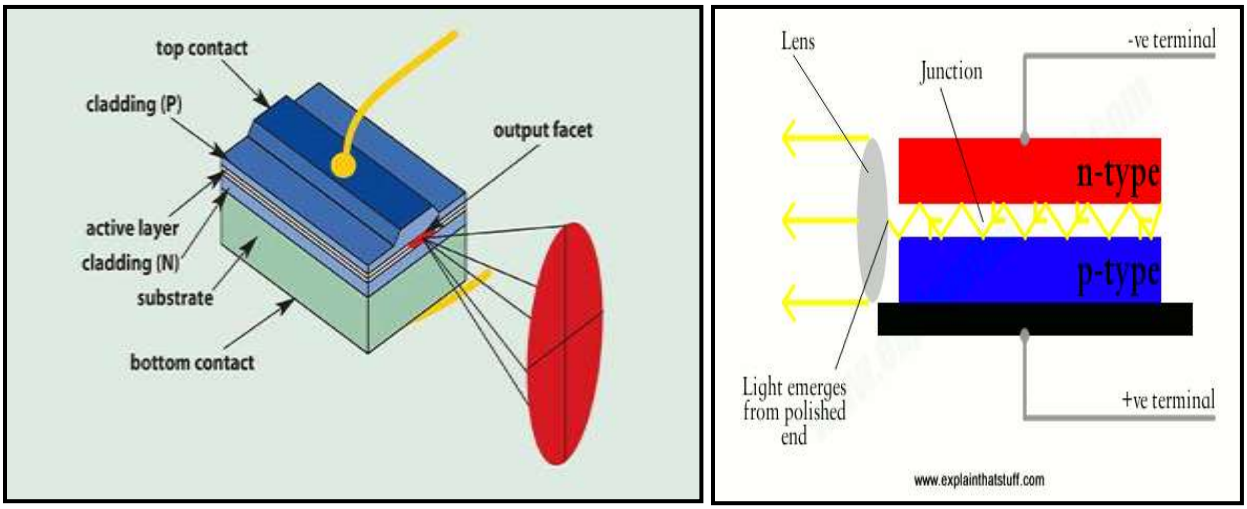


**Fig. 2.17.** Diode laser[17,18]

Laser diodes form a subset of the larger classification of semiconductor p-n junction diodes. Forward electrical bias across the laser diode causes the two species of charge carrier holes and electrons to be "injected" from opposite sides of the p-n junction into the depletion region. Holes are injected from the p-doped, and electrons from the n-doped, semiconductor. (A depletion region, devoid of any charge carriers, forms as a result of the difference in electrical potential

between n- and p-type semiconductors wherever they are in physical contact.) Due to the use of charge injection in powering most diode lasers, this class of lasers is sometimes termed "injection lasers" or "injection laser diode" (ILD). As diode lasers are semiconductor devices, they may also be classified as semiconductor lasers. Either designation distinguishes diode lasers from solid-state lasers.

## 6 . High resolution transmission electron microscope (HRTEM)

It is a modern cousin version of transmission electron microscopy (TEM). HRTEM is used for high magnification of nanomaterials. This high resolution makes HRTEM as a perfect imaging technique of nanomaterials in atomic scale. The TEM is a technique that uses energetic electron interaction with the sample and provides morphological, compositional, crystallographic information. In HRTEM, it uses both transmitted and scattered electron to produce an interference image. It is a phase contrast image and can be as small as the unit cell of a crystal. HRTEM has been extensively and successfully used for analyzing crystal structures and lattice imperfections in various kinds of advanced materials on an atomic resolution scale. It can be used for the characterization of point defects, stacking faults, dislocations, precipitates grain boundaries, and surface structures. The 2D spatial resolution of HRTEM is about 0.05 nm. In 3D crystal, it takes different view at different angles and combines them to produce a 3D map. This technique is called electron crystallography.

## 6.1 Working principle

Transmission electron microscope (TEM) has three essential sections:

1. The illumination system comprises of electron gun with two or more condenser lenses, which focuses electron beam on the sample. Here beam diameter is designed by specimen arrangement.
2. The specimen system may be stationary or moved slowly, as per requirement. The mechanical stability is an important part in determining the resolution of TEM.

3. The imaging system contains at least three lenses which produce magnified image of the sample on the fluorescent screen or on the monitor of an electronic camera system. This design of imaging lenses determines the special resolution of the microscope.

These components are discussed below.

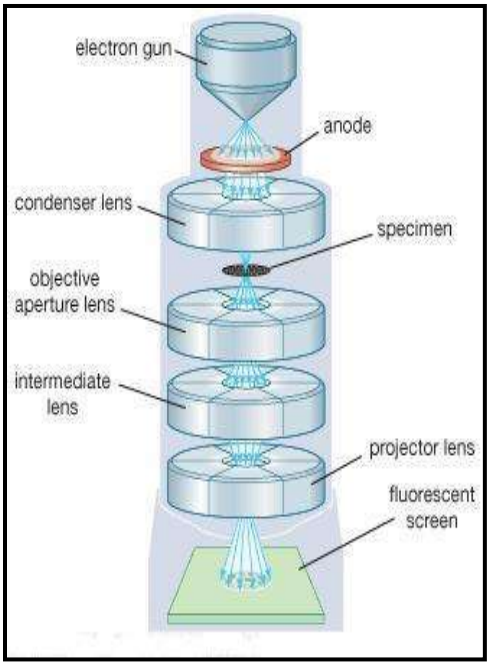


**Fig. 2.18.** Schematic diagram of HRTEM[19]

## 6.1.1 Illumination system

The electron beam produced by the electron gun has sufficiently high energy to pass through the sample specimen. This gun consists of electron source, cathode because it is at a high negative potential, and an electron-accelerating chamber. The electrons are emitted by thermonic emition. The electron source is a V-shaped filament made of tungsten wire, spot-welded to straight-wire leads that are mounted in a ceramic or glass socket. A direct (dc) current heats the filament to about 2700 K, at which temperature tungsten emits electrons into the surrounding vacuum. The filament of the electron gun can be made up of tungsten or lanthanum hexaboride ($LaB_6$). $LaB_6$ source it quite expensive than tungsten filament but it lasts long. The filament is

surrounded by a control grid, sometimes called a Wehnelt cylinder, with a central aperture arranged on the axis of the column; the apex of the cathode is arranged to lie at or just above or below this aperture. The cathode and control grid are at a negative potential equal to the desired accelerating voltage and are insulated from the rest of the instrument. After emission from the cathode, electrons are accelerated to their final kinetic energy $E_0$ with the help of an electric field parallel to the optic axis. This field is generated by applying a potential difference $V_0$ between the cathode and an anode. Anode is a round metal plate containing a central hole through which accelerated beam of electron emerges[20]. If the stabilization of the high voltage is adequate, pass through the central aperture at a constant energy. The control and alignment of the electron gun are critical in ensuring satisfactory operation.

In order to produce good quality magnified image of the sample, the condenser lense must contain at least two electron lenses. The first condenser lens is a strong magnetic lens. It uses virtual electron source and produce a real image. This lens current can be controlled by using spot size. Here second condenser lens is a weak magnetic lens, which produces little or no magnification. This lens contains a condenser aperture whose diameter can be changed to deviate the angle of illumination of electron form optic axis. The use of a small spot size minimizes disturbances in the specimen due to heating and irradiation. The illumination system also contain two pairs of coils that apply uniform magnetic fields in the horizontal (x and y) directions, in order to shift the electron beam (incident on the specimen) in the y and x directions, respectively. A second pair of coils is used to adjust the angle of the incident beam relative to the optic axis.

### 6.1.2 Specimen system

The specimen stage is designed to hold the specimen as stationary as possible, as any drift or vibration would be magnified in the final image. TEM specimens are always made circular with a diameter of 3 mm. Perpendicular to this disk; the specimen must be thin enough to allow electrons to be transmitted to form the magnified image. The specimen is placed initially and which can be evacuated before the specimen enters the TEM column. There are two basic designs of the specimen stage: side-entry and top-entry. In side-entry stage, the specimen is

clamped close to the end of a rod-shaped specimen holder and is inserted horizontally through the airlock and then activated by rotation of the specimen holder about its long axis. In top-entry stage, the specimen is clamped to the bottom end of a cylindrical holder that is equipped with a conical collar. The holder is loaded into position through an airlock by means of a sliding and tilting arm, which is then detached and retracted. Inside the TEM, the cone of the specimen holder fits snugly into a conical well of the specimen stage, which can be translated in the (x and y) horizontal directions by a precision gear mechanism.

### 6.1.3 Image producing system

The imaging system of TEM produces a magnified image of the specimen on the viewing screen or on the digital display system. The spatial resolution of the image is largely dependent on the quality and design of these lenses, especially on the first imaging lens i.e. objective lens. It is a strong lens, with a small focal length; because of its high excitation current. This lens must be cooled at room temperature to avoid drift in image due to thermal fluctuation. As the focusing power depends on lens excitation, hence current of the objective lens must be highly stabilized. The TEM also has fine controls that enable the operator to make small fractional adjustments to the objective current, to allow the specimen image to be accurately focused on the viewing screen. The first condenser lens with strong magnetic field has a strong focusing ability, so it's called condenser objective. The second condenser lens produces near parallel beam, which is used in analytical electron microscopy to obtain chemical information from very small regions of the specimen.

Accordingly, an electron that leaves the specimen parallel to the optic axis is deflected at the principal plane, at a focal distance below the principal plane. Using parallel illumination and correctly-adjusted tilt controls we can confine electrons to arrive at the specimen parallel to the axis and must remain unscattered during its passage through the specimen. When electron is scattered by one or more atoms of the specimen, it then leaves the specimen at same angle with the optic axis. Electrons scattered through larger angles are absorbed by the diaphragm surrounding the aperture and do not contribute to the final image. By making deflection angle

small, we can ensure that almost all scattered electrons are absorbed by the diaphragm. As a result, regions of specimen that scatter electrons strongly will appear as dark areas in the corresponding final image, which is said to display scattering contrast or diffraction contrast. In addition, this objective aperture limits the amount of image blurring that arises from spherical and chromatic aberration. In addition to this, electrostatic charging of contamination layers or hysteresis effects in the lens polepieces give rise to axial astigmatism that may be different for each specimen. So the TEM operator can correct for axial astigmatism in the objective using an objective stigmator located just below the objective lens. The stigmator controls are adjusted to minimize this streaking effect. Here we can also use a diaphragm, which limits the specimen region from which electron diffraction is recorded. Here electrons are transmitted through the aperture only if they fall within its diameter. So the introduction of this diaphragm provides diffraction information with good angular resolution, combined with good spatial resolution.

TEM system consists of several lenses between objective and final lens. This intermediate lenses serves mainly two purposes. First, by changing its focal length in small steps, image magnification can be changed, typically $10^3$ to $10^6$. Second, by making a larger change to the intermediate lens excitation, an electron diffraction pattern can be produced on the TEM viewing screen. Next there is a projector lens, which produces an image or a diffraction pattern across the entire TEM screen, with an overall diameter of several centimeters. Though, the final-image magnification is the algebraic product of the magnification factors of each of the imaging lenses.

## 6.2 Image Recording

The electron image is monochromatic and must be made visible to the eye either by allowing the electrons to fall on a fluorescent screen fitted at the base of the microscope column or by capturing the image digitally for display on a computer monitor. Computerized images are stored in a format such as TIFF or JPEG and can be analyzed or image-processed prior to publication. This electronic image recording is based on charged coupled diode (CCD) sensors, which contain an array of million photodiode. Electronic recording has numerous advantages. The recorded image can be inspected on a monitor screen, high magnification, makes focusing and

astigmatism correction a lot easier. The image information is stored digitally in computer memory and subsequently on magnetic or optical disks, from which previous images can be rapidly retrieved for comparison purposes. The digital nature of the image also allows various forms of image processing.

# References


1. K. K. Park, H. Jung, T. Lee, S. K. Kang, "Synthesis and structure of benzotriazolyl fluoresces", Bull. Korean Chem. Soc.,vol- 31, 984, 2010.
2. D.C. Marcano, D.V. Kosynkin, J.M. Berlin, A. Sinitskii, Z. Sun, A. Slesarev, L.B. Alemany, W. Lu and J.M. Tour, "Improved synthesis of graphene oxide", Am. Chem. Soc., vol-4, 8, 2010.
3. A. Mallick, A.S. Mahapatra, A. Mitra, J.M. Greneche, R.S. Ningthoujam and P.K. Chakrabarti, "Magnetic properties and bio-medical applications in hyperthermia of lithium zinc ferrite nanoparticle integrated with reduced graphene oxide", Journal of Applied Physics, 123, 055103, 2018.
4. T.D.W. Claridge, "High resolution NMR technique in organic chemistry ", Elsevier, vol-19, 2005.
5. E.D. Becker, "High resolution NMR: theory and chemical application", Third edition, Academic press, 2000.
6. https://medium.com/@ankur1857/principle-of-ultra-violet-uv-spectrophotometer-e6a1c435d258
7. https://bouman.chem.georgetown.edu/S00/handout/spectrometer.htm
8. Introduction to ultraviolet visible spectroscopy (UV); advancing chemical science, RSC, 2009.
9. L. Evans, "UV-VIS Spectrophotometry: A Brief Background to Spectrophotometry", Biochrom Ltd., Issue 1.0.
10. Y. Povrozin and B. Barbieri, "Fluorescence spectroscopy", J Wiley & Sons, vol-3, 2016
11. https://slideplayer.com/slide/4215694/
12. https://www.pharmatutor.org/pharma-analysis/draw-an-optical-diagram-of-spectrofluorometer
13. W. Becker, "Advanced time-correlated single photon counting applications", vol-111, DOI 10.1007/978-3-319-14929-5.
14. D.V. O'Connor and D. Philips, "Time correlated single photon counting", Academic press, 1984.
15. J. R. Lakowicz, "Principles of fluorescence spectroscopy", Third edition, 2006.

16. L. Coldren, S. Corzine, M. Mashanovitch, “Diode lasers and photonic integrated circuits”, Wiley, Second edition, 2012.
17. https://www.photonics.com/Articles/Semiconductor_Lasers_An_Overview_of_Commercial/a25099
18. https://www.explainthatstuff.com/semiconductorlaserdiodes.html
19. https://www.britannica.com/technology/transmission-electron-microscope
20. R. F. Egerton, “Physical principles of electron microscopy”, springer, 2005.

Chapter : 3

# *Effect of Graphene Oxide and Reduced Graphene Oxide on the energy storage capacity of a short chain dyad. A comparative study with the pristine dyad*

# Chapter 3 : Effects of Graphene oxide and Reduced Graphene oxide on the energy storage capacity of a short-chain dyad. A comparative study with the pristine dyad.

## 1. Introduction

Investigations on photoswitchableshort-chain dyads **[1-8]** are gradually becoming interesting topics of modern research due to their wide applications in molecular electronics, building of components of photovoltaic cells and artificial light energy converters, optical data storage devices etc. Recent studies by steady state and time resolved spectroscopic techniques demonstrate that when the short-chain dyads combine with nanoparticles of noble metals such as silver, gold , gold/silver core-shell nanocomposite systems **[2]** and carbon quantum dots **[1]** they exhibit efficient artificial light energy conversion materials. Investigations with the dyad MNTMA, where methoxynaphthalene donor is attached with the electron acceptor p-methoxyacetophenone, it was observed **[3]** that the dyad, in its pristine form, does not suffer any conformational changes even on photoexcitation. But when the dyad combines with the noble nanometals, significant conformational changes in the excited states occur. In these changes, the elongated conformer of the dyad facilitates the lowering of the energy destructive charge recombination rate processes as the two redox components donor and acceptor move far away from each other minimizing the overlapping of the charge clouds of both the redox components. In the present investigation, a novel synthesized dyad, organic (E)-4-(((9H-fluorene-2yl)imino)methyl)- N,N-dimethylaniline (NNDMBF) has been chosen where N,N-dimethyl amino donor (NNDMB) is being attached with the acceptor fluorene (F) **(Fig. 3.1a**) . Our primary aim is to perform comparative analysis to examine the suitability for designing efficient artificial light energy converter when it is in its pristine form and when combined with

graphene oxide (GO) and reduced graphene oxide (RGO) nanoparticles. From the NMR analysis it is apparent that there is a possibility of the co-existence of two conformers: Trans- and Cis- (**Fig. 3.1b**) of the dyad in its ground state. Detailed steady state and time resolved spectroscopic measurements were made to determine the two parameters, charge separation ($k_{CS}$) and energy wasting charge recombination rates ($k_{CR}$), without and in presence of GO and RGO to compare the efficiency of light energy conversion of the pristine dyad and when it adsorbs the nanosurfaces of GO and RGO ie., of the same dyad in nanocomposite forms.

## 2. Experimental details

## 2.1. Materials

The method of synthesis and characterization of the short chain dyad (E)-4-(((9H-fluorene-2-yl)imino)methyl)-N,Ndimethylaniline(NNDMBF) are described elsewhere [9]. The solvents acetonitrile (ACN) (SRL), and cyclohexane (CH) (Sigma Aldrich) of spectroscopic grade were purified following the standard procedures and tested before use for the absence of any impurity emission in the concerned wavelength region. Water was deionized using a Millipore Milli-Q system. The solutions were prepared by dissolving the appropriate amount of dyad in ACN and CH.

### 2.1.1 Graphene Oxide (GO) Synthesis Procedure

Here, 2g of graphite powder was mixed with 1g of $NaNO_3$by keeping it in an ice bath. Now, concentrated $H_2SO_4$ (130 ml) was added to the mixture under a stirring condition. Under the vigorous stirring condition, 6 g of $KMnO_4$ was added slowly maintaining the reaction temperature of the mixture around $20^0$ C. Gradually, the reaction temperature was elevated up to 40 $^0$C and stirred for 6 h. At this stage, the colour of the mixture changes from dark grey to

grayish green. An additional 6 g of $KMnO_4$ were added to the mixture and stirred for another 6 h so that the color of the mixture becomes grayish brown. Now, 250 ml of triple distilled water was slowly added to the solution which raises the temperature of the solution to around 96 $^0$C at which the mixture was stirred for 30 min. The solution was then cooled down to room temperature. Now, an additional 500 ml triple distilled water and 15 ml 30% $H_2O_2$were added to the solution to stop the oxidation. At this stage, the color of the solution becomes yellow ochre signifying the high oxidation level of graphite. The yellow solution was washed two times with 1M HCl solution and repeated washing was done with tripledistilled water until a pH of 5 was obtained. This was doneby centrifugation of the solution and decantation of thesupernatant. A rigorous washing and decantation step is necessaryto exfoliate the graphene oxide layers and to removethe unexfoliatedgraphene oxide layers. The thick yellowbrown gel was filtered and dried overnight to get a fine yellowgraphene oxide (GO) powder.A stoichiometric amountof GO was then taken in triple distilled water and ultrasonicatedfor 30 min to get a homogeneous solution [10].

## 2.1.2 Reduced Graphene Oxide (RGO) Synthesis Procedure

Bulk samples (GO) of the oxidized materials were reduced using hydrazine hydrate and then annealed at 300 and 900 °C in $Ar/H_2$. In general, for the hydrazine reduction, 100 mg of the improved GO materials is dispersed in 100 ml DI water, stirred for 30 min and then 1 ml of hydrazine hydrate is added. The mixture is heated at 95 $^0$C using water bath for 45 min, a black solid precipitated from reaction mixture. Products are isolated by filtration and washed with DI water, producing 54 mg of chemically reduced improved GO (RGO). After reduction no signal from oxidized carbon is detected by NMR spectra. This indicates the quality of RGO is very good. From AFM data we can say that individual flacks of RGO have a thickness ranging from 1 to 3 nm [11]. The measured lattice spacing value is 2 Å using HRTEM.

## 2.2. Spectroscopic Apparatus

UV–vis absorption and steady state fluorescence emission spectra of dilute solutions of the dyad were recorded at the ambient temperature (296 K) using 1 cm path length rectangular quartz cells by means of an UV–vis absorption spectrophotometer (JASCO UV–Vis absorption spectrometer, Model: V-630) and JASCO spectrofluorimeter Model: 8200) respectively.

Fluorescence lifetimes were determined by using a time correlated single-photon-counting (TCSPC) technique with the model FLUOROLOG TCSPC HORIBA JOBIN YVON using nanosecond diode lasers of 375 nm and 440 nm(Horiba scientific, DD-375L) as excitation source profiles. The decay kinetics are monitored at emission wavelengths of 480 nm and 550 nm. The quality of fit is assessed over the entire decay, including the rising edge, and tested with a plot of weighted residuals and other statistical parameters e.g., the reduced $\chi 2$ and the Durbin–Watson (DW) parameters. All the solutions prepared for room temperature measurements were deoxygenated by purging with an argon gas stream for about 30 min.

## 3. Results and discussion

## 3.1 UV-Vis Absorption and Steady State Fluorescence Measurements

From the theoretical computations on ground state optimized geometry of the dyad NNDMBF (**Fig. 3.1a and 3.1b**), by using BL-LYP/6-311 g (d,p) level of theory on HOMO – LUMO surfaces it appears that there may be the two types of conformers Cis- and Trans- , in which the latter form is found to be more stable in the ground state. Thus the above theoretical predictions suggest that both cis- and trans- forms of the dyad exist in the ground state (Fig. 3.2) with the preponderance of the latter. Moreover trans-form of the dyad NNDMBF appears to be more planar.

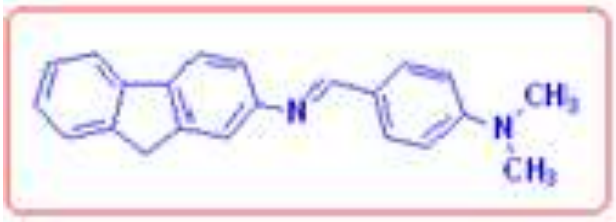


**Fig. 3.1a.** Molecular structure of the dyad NNDMBF

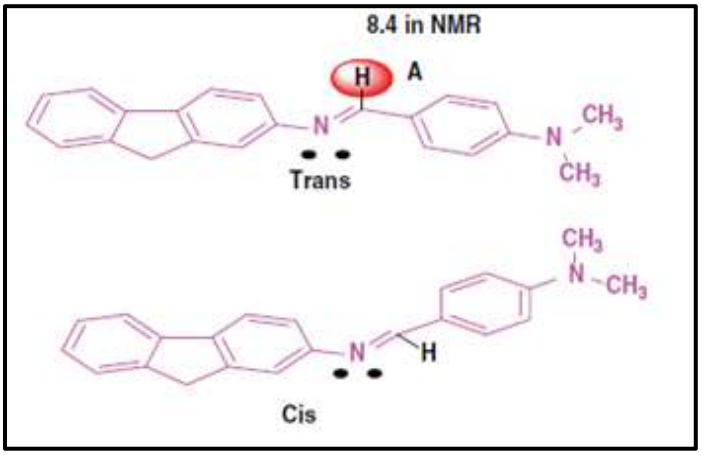


**Fig 3.1b.** Cis- and Trans-structure of the dyad

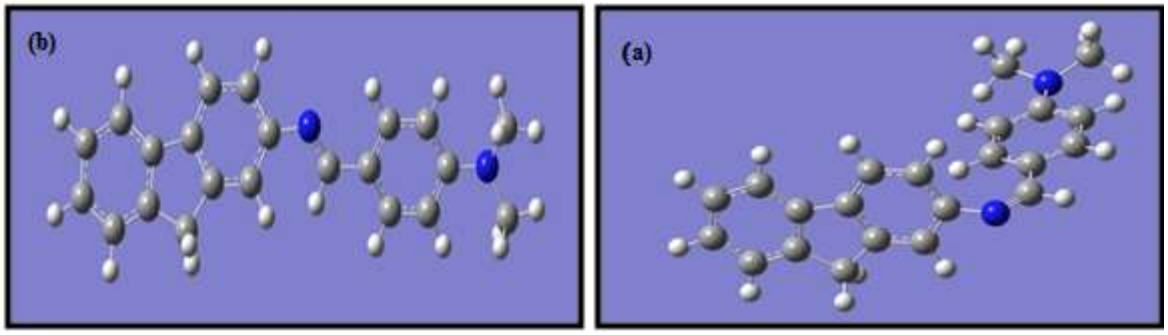


**Fig. 3.2 (**a)Cis form of dyad NNDMBF in vacuum**;**(b) Trans form of dyad NNDMBF in vacuum

Trans-form of the dyad appears to be more planar than the cis-one.

UV-vis absorption spectra of the pristine dyad in ACN solvent exhibits a broad long wavelength band at around 365 nm region **(curve 1 of Fig. 3(a))**. The charge transfer nature of this broad band has been confirmed from solvent polarity effect which shows blue shift in nonpolar environment relative to ACN solvent. This CT band originates due to partial transfer of electron from the highest occupied molecular orbital (HOMO) of the donor chromophore (D) to the lowest unoccupied molecular orbital (LUMO) of the acceptor fluorene (A). It is to be pointed out here that the UV-vis absorption spectra of the mixture of the free donor and acceptor components (when not present in the dyad) in ACN medium correspond to the superposition of the corresponding spectra of the donor and the acceptor moieties (**Fig. 3.3(c)**).

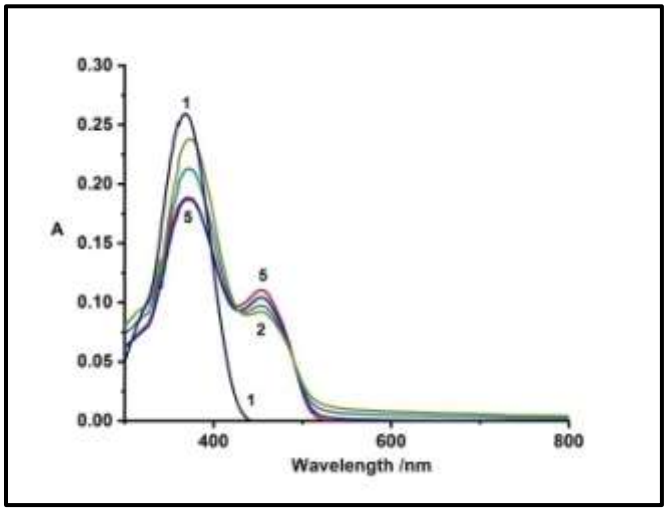


**Fig. 3.3 (a)** UVvis absorption spectra of the dyad NNDMBF in ACN in presence GO whose concentration (µg/ml) in 1:0; 2:0.5 ; 3: 1 ; 4: 1.5 ; 5:2.5at the ambient temperature.

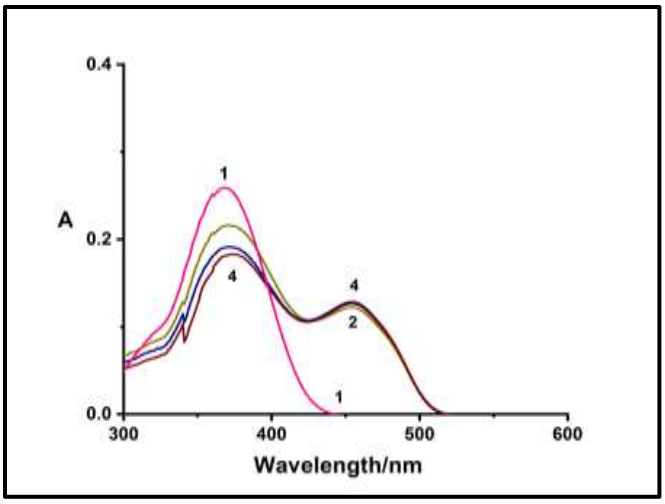


**Fig. 3.3 (b)** UVvis absorption spectra of the dyad NNDMBF in ACN in presence RGO whose concentration (µg/ml) in 1: 0; 2:3 ; 3: 4 ; 4:5 at the ambient temperature.

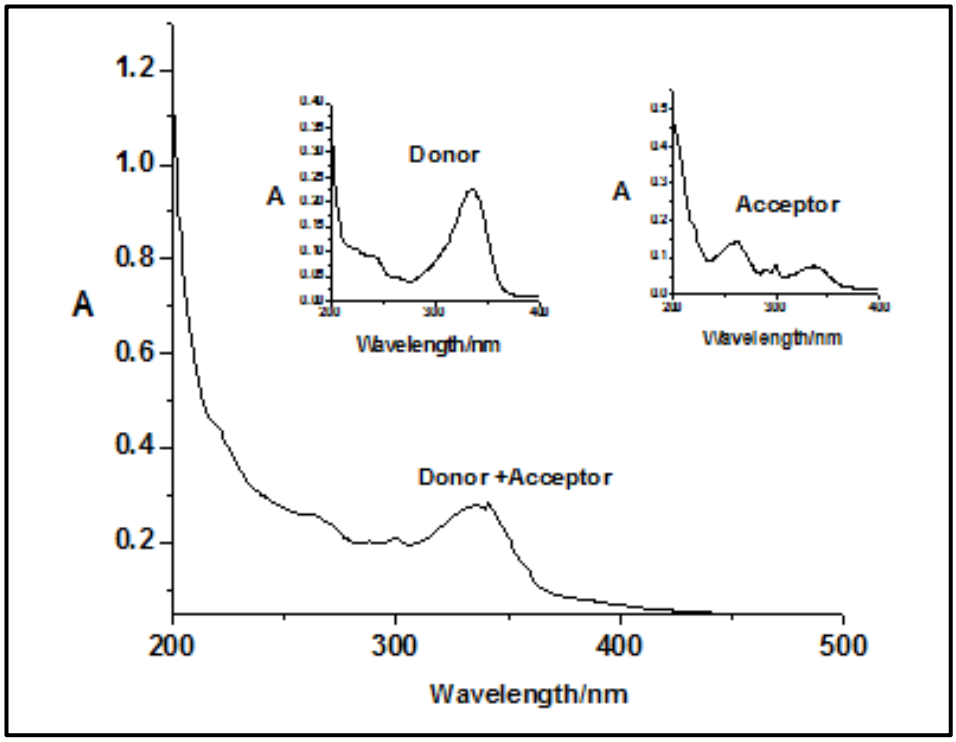


**Fig. 3.3(c).** UV-vis absorption spectra of the mixture of the donor and the acceptor in ACN medium. Inset: (right) UV-vis spectra of the acceptor and (right) UV-vis spectra of the donor only

This indicates the lack of formations of any interrmolecular ground state complex between the donor NNDMB and acceptor (F). However, in case of the dyad, intramolecular interaction between the donor NNDMB and the acceptor Fluorene (F) leads to the formation of Charge transfer band (broad band at 365 nm region). This indicates that within the dyad, the alignment of the donor and the acceptor moieties are such that it facilitates the formation of CT spectra in the ground state.

With addition of GO (**Fig. 3.3(a)**) or RGO **(Fig. 3.3(b))**, 365 nm band diminishes gradually with the concomitant development of another band near 440 nm region. Following the observations made earlier with gold nanoparticles of different morphologies, it appears that when the dyad adsorbs on the surface of GO or RGO, the band associated with the cis- conformation develops, peaking at about 440 nm, through interconversion (trans to cis) process in the ground state.

On exciting the CT absorption band of the dyad NNDMBF-GO (or RGO) system (CT nature has been conformed from the solvent polarity effect) at 365 nm region, CT fluorescence band peaking at around 470 nm was observed (**Figs 3.4 (a**) **and 3.4(b)))** along with a very weak shoulder –like band at 550 nm. The 470 nm as well as 550 nm band become gradually enhanced

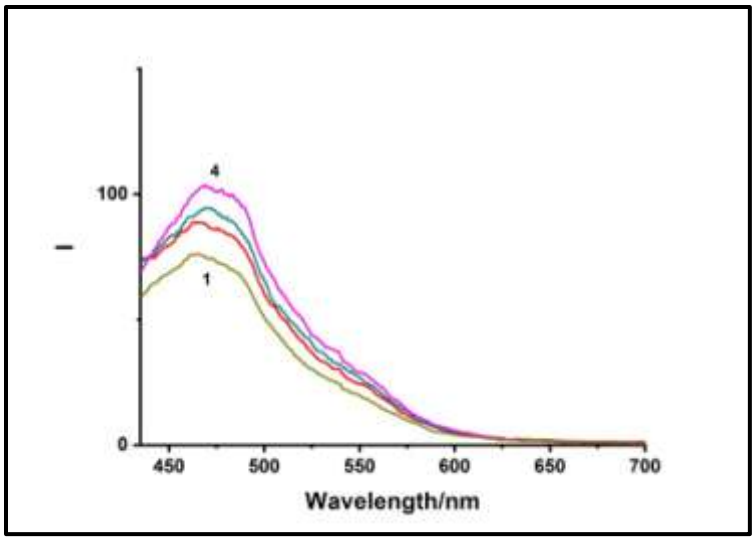


**Fig. 3.4(a)** Fluorescence CT emission spectra (exc~ 365 nm) of dyad NNDMBF in presence of GO nps of conc. (µg/ml) in 1: 0; 2: 1;3:2;4: 2.5 at the ambient temperature.

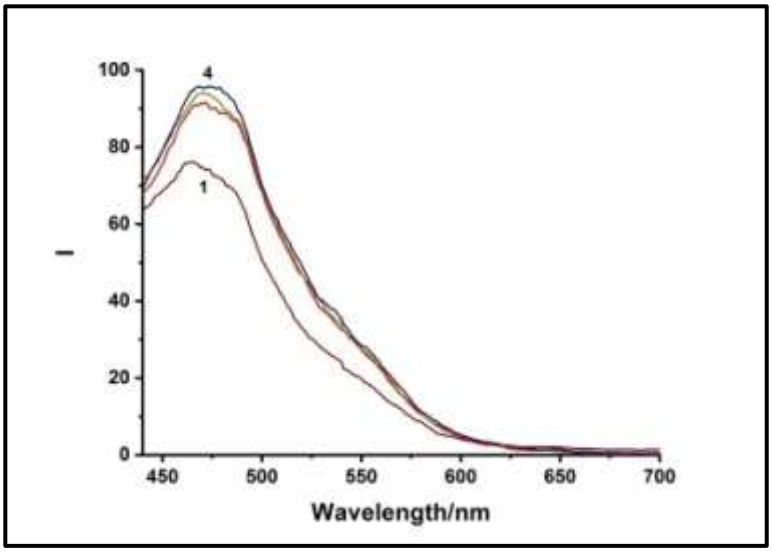


**Fig. 3.4(b)** Fluorescence CT emission spectra (exc~ 365 nm) of dyad NNDMBF in presence of RGO nps of conc. (µg/ml) in 1: 0; 2: 4;3: 5at the ambient temperature.

with increase of concentrations of GO **(Fig. 3.4(a))** or RGO**(Fig. 3.4(b))**. The above findings demonstrate that even with the 365 nm excitation (region of mostly trans-isomers)emitting region of cis-isomer at 550 nm appear to be formed in the excited state. This observation demonstrates thatphotoswitchable conversion of the trans-dyad to the cis-form facilitates when

combined with graphene nanoparticles, GO and RGO. From the observed enhancement of the fluorescence band throughout its entire region **(Figs 3.4(a) and 3.4 (b))** indicates that both trans- and cis –species are formed by exciting the ground state trans-conformers.

On the other hand, when the excitation was made at 440 nm wavelength (the region of cisisomer of UV-vis absorption spectra) of CT absorption band of the dyad-GO (or RGO) system, the CT fluorescence emission mostly originates from 550 nm region (**Fig. 3.4(C))** indicating in this region mostly excited cis-isomeric species of the dyad predominates.

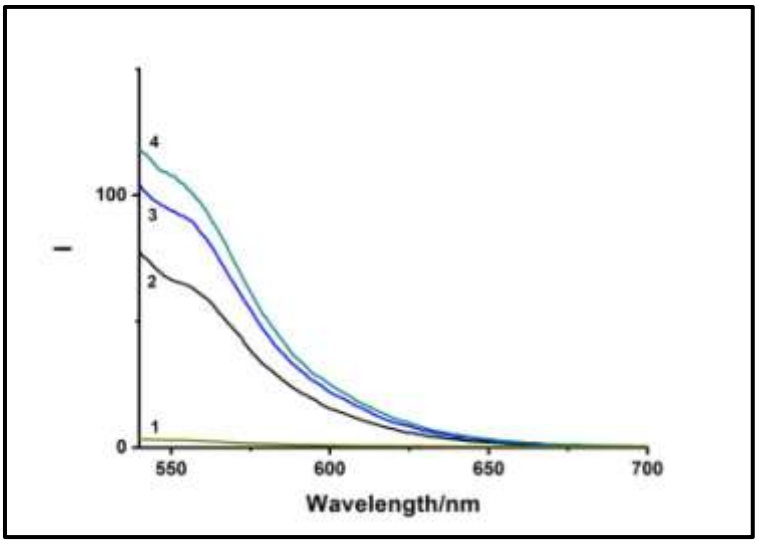


**Fig. 3.4(c)** Fluorescence emission spectra (exc~ 450 nm) of dyad NNDMBF in presence of GO of conc. (µg/ml) in 1:0; 2:0.5; 3:1.5; 4: 2 at the ambient temperature.

From this Fig. it is apparent that though the pristine dyad (curve 1 of **Fig. 3.4c**) exhibits very weak emission at 550 nm but the emission becomes significantly strong when the dyad adsorbs the surface of GO or RGO. This indicates in this environment formation of cis-isomer facilitates largely and the production of cis-species in the excited state occur directly from the ground state cis-isomer and also from ground trans-isomer through interconversion process. This observation indicates the photoswitchablecharacter of the dyad NNDMBF.

The fluorescence excitation spectra of the pristine dyad and its nanocomposite forms with GO and RGO were measured by monitoring at 480 nm and 550 nm wavelengths (**Figs. 3.5 a -d)**. In the cases of the monitoring wavelengths 480 nm and 550 nm (**Fig. 3.5aand b)** the observed excitation spectra correspond well to the CT absorption band of the dyad-GO system where both the bands at 365 nm and 440 nm region were present. In the case of the pristine dyad (where no GO and RGO were present) the excitation spectra show only 375 nm band, which corresponds only CT absorption species having trans-nature whatever be the monitoring wavelength 480 nm or 550 nm. This observation infers that in the case of the pristine dyad, the excited cis-species are mostly formed due to photoconversion originate from the ground state trans-isomers. In the case of the nanocomposite dyads (dyad-GO or dyad-RGO), from the **Figs. 3.5b and d** where monitoring wavelength is at 550 nm, the region of mostly cis-conformer) the excitation spectra clearly show that cis-forms in the excited state are produced from the ground trans-state on photoexcitationie., through interconversion processes. Moreover, presence of 440 nm band in the excitation spectra (possesses clear resemblance with the corresponding absorption spectra of the nanocomposite dyad) indicates that some direct conversion of ground state cisto excited cis is also possible. **Fig. 3.5** of excitation spectra clearly demonstrates that the steady state intensities of two excited conformers, trans-and cis-, could be varied by changing the excitation wavelength from 375nm (region of mostly trans-isomer) to 440 nm regime, the domain of primarily cis-conformers. The fluorescence lifetime measurements by TCSPC techniques further corroborate this view.The results obtained from TCSPC method has been discussed below.

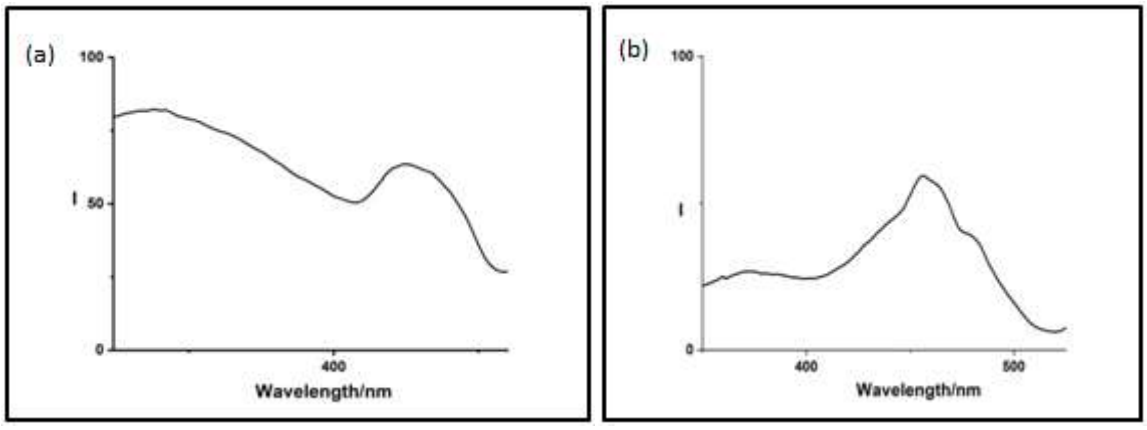

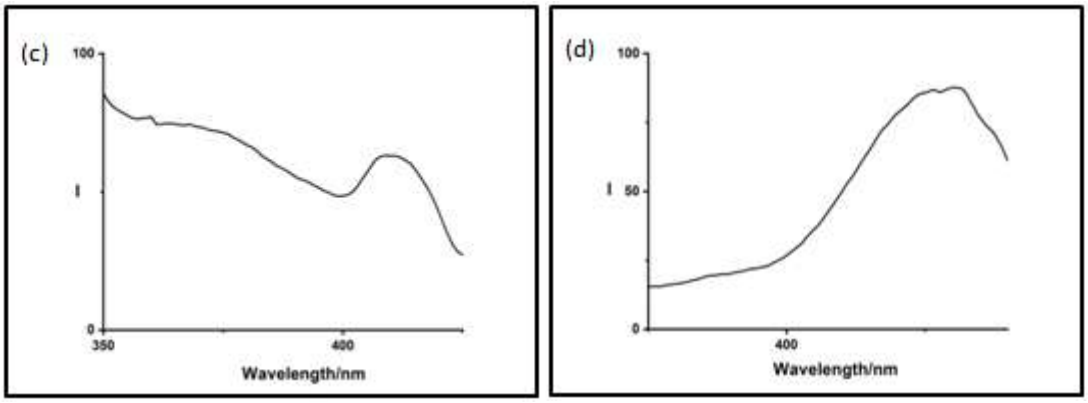


**Fig. 3.5** Fluorescence excitation spectra of the dyad-GO nanocomposite system in (a) mon wavelength ~ 480 nm, (b) mon wavelength ~ 550 nm and Fluorescence excitation spectra of the dyad –RGO nanocomposite system in ( c ) mon wavelength ~ 480 nm, (d) mon wavelength ~ 550 nm (mon wavelength ~ monitoring wavelength)

## 3.1 Fluorescence lifetime measurements by TCSPC method

Measurements of the fluorescence lifetimes of the dyad were made by using the time correlated single photon counting (TCSPC) technique. By monitoring the different positions of the steady state fluorescence spectra the possibility of formations of different conformer, apart from trans- one, in the excited state due to photoexcitation has been examined. These findings further provide us the idea that the present short-chain dyad NNDMBF possesses photoswitchable character, especially in its pristine form.

When excitation was made at 375 nm (using diode laser) in case of the pristine dyad NNDMBF, it was found that at the monitoring wavelength 480 nm (the peak region), majority emission originates from a species having lifetime of 15 ps. (**Table 1**).

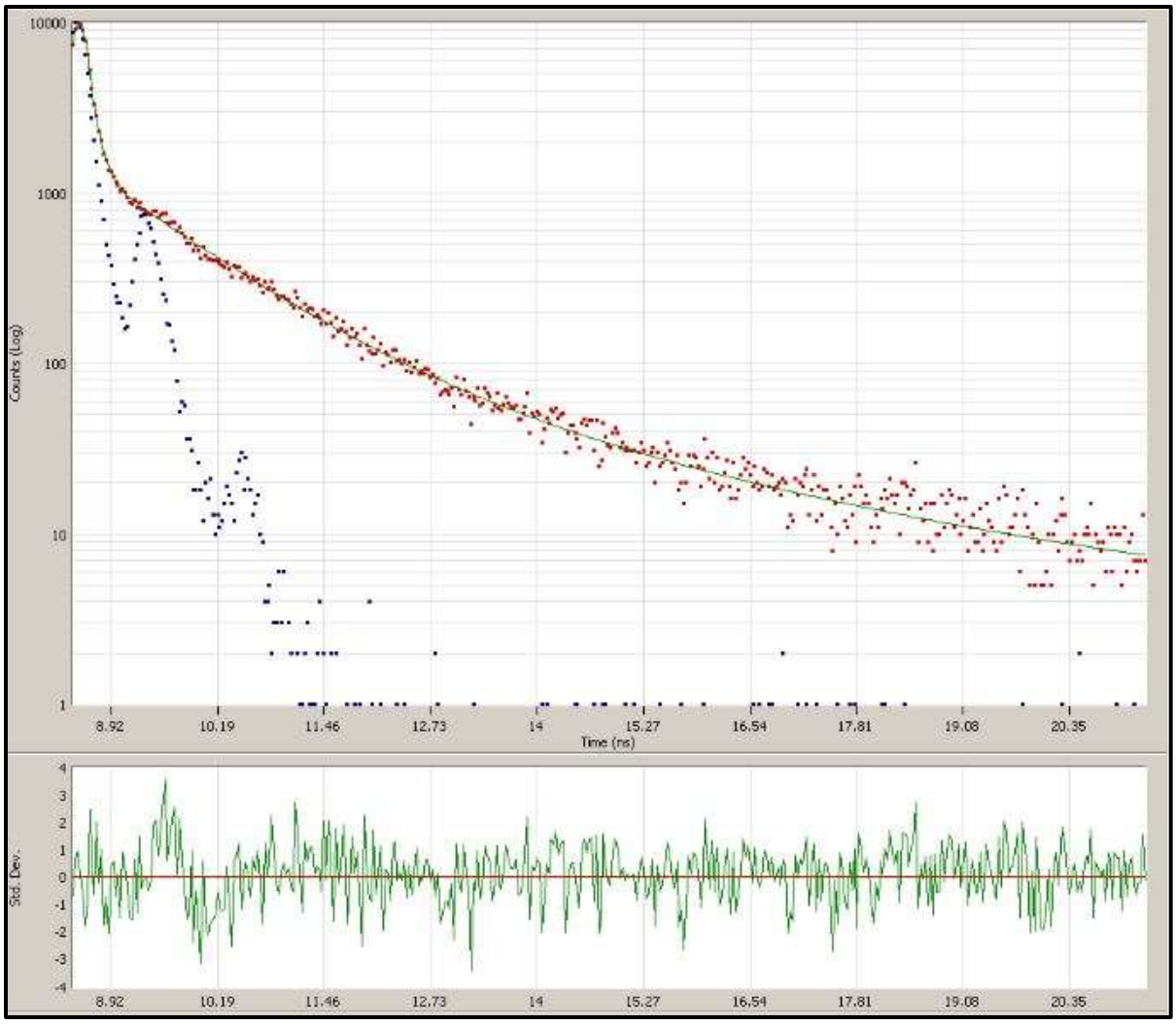


**Fig. 3.6(a)** Fluorescence decay of the dyad –GO system in ACN ex =375 nm, em = 480 nm, the fast (blue) decaying component represents impulse response (diode laser) ($\chi^2$~ 1.196). The residual is also shown.

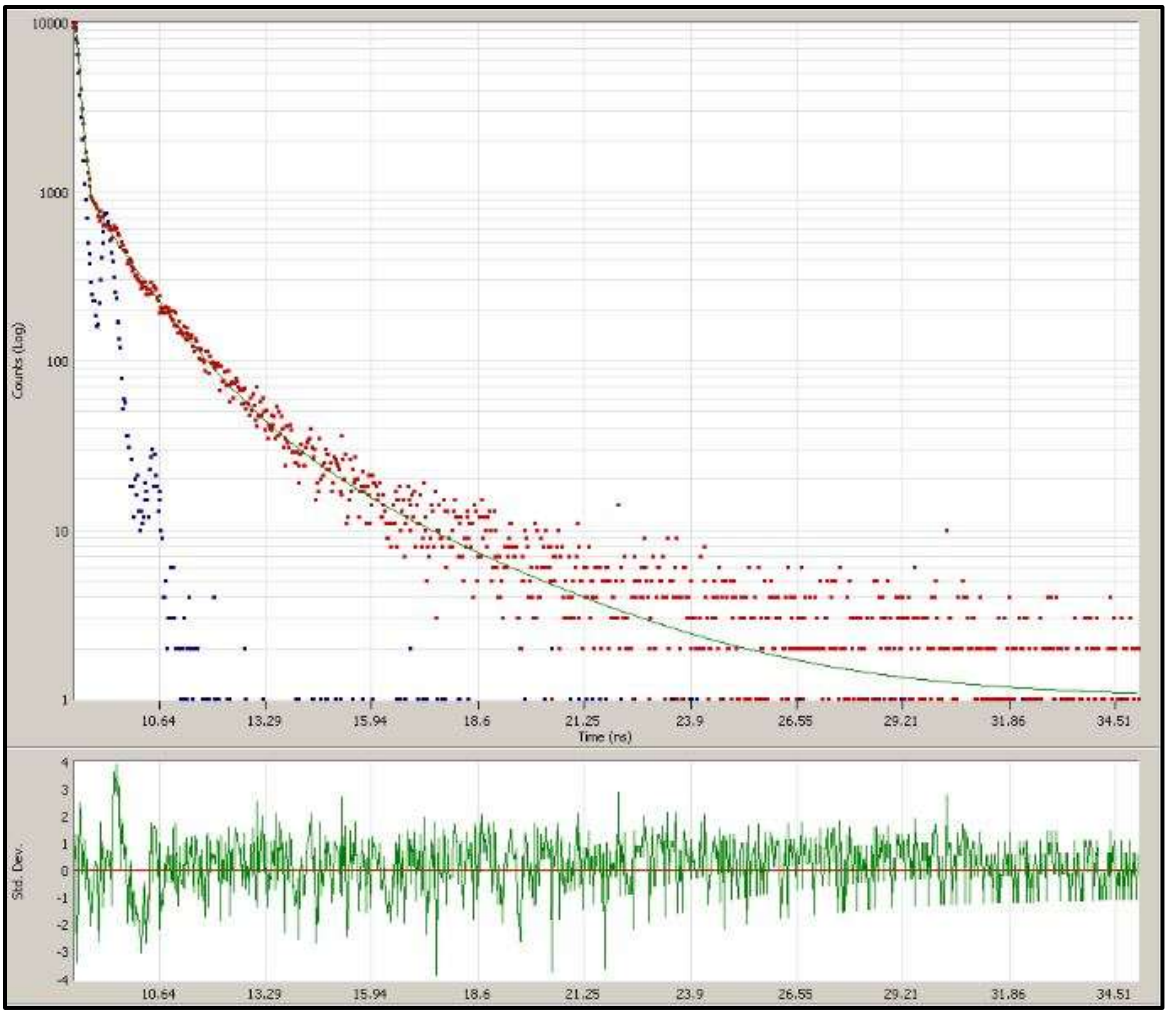


**Fig. 3.6(b)** Fluorescence decay of the dyad-RGO in ACN ex =375 nm, em = 480 nm, the fast (blue) decaying component represents impulse response (diode laser) ($\chi^2$~1.143). The residual is also shown.

On monitoring at the 550 nm region again only faster component of lifetime of picoseconds (ps) order was observed. We measured the fluorescence lifetimes of the dyad in presence of GO or RGO (nanocomposite systems)by using the excitation wavelength at 375 nm, the region of mostly trans-isomer. By monitoring at the different positions of the steady state fluorescence band on the longer wavelength side of the excitation wavelength 375 nm, primarily two lifetimes, one in the range of nanoseconds (slower component) and the other in picoseconds range (faster component) wereapparent (**Table 1**). By exciting the 440 nm wavelength and

monitoring at 550 nm region, mostly picosecond component was apparent. This it appears that the picoseconds species, in high probability, should originate from cis-conformers which are of folded nature. Another interesting findings are that in presence of both GO and RGO (Table 1) contribution from the faster component (~ps order) decreases, though the decrement is not very significant, along with concomitant increase of the slower component (in ns order).as one moves from 550 nm to the peak position of 480 nm of the dyad fluorescence emission band produced by the excitation at 375 nm.

Hence the above findings demonstrate that when the trans-type dyad in its pristine form is excited by using 375 nm wavelength, most ground state trans isomers convert to the cis-type isomers having faster component (~ ps) lifetime. Thus the dyad NNDMBF appears to behave as photoswitchable dyad. However, when the dyad combines with GO or RGO nanoparticles, some amounts of slower component species, appearing to possess trans-type structure, are found to be present along with the faster component which corresponds to cis-isomer. Thus , by developing nanocomposite systems with graphenes, photoconversion (from trans to cis) could be retarded though not significantly unlike the situation observed in the cases of dyad-CQDs systems where more than 80% trans-conformation formed in the ground state could be retained even on photoexcitation. Thus dyad- CQDs systems appear to be more efficient light energy converter than dyad-GO (or RGO) nanocomposites as in the former case elongated nature (trans) of the conformers help to retard energy wasting charge recombination processes.

**Table 1:** Fluorescence Lifetime data of the the short chain dyad NNDMBF in absence (pristine) and presence of GO and RGO at the different excitation and emission wavelengths at the ambient temperature. Values in parentheses besides lifetimes correspond to fractional contributions (f) of the particular species in the total steady state fluorescence emission intensity

| Samples | $\lambda_{exc}$ (nm) | $\lambda_{em}$(nm) | $\tau_1$ /ns ($f_1$) | $\tau_2$ ($f_2$) | $\chi^2$ |
|---|---|---|---|---|---|
| Dyad in ACN | 375 | 480 | - | 15ps (1.0) | 1.088 |
| | | 550 | - | 1.9ps (1.0) | 1.092 |
| | 440 | 550 | - | - | --- |
| Dyad + GO ($1x10^{-6}$ M) | 375 | 480 | 3.61(0.21) | 91 ps(0.79) | 1.080 |
| | | 550 | 3.44 (0.17) | 82 ps(0.83) | 1.09 |
| | 440 | 550 | 3.01 (0.09) | 100 ps (0.91) | 1.16 |
| Dyad + RGO ($4\times10^{-6}$ M) | 375 | 480 | 3.61(0.27) | 88 ps (0.73) | 1.138 |
| | | 550 | 3.00 (0.13) | 87 ps(0.87) | 1.18 |
| | 440 | 550 | 3.00 ( 0.10) | 100 ps (~0.90) | 1.178 |

.

Thus the experimental observations made from the fluorescence lifetime measurements reveal that though trans-isomer primarily dominates in the ground state but on photoexcitation, most of the trans components convert (photoconversion) to the cis-form in the excited level. However this photoconversion is somewhat impeded when the dyad adsorbs the GO and RGO nanoparticles.

From the above results and following the observations made earlier [1] it could be hinted that relatively stable trans-conformer in the excited state in case of the nanocompositedyad NNDMBF-GO (or RGO) in comparison to the pristine form may arise from the surface trap effects **[12]**. The phenomenon should be clearly understood if one compares with dyad-CQD systems where the situations were more prominent. As smaller size of carbon quantum dot (CQD) **[13]** (~2-5 nm) relative to GO or RGO, a larger fraction of the atoms in the former case being on the surface may form electronic states which may act as traps **[14]** for electrons or holes . These trap states may hinder the photoconversion of trans-to cis- isomeric forms of the dyad.

As the theoretical predictions along with the steady state and time resolved spectral measurements clearly reveals that though in the ground state trans-isomer of the dyad prevails but on photoexcitationcis-isomeric species of the dyad predominates and this cis-form having folded nature generates from the relatively planar trans conformer through interconversion processes. In presence of GO and RGO, the photoconversion is somewhat hindered resulting the presence of excited trans-isomers along with the cis-ones.The hindrance effect for photoconversion is not as efficient as observed in the case of carbon quantum dots (CQDs) where more than 80% of the ground state trans-conformers were able to retain their identity of trans-configuration even on photoexcitation. Thus dyad-CQD systems appear to be better artificial light energy conversion devices relative to the present dyad-GO or RGO nanocomposites. However, if the light energy conversion efficiencies of the dyad-GO or the dyad-RGO is compared with the pristine dyad system, the former looks better light energy converters due to ability of retention of trans-conformers even on photoexcitation, though in small amount as evidenced from low value of fractional contributions, f, (Table 1). This conformation will help to impede energy wasting charge recombination processes and may serve as better candidate for artificial light energy conversion systems relative to its pristine form.

## Conclusions

On comparing the dyad-GO or the dyad-RGO systems with the pristine dyad, the former looks better light energy converters due to ability of retention of trans-conformers even on photoexcitation, though in small amount as evidenced from low value of fractional contributions, f, (Table 1). This trans conformation being of elongated nature, where the redox partners the donor and the acceptor within the dyad would be far apart, will help to impede energy wasting charge recombination processes within the electron donor and acceptor moieties and may serve as better candidate for artificial light energy conversion systems relative to its pristine form which on photoexcitation converts mostly into folded structure cis-form from its ground extended trans-structure.

## References


1. I. Mitra, S. Paul, M. Bardhan, S.Das, M.Saha, A.Saha and T. Ganguly, "Effects of carbon quantum dots (CQD) on the energy storage capacity of a novel synthesized short-chain dyad", Chem, Phys Letts, 726, 1, 2019.
2. G. Dutta (Pal), S. Paul, M. Bardhan, A. De, and T. Ganguly, "Designing of an artificial light energy converter in the form of short chain dyad when combined with the core-shell gold/silver nanocomposite", SpectrochimicaActa Part A, 180, 168, 2017.
3. G. Dutta (Pal), P. Chakraborty , S. Yadav, A. De, M. Bardhan, P. Kumbhakar,S. Biswas, H.S. DeSarkar, and T. Ganguly, "Time resolved spectroscopic investigations to compare photophysical properties of a short chain dyad when combined with silver and gold nanoparticles to form nanocomposite system", J NanosciNanotechnol, 16, 7411, 2016.
4. G. Pal, A. Paul, S. Yadav,M.; Bardhan, A.. De, J. Chowdhury, A. Jana, and T. Ganguly, "Time resolved spectroscopic studies on a novel synthesized photo-switchable organic dyad and its nanocomposite form in order to develop light energy conversion device", J Nanosci Nanotechnol, 15, 5775, 2015.
5. G. Zaragoza-Galán, J. Ortíz-Palacios , B.X. Valderrama , A.A. Camacho-Dávila , D. Chávez-Flores , V.H. Ramos-Sánchez , and E. Rivera, "Pyrene fullerene $C_{60}$ dyads as light harvesting antennas", Molecules, 19, 352, 2014.
6. S. Bhattacharya, T.K. Pradhan, A. De, S.RoyChowdhury, A.K.De, and T. Ganguly, "Photophysical process involved within the Anisole-Thioindoxyl dyad system", J Phys Chem A, 110, 5665, 2006.
7. E. Allard, J.Cousseau, J. Ordúna, J. Garín, H. Luo, Y. Araki, and O.Ito, "Photoinduced electron transfer processes in C60-Tetrathiafulvalene dyad containing a short or long flexible spacer", Phys. Chem. Chem. Phys., 4, 5944, 2002.
8. S. Fukuzumi, K. Ohkubo, H. Imahori, J. Shao, Z.Ou, G. Zheng, Y. Chen, R.K. Pandey, M. Fujitsuka, O.Ito, and K.M. Kadish, "Modulating charge separation and charge recombination dynamics in porphyrin-fullerene linked dyads and triads: marcus-normal versus inverted region", J Am Chem Chem Soc., 123, 10676, 2001.
9. S. Paul, I. Mitra, R. Dutta, M. Bardhan,M. Bose, S. Das, M. Saha and T Ganguly, "Comparative analysis to explore the suitability of a short chain dyad in its pristine and

nanocomposite forms for designing artificial light energy conversion device", J Nanosci Nanotechnol, 18, 7873, 2018.

10. D.C. Marcano, D.V. Kosynkin, J.M. Berlin, A. Sinitskii, Z. Sun, A. Slesarev, L.B. Alemany, W. Lu and J.M. Tour, "Improved synthesis of graphene oxide", Am. Chem. Soc., 4, 8, 2010.
11. A. Mallick, A.S. Mahapatra, A. Mitra, J.M. Greneche, R.S. Ningthoujam and P.K. Chakrabarti, "Magnetic properties and bio-medical applications in hyperthermia of lithium zinc ferrite nanoparticle integrated with reduced graphene oxide", Journal of Applied Physics, 123, 055103, 2018.
12. C T Smith, M A Leontiadou, R Page, P.O.Brien, D.J.Binks, "Ultrafast charge dynamics in trap-free and surface trapping colloidal quantum dots", Adv Sci, 2, 1500088, 2015
13. Y. Wang, A Hu, "Carbon quantum dots: synthesis, properties and applications", J Mater Chem C, 2, 6921, 2014.
14. H. Zou, C. Dong, S. Li, C. Im, M. Jin, S. Yao, T. Cui, W. Tian, Y. Liu, H. Zhang, "Effect of surface trap states on photocatalytic activity of semiconductor quantum dots", J. Phys. Chem. C, 122, 9312, 2018.

Chapter : 4

# *Comparative analysis between nanocomposite dyads when NNDMBF dyad combined with Graphene oxide and Spherical gold nanoparticles to explore the suitability for designing artificial light energy conversion device*

# Chapter 4 : Comparative analysis between the nanocomposite dyads when NNDMBF dyad combined with Graphene oxide (GO) and spherical gold nanoparticles to explore the suitability for designing artificial light energy conversion device

From the UV-vis, steady state and time resolved spectroscopic investigations on the pristine dyad , dyad-spherical gold nanoparticles (GNP) and dyad-Graphe oxide (GO) , it was observed that though in the ground state the pristine dyad in its pristine form possesses trans-type (elongated and planar) isomer but on photoexcitation trans-form converts into cis-structure (folded). Interestingly, the dyad exhibits different behavior when it combines with GNP. In nanocomposite form of dyad-GNP, even on photoexcitation some ground state trans-structure still retains its identity in the excited state. The 16% of the trans-species remains unchanged in the excited state due to excitation of dyad-GNP system and possibly this configuration facilitates the hindrance of energy destructive charge recombination processes as in this conformer the donor and acceptor moieties tend to move far away from each other causing lack of overlapping of charge clouds of the reactants, the electron donor and acceptor moieties.

Measurements of the fluorescence lifetimes (**Table 1**) of the dyad were made by using the time correlated single photon counting (TCSPC) technique. By monitoring the different positions of the steady state fluorescence spectra the possibility of formations of another type of conformer, apart from trans, in the excited state due to photoexcitation has been examined. These findings further provide us the idea that the present short-chain dyad possesses photoswitchable character.

When excitation was made at 375 nm (using diode laser) in case of the pristine dyad NNDMBF , it was found that at the monitoring wavelength 480 nm (the peak region), majority emission originates from a species of lifetime 15 ps.

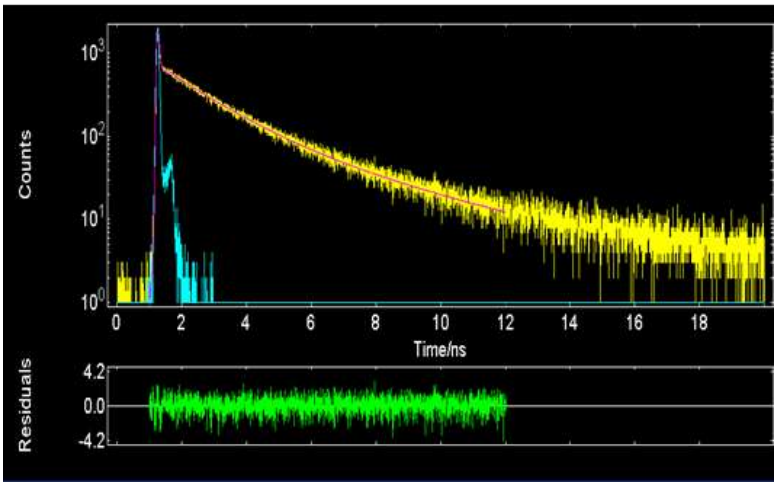


**Fig. 4.1 (a)** Fluorescence decay of the dyad –GNP system (yellow) in ACN ex =375 nm, em = 480 nm, the fast (blue) decaying component represents impulse response (diode laser) ($\chi^2$~ 1.088). The residual is also shown.

On monitoring at the 550 nm region (**Table 1)** only faster component of lifetime of picoseconds (ps) order was apparent. The fluorescence lifetimes of the dyad in presence of GNP (nanocomposite system ) by using the excitation wavelengths at 375 nm (region of mostly trans-isomer) and 440 nm (mostly relatively folded cis-isomeric regime) were measured. By monitoring at the different positions of the steady state fluorescence band on the longer wavelength side of the excitation wavelengths of 375 nm and 440 nm, both nanoseconds (slower component) and picoseconds (faster) component were observed. Another interesting findings are that in presence of both GNP and GO (Table 1) contribution from the faster component (~ps order) decreases along with concomitant increase of the slower component (in ns order).in the peak position of 480 nm of the dyad fluorescence emission band produced by the excitation at 375 nm.

Hence the above findings demonstrate that when the trans-type dyad in its pristine form is excited using 375 nm wavelength, most ground state trans isomers convert to the cis-type isomers having faster component (~ ps) lifetime. Thus the dyad NNDMBF appears to behave as photoswitchable dyad. However, when the dyad combines with GNP or GO nanoparticles, significant amounts of slow component species, appearing to possess trans-type structure, are found to be present along with the faster component which corresponds to cis-isomer.

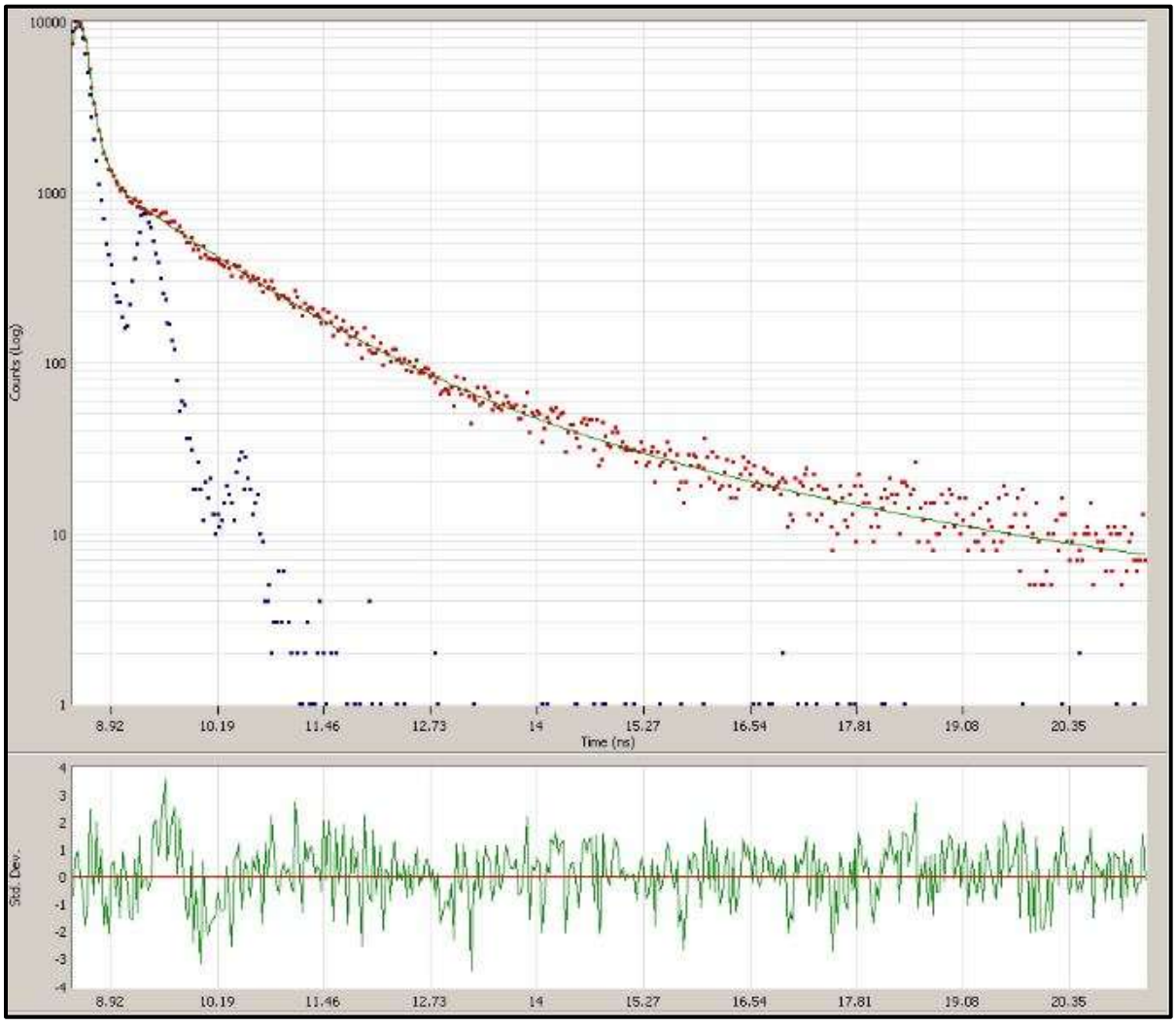


**Fig. 4.1 (b)** Fluorescence decay of the dyad –GO system in ACN ex =375 nm, em = 480 nm, the fast (blue) decaying component represents impulse response (diode laser) ($\chi^2$~ 1.196). The residual is also shown

**Table 1:** Fluorescence Lifetime data of the the short chain dyad NNDMBF in absence (pristine) and presence of **GNP** and **GO** at the different excitation and emission wavelengths at the ambient temperature. Values in parentheses besides lifetimes correspond to fractional contributions (f) of the particular species in the total steady state fluorescence emission

| Samples | $\lambda_{exc}$ (nm) | $\lambda_{em}$ (nm) | $\tau_1$ /ns ($f_1$) | $\tau_2$ ($f_2$) | $\chi^2$ |
|---|---|---|---|---|---|
| Dyad in ACN | 375 | 480 | 1.50(0.06) | 15ps (0.94) | 1.088 |
| | | 550 | - | 19ps(~ 1.0) | 1.068 |
| | 440 | 550 | - | 15ps(`1.0) | 1.15 |
| Dyad + GNP ($1x10^{-6}$ M) | 375 | 480 | 1. 51 (0.16) | 20 ps(0.84) | 1.080 |
| | | 550 | - | 20ps(1.0) | 1.09 |
| | 440 | 550 | - | 25 ps (1.0) | 1.16 |
| Dyad + GO ($4\times10^{-5}$ M) | 375 | 480 | 3.61(0.21) | 91 ps(0.79) | 1.080 |
| | | 550 | 3.44 (0.17) | 82 ps(0.83) | 1.09 |
| | 440 | 550 | 3.01 (0.09) | 100 ps (0.91) | 1.16 |
| Dyad+ CQD | 375 | 480 | 6.4 (0.84) | 256 ps (0.16) | 1.156 |
| | | 550 | 6.0 (0.77) | 260 ps (0.23) | 1.077 |

. Thus the experimental observations made from the fluorescence lifetime measurements reveal that though trans-isomer primarily dominates in the ground state but on photoexcitation, most of the trans components convert (photoconversion) to the cis-form in the excited level of the pristine dyad. However this photoconversion is somewhat impeded when the dyad adsorbs the

GNP or GO nanoparticles (nearly similar magnitudes of trans-structured species (Table 1), as evidenced from the fractional contribution values f, still retains even on photoexcitation). Thus in comparison to the pristine dyad, nanocomposite dyads appear to behave better light energy converters as trans-form impedes energy wasting charge recombination rates.

The hindrance effect for trans-cis photoconversion in the cases of dyad-GO and the dyad-GNP systems are not as efficient as observed in the case of carbon quantum dots (CQDs) where more than 80% of the ground state trans-conformers were able to retain their identity of trans-configuration even on photoexcitation. Thus dyad-CQD systems appear to be better artificial light energy conversion devices relative to the present dyad-GO or dyad-GNP nanocomposites.

# Chapter : 5

# *Overall conclusions*

# Chapter 5 : **Overall conclusions**

From our present investigation we can state following conclusions

(i) The time resolved measurements reveal that with dyad-GO and dyad-RGO around 20% trans structure of the ground state dyad could be protected even on photoexcitation.

(ii) In the case of the pristine dyad NNDMBF all the ground state trans-conformers would be converted to relatively folded structure cis on photoexcitation.

(iii) The retention of elongated conformation in trans-form will help to impede energy wasting charge recombination processes within nanocomposite dyads and may serve as better candidate for artificial light energy conversion systems relative to its pristine form.

(iv) The hindrance effect for trans-cis photoconversion in the cases of **dyad-GO** and the **dyad-GNP** systems are not as efficient as observed in the case of **carbon quantum dots (CQDs)** where more than **80% of the ground state trans-conformers** were able to retain their identity of trans-configuration even on photoexcitation.

(v) From the time resolved spectroscopic investigations it could be hinted that relatively stable trans-conformer in the excited state in case of the nanocomposite system of dyad NNDMBF-GO (or RGO) in comparison to the pristine form may arise from the surface trap effect.